University of Oxford

Radiative Processes in Astrophysics

Dr Adam Ingram

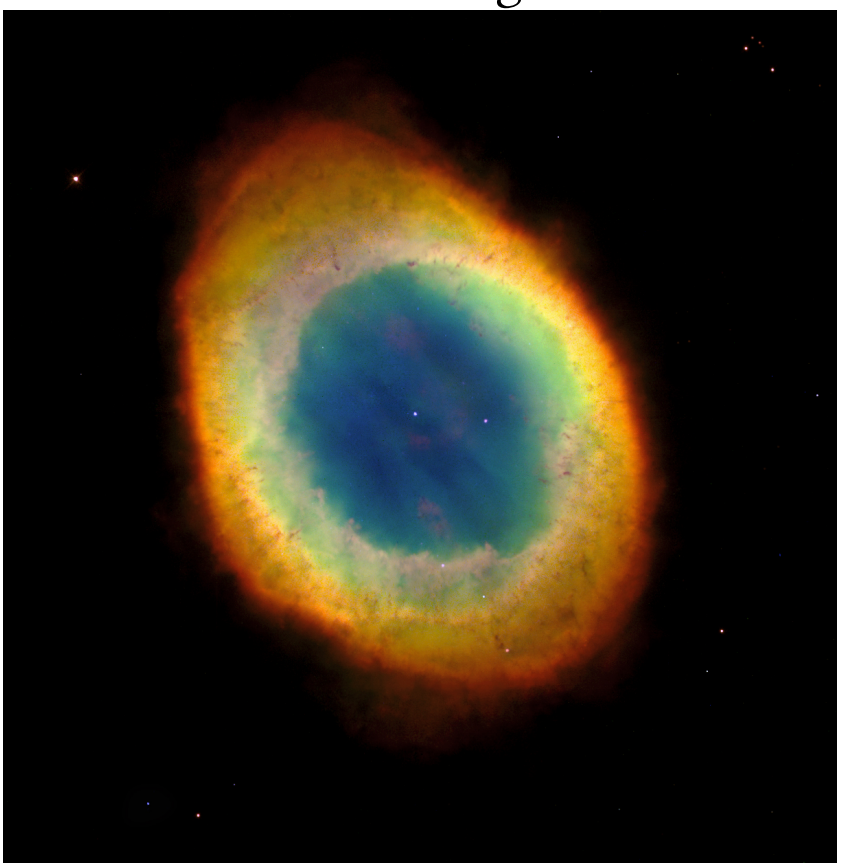

Hilary Term 2020

Contents

1 Basics of Radiative Transfer

1.1 Introduction

In this Lecture course, we will be learning about radiative transfer theory: the theory of how light propagates through an absorbing and emitting medium. We will use this theory in order to calculate the spectrum of astrophysical objects, including understanding the formation and strength of emission and absorption lines. In order to understand spectral lines, we must understand ionization and recombination of atoms/ions, and we must also of course understand excitations and de-excitations of electrons between bound energy levels in atoms/ions.

We will be applying our theory to several classes of astrophysical object:

Stars: We all know what stars are, so no need for an introduction!

Planetary Nebulae: A planetary nebula is a slowly expanding shell of gas that has been lost from a red giant star (i.e., on the asymptotic giant branch of the Hertzsprung-Russell diagram). This is a relatively short-lived ($\sim$ 10s of thousands of years) phase of stellar evolution for $\sim 1-8\ M_\odot$ stars. When the star runs out of fuel for nuclear fusion, its envelope expands to form a red giant and eventually this material is lost to the surroundings via a stellar wind. This diffuse material is then ionized by the remaining core, which becomes hotter as it fuses the remaining light elements into heavier elements. The ionized gas then glows with a spectrum dominated by strong emission lines. Examples of planetary nebulae are shown in Fig 1.1. Eventually, the central star will become a white dwarf and the gas will expand so much that it recombines and becomes invisible to us. Planetary nebulae play an important role in the chemical evolution of galaxies, since they expel the heavy elements that were created inside the star into the surrounding interstellar medium (ISM). As we will see, we can also use planetary nebulae to measure chemical abundances, because they exhibit strong emission lines – including 'forbidden' lines that are only produced in very tenuous environments. Note that the term 'planetary nebula' is a misnomer – these objects are nothing to do with planets. The term is just historical, since the first nebulae observed in the ~1700s looked spherical and a little like planets. As often happens in astronomy, the original, incorrect, name stuck!

Active Galactic Nuclei (AGN): An AGN is a supermassive black hole at the centre of a galaxy accreting material via an accretion disc (see Fig 1.2). During this course, we will only really be considering AGN as background sources of light, but we will cover them in a lot more detail in the following High Energy Astrophysics course. It is important to note that there are *lots* of different names for AGN. According to the unification theory, many different classes of objects are just AGN viewed from a different angle. During this course, I will talk most about *quasars*. These were originally called quasi-stellar objects, because they were optical point sources and

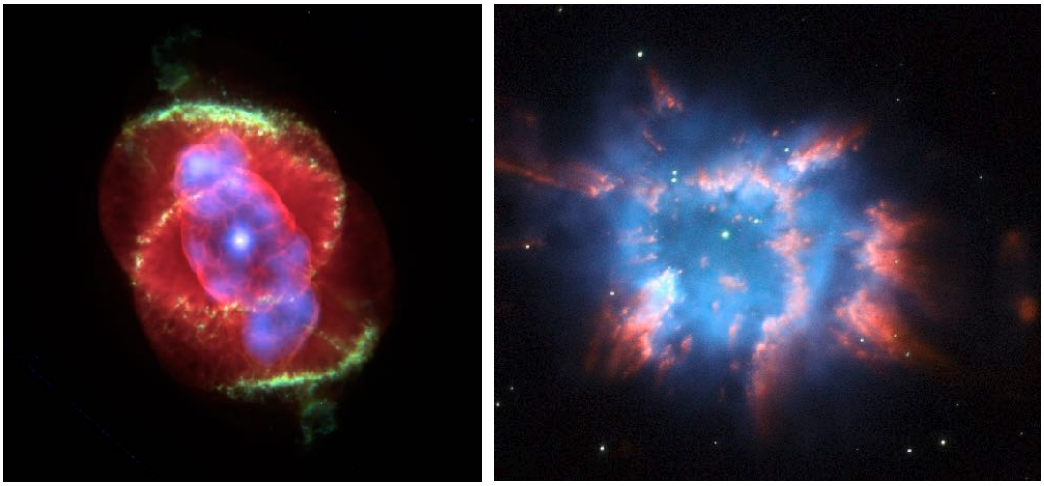

Figure 1.1: Examples of planetary nebulae. *Left:* Cat's Eye Nebula (NGC 6543), X-ray / optical composite image. *Right:* NGC 6326, here the central star is a binary.

therefore not e.g. galaxies or nebulae, but it later became apparent that they are actually very far away and very intrinsically bright. Galaxies that can be resolved as larger than a point source, but with a similar optical spectrum to that of quasars, were called *Seyfert* galaxies. These are just AGN that are close enough for us to spatially resolve. Consequently, the most distant (and therefore most intrinsically bright) objects that we can see in the Universe are quasars.

1.2 Radiative flux

Radiation theory applies when the scale of the system greatly exceeds the wavelength of radiation – e.g. shining a torch through a keyhole. In this case, we can consider light to travel along rays. If a detector of area dA faces a light source for a time interval dt, the amount of energy passing through the detector is $F\,dA\,dt$, where F is the *energy flux*. In the simplest case, we can consider an isotropic source of radiation emitting energy equally in all directions (e.g. a spherically symmetric, isolated star). If we put imaginary spherical surfaces around the source with radii r_0 and r, we know from simple energy conservation that the total energy passing through one sphere must be equal to the total energy passing through the second sphere. Therefore

$$F(r_0)\,4\pi r_0^2 = F(r)\,4\pi r^2. \tag{1.1}$$

Re-arranging gives

$$F(r) = \frac{\text{constant}}{r^2}, \tag{1.2}$$

which is the well-known *inverse square law*.

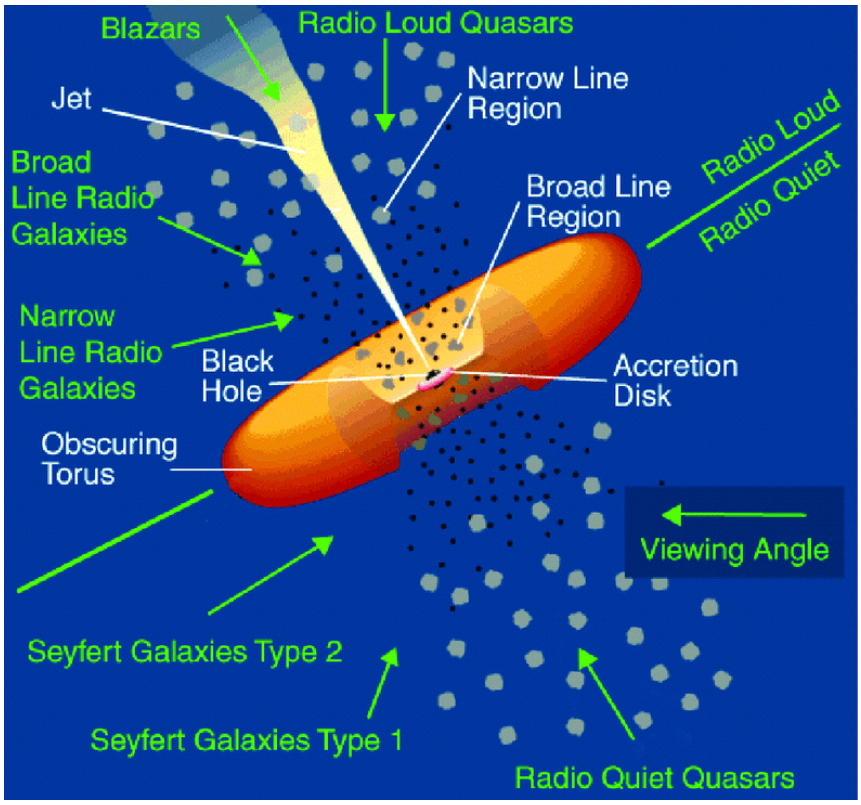

Figure 1.2: Schematic diagram of an active galactic nucleus (AGN). According to the unification theory, many different classifications of object are actually AGN viewed from a different angle.

1.2.1 Intensity

We can express the flux crossing the detector in a different, ultimately more useful way (although admittedly, much more confusing initially). Fig 1.3 illustrates a source element with area dA_s radiating energy dE in a time interval dt. A detector with surface area $dA_{\rm det}$ located a distance r from the source faces the source. We see from the sketch that rays with polar angle in the range $\theta - d\theta/2 \rightarrow \theta + d\theta/2$ and azimuthal angle in the range $\phi - d\phi/2 \rightarrow \phi + d\phi/2$ hit the detector, and all other rays miss the detector. From polar coordinates, we can see that

$$dA_{\rm det} = r^2 \ \sin\theta \ d\theta \ d\phi = -r^2 \ d\cos\theta \ d\phi = r^2 \ d\Omega_{\rm det}. \tag{1.3}$$

Here, $d\Omega_{\rm det}$ is the *solid angle* subtended by the detector. It is useful to define the *intensity*, which is the energy flux per unit solid angle:

$$I = \frac{dE}{dA_\perp \ dt \ d\Omega} = \frac{dE}{dA_s \ \cos\theta \ dt \ d\Omega}, \tag{1.4}$$

where $dA_\perp = dA_s \cos\theta$ is the area of the source element projected onto the trajectory of the ray. But why is this useful? Well, it is because the flux corresponds to the energy carried by *all rays* passing through a given area. Since there are many, many rays, the energy carried by an individual ray is essentially zero. We must therefore consider *bundles* of rays; i.e. all of the rays oriented within some solid angle of one central ray.

The total energy flux emitted by the source is related to the intensity as

$$F = \int \frac{dE}{dA_s \ dt \ d\Omega} d\Omega = \int I \ \cos\theta \ d\Omega = \int_0^{2\pi} \int_{-1}^{1} I \ \cos\theta \ d\cos\theta \ d\phi. \tag{1.5}$$

For an isotropic source radiating from only the upper surface, this becomes $F = I \ \pi$. Therefore a fraction $d\Omega_{\rm det}/\pi$ of the rays emitted from the source cross the detector and the rest miss. The energy flux crossing the detector is therefore

$$F_{\rm det} = \frac{d\Omega_{\rm det}}{\pi} \ \frac{dE}{dA_{\rm det} \ dt}. \tag{1.6}$$

We can make this expression much simpler by appreciating that the solid angle subtended by the source according to the detector is $d\Omega_s = dA_s/r^2$ (see Fig 1.4), giving rise to the *reciprocity theorem*:

$$\frac{dA_{\rm det}}{d\Omega_{\rm det}} = \frac{dA_s}{d\Omega_s}. \tag{1.7}$$

We therefore find that the detected flux is

$$F_{\rm det} = \frac{d\Omega_s \ dA_{\rm det}}{\pi \ dA_s} \ \frac{dE}{dA_{\rm det} \ dt} = \frac{d\Omega_s}{\pi} \ \frac{dE}{dA_s \ dt} = I \ d\Omega_s. \tag{1.8}$$

Even though this expression was derived for a flat isotropic source, it is true in general.

Intensity is very useful because it is an invariant quantity. Whereas flux always depends on what surface area we are considering, intensity is measured to be the same by any observer.[1]

[1] Except there is a modification to this in relativity, but that is beyond the scope of this course.

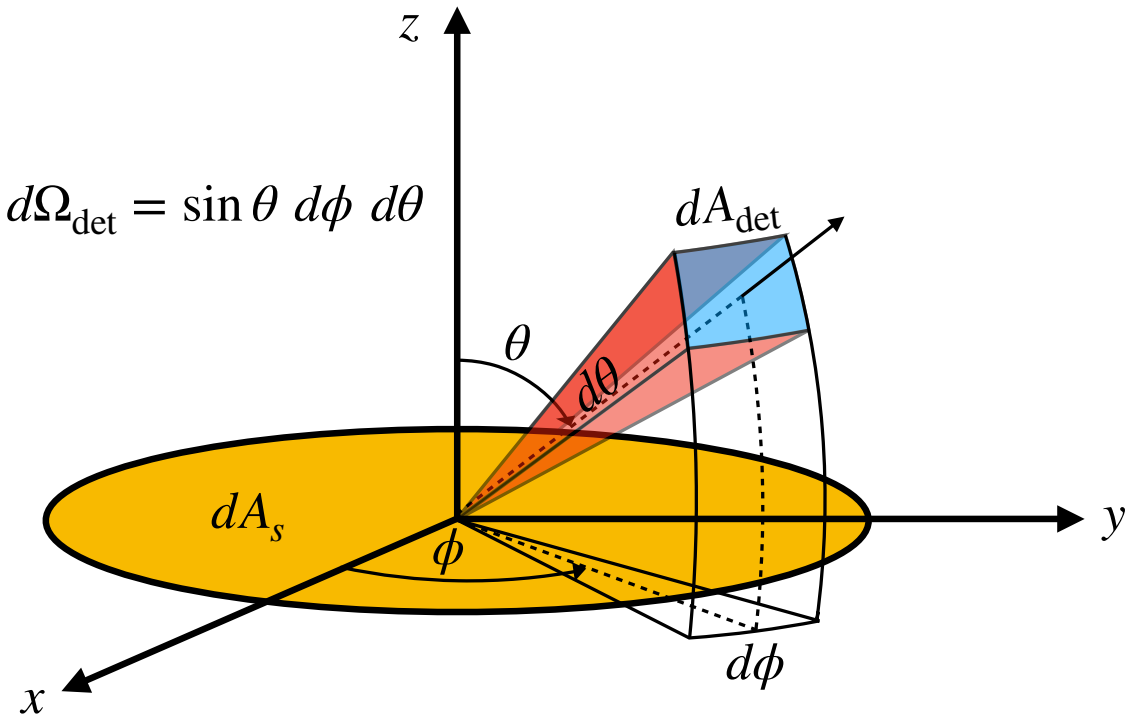

Figure 1.3: A source of surface area dA_s (yellow) radiates light that crosses a detector with surface area $dA_{\rm det}$ placed a distance r away (blue). The detector subtends a solid angle $d\Omega_{\rm det} = dA_{\rm det}/r^2$.

We can see this quite simply from the above equation: the intensity is just defined by how the source radiates, and the flux observed by an observer just depends on the intensity and the apparent size of the source on the observer's sky. We can also recover the inverse square law from the above equation by imagining two detectors with the same area dA, one placed a distance r_0 from the source and detecting a flux F_0 and the other at a distance r detecting a flux F. It is simple to show from Equation (1.8) that $F \propto 1/r^2$.

1.2.2 Specific intensity

The *specific intensity* (sometimes referred to as the *surface brightness*) is simply the intensity per unit photon frequency, $I_\nu = dI/d\nu = dE/[dA\,dt\,d\Omega\,d\nu]$. We could alternatively think in terms of wavelength, $I_\lambda = dI/d\lambda$, or even photon energy $I_E = dI/(h\,d\nu)$. Traditionally, different notations tend to be employed in different branches of astronomy. Optical and infrared astronomers tend to use wavelength, X-ray and $\gamma-$ray astronomers tend to use photon energy, and photon frequency is normally preferred in radio astronomy, multi wave-length and theoretical studies. These differences often reflect the different detection techniques employed for different wavelengths of radiation, but ultimately the three can be used interchangeably as long as you are careful. I'm

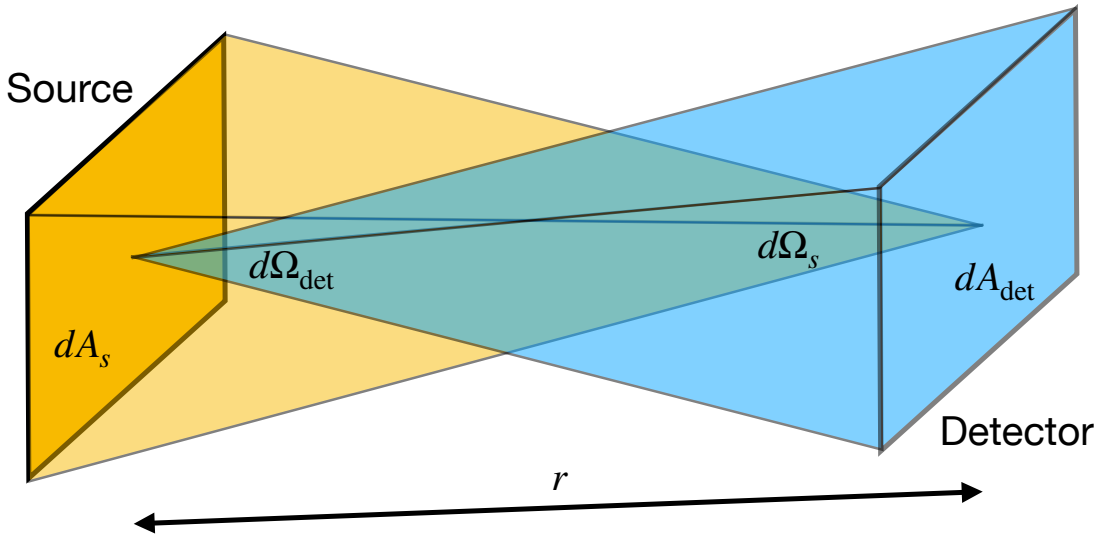

Figure 1.4: Demonstration of the reciprocity principle. A source and detector are a distance r from one another. The detector has a surface area $dA_{\rm det}$ and subtends a solid angle $d\Omega_{\rm det}$. The source has a surface area dA_s and subtends a solid angle $d\Omega_s$.

mainly an X-ray astronomer, so naturally think in terms of photon energy, but photon energy can be too easily confused with the radiated energy (and the radiated energy is the photon energy multiplied by the number of photons) and so I will use photon frequency or wavelength throughout this course. In general, the word *specific* can just be used to mean 'per unit photon frequency', such that e.g. specific flux is $F_\nu = dF/d\nu$, or 'per unit wavelength' (e.g. $F_\lambda = dF/d\lambda$). The specific flux in terms of frequency and wavelength can be related by starting with their definitions:

$$\int_{\nu=0}^{\nu=\infty} I_\nu d\nu = \int_{\lambda=0}^{\lambda=\infty} I_\lambda d\lambda. \tag{1.9}$$

Since $\lambda = c/\nu$, $d\lambda = -c\nu^{-2}d\nu = -(\lambda/\nu)d\nu$, therefore

$$\int_{\nu=0}^{\nu=\infty} I_\nu d\nu = -\int_{\nu=\infty}^{\nu=0} I_\lambda \frac{\lambda}{\nu} d\nu = \int_{\nu=0}^{\nu=\infty} I_\lambda \frac{\lambda}{\nu} d\nu. \tag{1.10}$$

We therefore see that

$$I_\nu = \frac{\lambda}{\nu} I_\lambda. \tag{1.11}$$

Specific intensity is a very useful quantity to work with because it is something intrinsic to the source that we can actually measure. For instance, say we observe a galaxy to have an angular diameter on the sky θ. If the projected shape of the galaxy on the sky is circular, then the solid angle it subtends is $d\Omega_s = \pi(\theta/2)^2$. The raw quantity we measure with our telescope is the specific flux crossing the detector, $F_\nu^{\rm det}$. It is straight forward to then derive the specific intensity of the source, $I_\nu = F_\nu^{\rm det}/d\Omega_s$. Even if the source is unresolved (i.e. appears as a point source

and therefore we only have an upper limit on it's angular extent), we can estimate the specific intensity if we have some idea of the physical size of the source and its distance from us.

1.2.3 Radiative energy density

The specific energy density u_ν – a quantity we will need in the following lecture – is defined as the energy per unit volume per unit frequency range. We can derive the relation between this quantity and the specific intensity by imagining a cylinder with cross-sectional area dA and length $c\ dt$. The specific energy density per unit solid angle relates to the radiated energy as

$$dE = (du_\nu/d\Omega)\ dA\ c\ dt\ d\Omega\ d\nu. \tag{1.12}$$

Light travels at speed c, therefore we also have that $dE = I_\nu\ dA\ d\Omega\ dt\ d\nu$. Equating the two expressions for dE and integrating over the full range of solid angles gives

$$u_\nu = \frac{1}{c}\int I_\nu d\Omega. \tag{1.13}$$

1.3 Thermal radiation

Thermal radiation is radiation emitted by matter in thermal equilibrium. This means, for instance, that the speed distribution of the free electrons in the matter is the Maxwellian distribution. That is, the fraction of electrons with speed in the range v to $v + dv$ is

$$f(v)\ dv = 4\pi \left[\frac{m_e}{2\pi k T_e}\right]^{3/2} v^2\ \exp\left(-\frac{m_e\ v^2}{2kT_e}\right), \tag{1.14}$$

where T_e is the electron temperature (or *kinetic temperature*), m_e the electron mass and k is the Boltzmann constant. However, even if the *particles* in the medium are in thermal equilibrium, the *photons* radiated from the medium do not necessarily need to be in thermal equilibrium.

1.3.1 Blackbody radiation

Blackbody radiation is radiation which is itself in thermal equilibrium; i.e. the photons are in thermal equilibrium with one another. The specific intensity of blackbody radiation is given by the familiar Planck function

$$I_\nu = B_\nu = \frac{2h\nu^3/c^2}{\exp(h\nu/kT) - 1}, \tag{1.15}$$

where T is the *photon* temperature. Examples of the Planck function for different temperatures are shown in Fig 1.5. For brevity, we will not derive this function, but I point interested students to Rybicki & Lightman (Section 1.5).

One important property of blackbody radiation is that the specific intensity is a universal function of T, which we can see from the above equation (i.e. B_ν depends *only* on T and fundamental constants). We can understand this with a thought experiment illustrated in Fig 1.6.

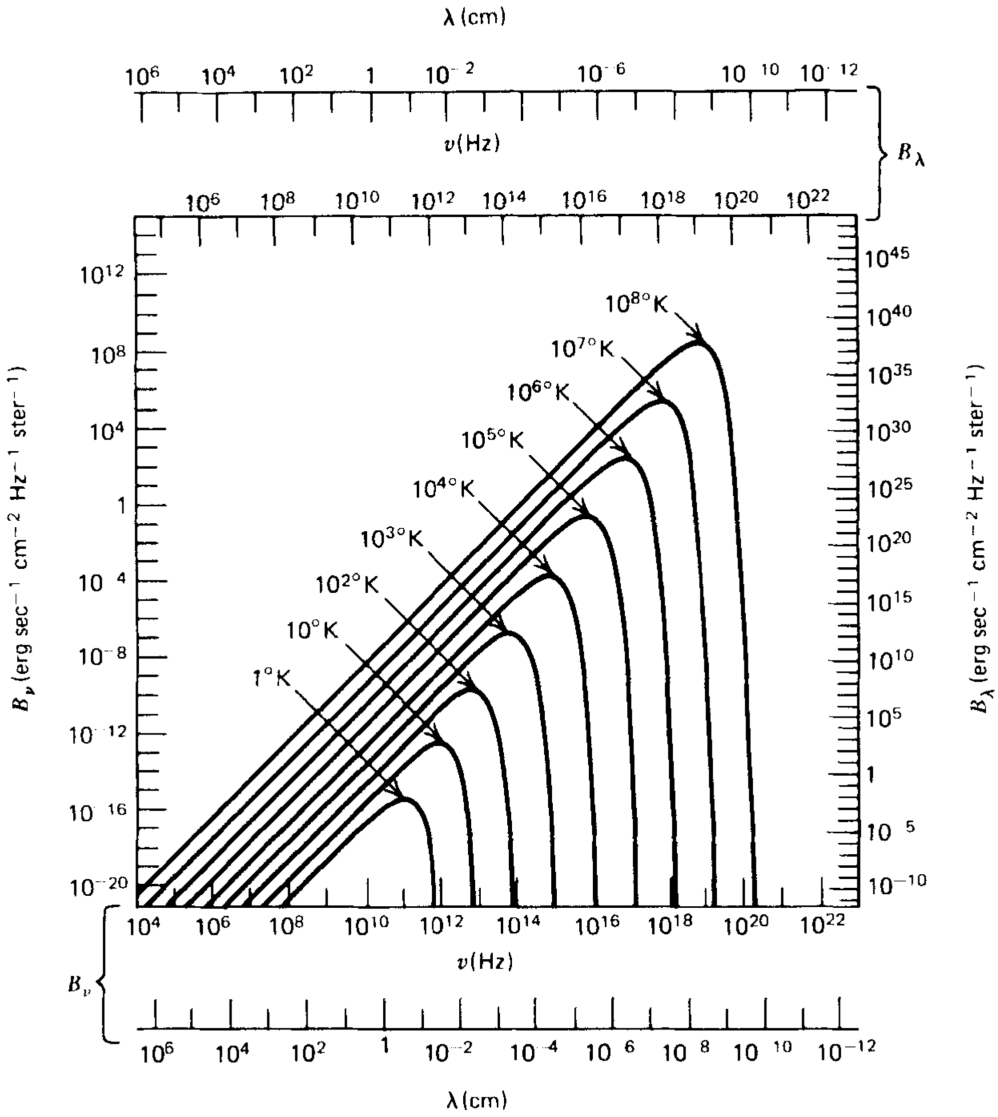

Figure 1.5: Examples of black body spectra at various temperatures (reproduced from Rybicki & Lightman; originally taken from Kraus 1966).

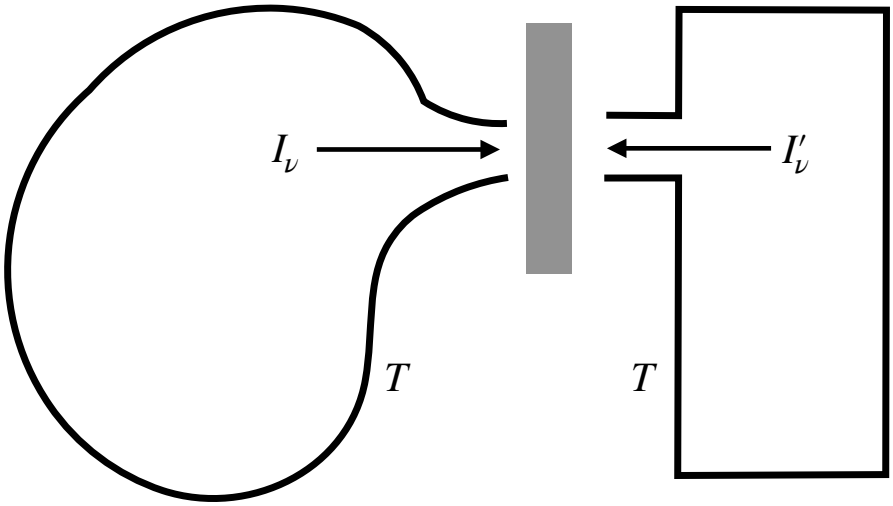

Figure 1.6: Two containers, both at temperature T, separated by a filter (grey).

Imagine we keep two containers at temperature T, and we do not let radiation in or out until equilibrium has been achieved separately in each container. Let's denote the specific intensity of radiation in the left and right hand containers I_ν and I'_ν respectively. These two containers can have different shapes or any other properties for that matter, but importantly they are the same temperature. We now place a filter between the two containers that enables photons in a narrow frequency range centered on ν_0 to pass between the two containers. If $I_{\nu_0} \neq I'_{\nu_0}$, energy will flow spontaneously between the two enclosures. Since the two are of the same temperature, this would violate the second law of thermodynamics. Therefore $I_\nu = I'_\nu$ and thus the specific intensity of blackbody radiation is a function of temperature only.

There are a number of other important characteristics of black body radiation, such as the *Stefan-Boltzmann* law

$$F = \sigma\, T^4, \tag{1.16}$$

where σ is the Stefan-Boltzmann constant. We can also simplify Planck's law for very low and very high frequencies. In the $h\nu << kT$ limit, the exponential can be Taylor expanded to give the *Rayleigh-Jeans law*:

$$I_\nu = \frac{2\nu^2}{c^2} kT. \tag{1.17}$$

We indeed see in Fig 1.5 that the function is simply a power-law at small ν. In the $h\nu >> kT$ limit, the exponential can be assumed to completely dominate the denominator, giving the *Wien law*:

$$I_\nu = \frac{2h\nu^3}{c^2} \exp\left(-\frac{h\nu}{kT}\right). \tag{1.18}$$

Again comparing with Fig 1.5, we see that the function drops off very quickly with frequency at the high end. Finally, it is straightforward to show that the peak of B_ν is at frequency $\nu = \nu_{\max}$, where

$$h\nu_{\max} = 2.82\, kT. \tag{1.19}$$

This is the *Wien displacement law.*

1.3.2 Characteristic temperatures

It is useful to define a number of characteristic temperatures related to the Planck spectrum. The first is the *brightness temperature.* Say we measure the specific flux of an astrophysical object, I_ν, in one narrow frequency range. The brightness temperature, T_b, is the temperature of the blackbody function that has that specific intensity at that frequency:

$$I_\nu = B_\nu(T_b). \tag{1.20}$$

The brightness temperature is often used in radio astronomy, since the Rayleigh-Jeans law is often applicable, giving

$$T_b = \frac{c^2}{2\nu^2 k} I_\nu \tag{1.21}$$

for $h\nu << kT$. Often, of course, the spectrum of the object is wildly different from a blackbody function (e.g. synchrotron radiation, Compton scattering etc). As an example, the quasar 3C 273 has a flux density of 12 Jy at 100 GHz, and subtends an angular diameter on the sky of 0.1 milli-arcseconds (data from Greve et al 2002). Since 1Jy = 10^{-26} W Hz^{-1} m^{-2} and the solid angle subtended by 3C 273 is related to the angular diameter $d\theta$ as $d\Omega = (\pi/4)\theta^2$, this means that the specific intensity at 100 GHz is $I_\nu = 6.9 \times 10^{-7}$ W Hz^{-1} m^{-2} St^{-1}, where St is a steradian (see Fig 1.7). It can be shown (and you will be showing this yourself in the coming problem set) that the brightness temperature for this specific intensity at this frequency is $T_b = 10^{10}$ K, which is *enormous*! The figure shows the unique blackbody function that gives the measured flux density at 100 GHz, and for reference also a blackbody function with $T = 2.4$ K. The conclusion is that the spectrum of 3C 273 is not described by a blackbody function. In the coming High Energy Astronomy course, we will see many examples of objects with spectra very different from a that of a blackbody.

Colour temperature can instead be measured from the *shape* of the spectrum. For example, the spectrum of a source may be the shape of a blackbody, but we may not know the distance to the source and/or the source may be spatially unresolved. We therefore cannot measure I_ν, only the flux crossing our detector. Alternatively, the source spectrum may be only approximately blackbody – for instance an initially blackbody spectrum may be modified by scattering in an atmosphere. We can still, however fit a blackbody function to the observed spectrum. The temperature of that blackbody function is the colour temperature, T_c. A cruder measurement of T_c can be obtained by measuring the peak frequency of the spectrum and applying Wien's law.

Finally, the *effective temperature* of a source, $T_{\rm eff}$, is derived from the total amount of flux integrated over all frequencies radiated at the source:

$$F = \int \cos\theta \, I_\nu \, d\nu \, d\Omega \equiv \sigma \, T_{\rm eff}. \tag{1.22}$$

Again, this is useful if the source spectrum is only approximately blackbody.

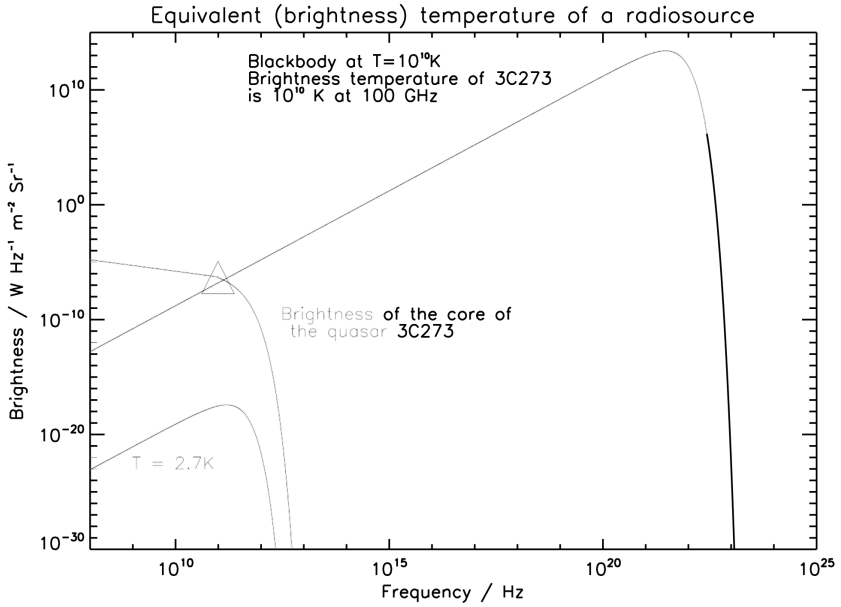

Figure 1.7: Specific intensity of quasar 3C 273 at 100 GHz (triangle) alongside the unique Planck function that passes through this data point, a Planck function with $T = 2.4$ K, and the true spectrum of the source. The brightness temperature of 3C 273 is so large, we can cnclude that it's spectrum is not described by Planck's law.

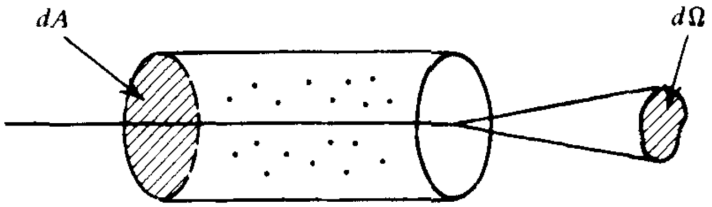

Figure 1.8: Bundle of rays (solid angle $d\Omega$) passing through a medium of absorbers, each with absorption cross-section σ_ν. Reproduced from Rybicki & Lightman.

1.4 Radiative transfer

So far, we've been thinking about light rays propagating through free space. Now we need to move on to thinking about light propagating through a medium. This medium can, in general, generate further emission and can also absorb existing emission.

1.4.1 Emission

The spontaneous *specific emission coefficient*, j_ν, is defined as the energy emitted by a medium per unit time per unit solid angle per unit volume:

$$j_\nu = \frac{dE}{dV\, d\Omega\, dt\, d\nu}. \tag{1.23}$$

When a beam of cross section dA moves a distance ds, it travels through a volume $dV = dA\, ds$. Thus the intensity added to the beam by spontaneous emission in the medium is

$$dI_\nu = j_\nu\, ds. \tag{1.24}$$

Therefore, if a beam has specific intensity $I_\nu(s = 0)$ upon entering a purely emitting medium, the specific intensity of the beam after travelling a distance s through the medium is given by

$$I_\nu(s) = I_\nu(0) + \int_0^s j_\nu(s')\, ds'. \tag{1.25}$$

The increase of brightness is equal to the emission coefficient integrated along the line of sight.

1.4.2 Absorption

Intensity will also, in general, be taken out of the beam as it propagates through a medium by absorption. The *absorption coefficient* α_ν (units: 1/distance) is defined by the equation

$$dI_\nu = -\alpha_\nu\, I_\nu\, ds, \tag{1.26}$$

and by convention α_ν is positive if net energy is taken out of the beam. It is useful to understand this law by imagining a cylinder with cross-section dA and length ds that contains n randomly

distributed particles per unit volume. Each particle has an absorbing cross-section σ_ν^2 (dimension: [distance]^2). The number of absorbers in the cylinder is $n\ ds\ dA$ and so the total absorbing area for photons with frequency ν is $\sigma_\nu\ n\ ds\ dA$. The energy absorbed out of the beam is

$$-\ dI_\nu\ dA\ d\Omega\ dt\ d\nu = I_\nu\ (n\ \sigma_\nu\ ds\ dA)\ dt\ d\Omega\ d\nu, \tag{1.27}$$

therefore

$$dI_\nu = -n\ \sigma_\nu\ I_\nu\ ds. \tag{1.28}$$

And so we can see from Equation (1.26) that the absorption coefficient is related to the absorption cross-section of the individual absorbers as

$$\alpha_\nu = n\ \sigma_\nu. \tag{1.29}$$

We will be using the absorption coefficient in this course, but there are a lot of different conventions. One common one is to use the *opacity* coefficient κ_ν (also known as the *mass absorption coefficient*), which relates to the absorption coefficient as $\alpha_\nu = \rho\ \kappa_\nu$, where ρ is the mass density. It is important to mention this, as it is common to talk about the opacity of a medium or 'the sources of opacity' in a medium. We can see from these equations that the opacity is simply a slightly different definition of absorption.

From the definition of the absorption coefficient (Equation 1.26) we can see that if a beam has specific intensity $I_\nu(0)$ upon entering a purely absorbing medium, the specific intensity of the beam after travelling a distance s through the medium is given by

$$I_\nu(s) = I_\nu(0) \exp\left\{-\int_0^s \alpha_\nu(s')\ ds'\right\}. \tag{1.30}$$

The brightness decreases along the ray by the exponential of the absorption coefficient integrated along the line of sight.

1.4.3 The Radiative Transfer Equation

It is fairly straightforward to combine the previous discussions on emission and absorption into one equation. This is the *radiative transfer equation*:

$$\frac{dI_\nu}{ds} = -\alpha_\nu\ I_\nu + j_\nu. \tag{1.31}$$

In the next lecture, we will solve this equation to calculate the intensity of a beam of light propagating through an emitting and absorbing medium as a function of photon frequency. Of course, all of the complicated physics comes in calculating the correct forms for α_ν and j_ν, which we will discuss next time.

Adam Ingram

2 Formation of Emission Lines

2.1 Introduction

Last lecture, we derived the radiative transfer equation (Equation 1.31):

$$\frac{dI_\nu}{ds} = -\alpha_\nu I_\nu + j_\nu,$$

Which describes how the specific intensity of a beam of light is modified when it passes through a medium with absorption coefficient α_ν and emission coefficient j_ν. This time, we will solve this equation and use it to determine whether we will see emission lines or absorption lines when a beam of light passes through a medium with given properties. We will then consider the case of emission lines and ultimately calculate the relative flux of different emission lines.

2.2 Solving the radiative transfer equation

2.2.1 Optical depth and source function

Equation (1.31) already looks fairly simple, but it simplifies even further when we introduce a few more key quantities (I promise the frequency that I define new quantities will reduce soon – radiative transfer theory is fairly heavy on definitions). A very important quantity that we can use in place of the path length s is the *optical depth*, τ_ν, defined by

$$d\tau_\nu = \alpha_\nu \, ds, \tag{2.1}$$

or

$$\tau_\nu(s) = \int_0^s \alpha_\nu(s') \, ds'. \tag{2.2}$$

Here we are defining the optical depth along the path of a travelling ray, and so $\tau_\nu = 0$ when the beam enters the medium. Note that the optical depth is dimensionless. A medium is said to be *optically thick* or *opaque* when τ_ν integrated along a typical path length is $\tau_\nu > 1$. When $\tau_\nu < 1$, the medium is said to be *optically thin*. Basically, in an optically thick medium, a typical photon can pass through the medium without being absorbed.

We can additionally define the *source function* $S_\nu = j_\nu/\alpha_\nu$ to re-write the radiative transfer equation as

$$\frac{dI_\nu}{d\tau_\nu} = -I_\nu + S_\nu. \tag{2.3}$$

2.2.2 The formal solution

We can use our newly defined quantities to solve the equation. Multiplying the above equation by e^{τ_ν} and using the chain rule gives

$$\begin{aligned} \frac{dI_\nu}{d\tau_\nu} e^{\tau_\nu} + I_\nu\, e^{\tau_\nu} &= S_\nu\, e^{\tau_\nu} \\ \frac{d[I_\nu\, e^{\tau_\nu}]}{d\tau_\nu} &= S_\nu\, e^{\tau_\nu}, \end{aligned} \tag{2.4}$$

which has the solution

$$I_\nu(\tau_\nu) = I_\nu(0)\, e^{-\tau_\nu} + \int_0^{\tau_\nu} e^{\tau'_\nu - \tau_\nu}\, S_\nu(\tau'_\nu)\, d\tau'_\nu. \tag{2.5}$$

The two terms can be interpreted as: the initial intensity diminished by absorption plus the integrated emission from the medium diminished by absorption. As an illustrative example, let's consider a medium with a constant source function. For such as medium, illustrated in Fig 2.1, a beam of light with initial specific intensity $I_\nu(0)$ is incident on some medium, travels a total optical depth of τ_ν through that medium, and emerges with specific intensity $I_\nu(\tau_\nu)$. Since the source term is constant, our solution to the radiative transfer equation becomes:

$$I_\nu(\tau_\nu) = S_\nu + e^{-\tau_\nu}[I_\nu(0) - S_\nu]. \tag{2.6}$$

We therefore see that the specific intensity emerging out of a medium with optical depth $\tau_\nu = 0$ is simply $I_\nu(0)$ – i.e. just the specific intensity that went in to the medium. In the opposite case of $\tau_\nu \longrightarrow \infty$, we see that the emergent specific intensity is S_ν – i.e. all of the initial intensity has been absorbed, and what emerges is the radiation that was produced in the medium, diminished by absorption.

2.2.3 Mean Path Length

The optical depth can be understood a little better in terms of *mean free path*, ℓ: the mean distance that a photon can travel in a medium before being absorbed. From the formal solution to the radiative transfer equation, we see that the probability of a photon traveling at least an optical depth τ_ν without being absorbed is $e^{-\tau_\nu}$. The mean optical depth travelled is therefore:

$$\langle \tau_\nu \rangle = \int_0^\infty \tau_\nu e^{-\tau_\nu} d\tau_\nu = 1. \tag{2.7}$$

Therefore photons in a given medium travel on average an optical depth of $\tau_\nu = 1$ before being absorbed. Since $d\tau_\nu = \alpha_\nu ds$, we see that the mean path length is $\ell = 1/\alpha_\nu$. This perhaps gives a more intuitive interpretation of the absorption coefficient.

2.2.4 Formation of emission and absorption lines

Fig 2.2 is a sketch illustrating the frequency dependence of the absorption coefficient α_ν. Two types of absorption are considered here: *bound-bound*, whereby the absorbed photon excites a

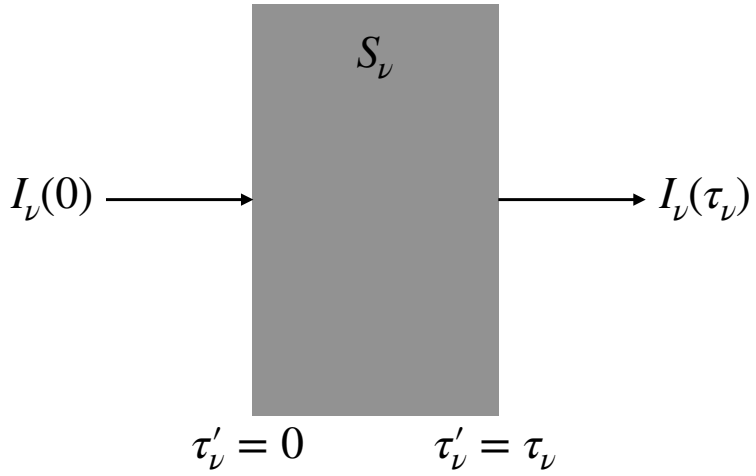

Figure 2.1: Schematic sketch of a beam of radiation passing an optical depth τ_ν through a medium that has source function S_ν.

bound electron to a higher bound state, and *bound-free*, whereby the photon gives an initially bound electron enough energy to escape the atom entirely (i.e. photo-ionisation). The cross-section for bound-bound transitions, σ_ν^{bb}, is a narrow spike centered at $h\nu$ equal to the energy difference between levels (with the width due to quantum effects we will briefly discuss later). The cross-section for a given bound free transition, σ_ν^{bf}, is zero for $h\nu$ below the ionisation potential energy and drops off as ν^{-3} for $h\nu$ above that energy, such that a photon has no hope of liberating an electron in a given shell if it has energy less than the relevant ionisation potential but always has a chance of liberating the electron if its energy is greater than the ionisation potential. The absorption coefficient for a particular species of a particular element in the medium is

$$\alpha_\nu = \sum_i \left[\sum_{j>i} n_i \, (\sigma_\nu^{bb})_{ij} + n_i (\sigma_\nu^{bf})_i \right], \tag{2.8}$$

where n_i is the number density of electrons in the i^{th} energy level. We then need to sum the absorption coefficients for each ionic species of each element in order to get the absorption coefficient for the medium. As is illustrated in Fig 2.2, this means that the absorption coefficient has a number of narrow spikes from bound-bound absorption and a number of 'edges' from bound-free interactions.

The spikes in the absorption coefficient will imprint narrow dips in the emergent spectrum – absorption lines. However, electrons *decaying* from a higher to a lower energy level in the medium will emit fluorescence lines at the same frequency as the absorption lines. So, when do we see absorption lines and when do we see emission lines? Well, we can get an intuitive handle on this by considering the optically thin case: $\tau_\nu << 1$, such that $e^{-\tau_\nu} \approx 1 - \tau_\nu$. In this case, Equation 2.6 becomes:

$$I_\nu(\tau_\nu) = I_\nu(0) + \tau_\nu [S_\nu - I_\nu(0)]. \tag{2.9}$$

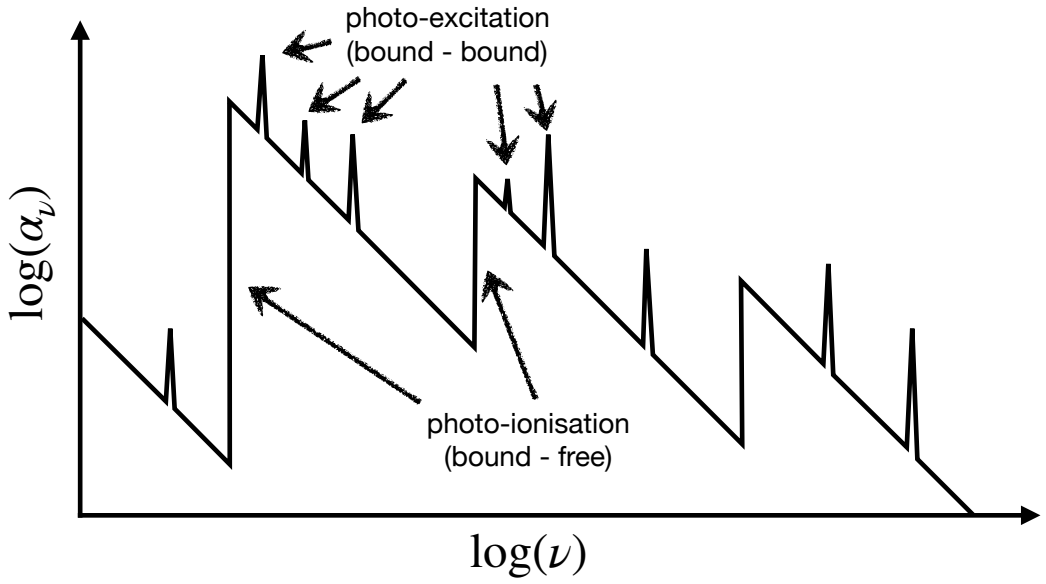

Figure 2.2: Sketch of the frequency dependence of the absorption coefficient. Bound-bound absorption results in a narrow line for each electron transition in each ionisation species of each element. The cross-section of bound-free absorption for a given bound electron energy level is zero for $h\nu$ below the ionisation potential and drops off as ν^{-3} for $h\nu$ above the ionisation potential.

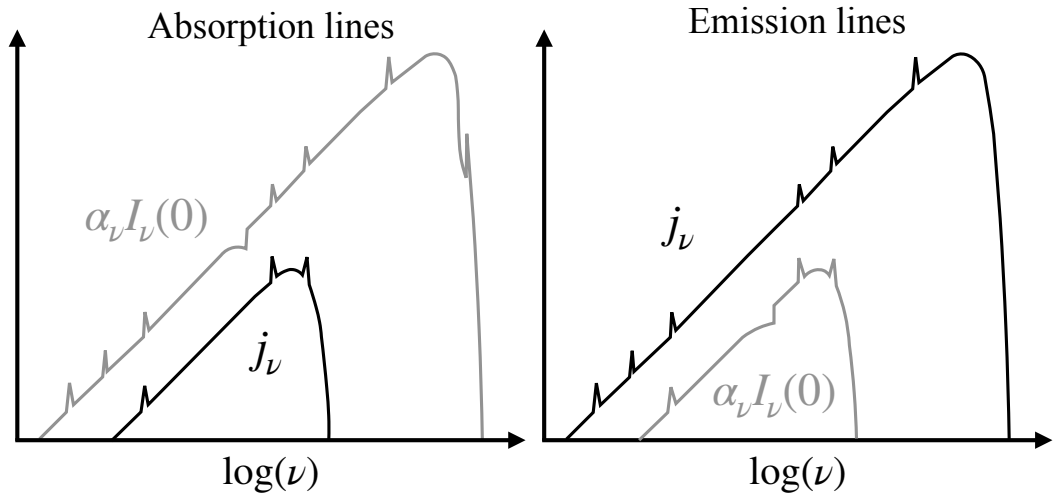

Figure 2.3: Cases whereby the emergent spectrum includes absorption (left) or emission (right) lines.

This form of the equation makes it very easy to see that when $S_\nu > I_\nu(0)$, the beam *increases* in brightness as a result of passing through the medium and when $S_\nu > I_\nu(0)$, the beam *decreases* in brightness. Therefore:

If $S_\nu > I_\nu(0)$: $I_\nu(\tau_\nu)$ has emission lines;

If $S_\nu < I_\nu(0)$: $I_\nu(\tau_\nu)$ has absorption lines.

Therefore, for there to be emission lines, we need $j_\nu > \alpha_\nu I_\nu(0)$, and for absorption lines $j_\nu < \alpha_\nu I_\nu(0)$. Fig 2.3 is a sketch of a specific illustrative example. In this example, the incident spectrum is a blackbody, and the spectrum emitted by the medium has a continuum with a *nearly* blackbody spectral shape (but, crucially, not exactly blackbody) plus fluorescence lines. In this case, whether we see emission or absorption lines simply depends on the relative temperature of the initial emitter and the absorbing material. If the absorber is hotter than the emitter (right) we get emission lines, and if it is cooler (left), we get absorption lines. In the case of planetary nebulae, j_ν is the gas is dominated by emission lines, and so the spectrum we see has many strong emission lines (Fig 2.4).

2.3 Excitation and De-excitation mechanisms

Now we have some understanding of the basics of radiative transfer, we can start to think about the detailed physics. Eventually, the goal is to calculate the expected flux of emission and absorption lines, and ultimately use line flux ratios to measure things such as elemental abundance, electron density and electron temperature in astrophysical objects such as stars,

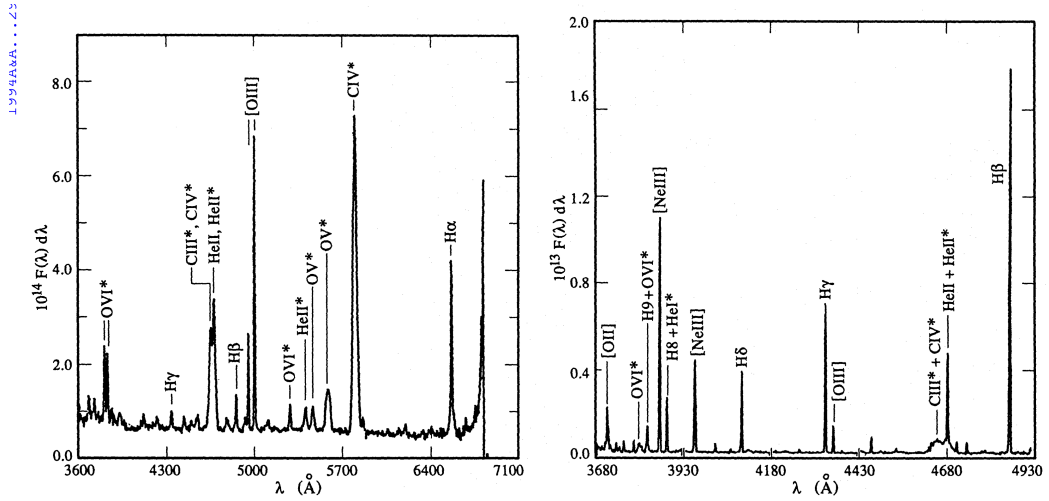

Fig. 1. The complete spectrum of NGC 1501 (Jan. 1988)

Fig. 3. The complete spectrum of IC 1747 (Sept 1983)

Figure 2.4: Examples of spectra from planetary nebula showing strong emission lines (from Stanghellini, Kaler & Shaw 1994).

planetary nebulae, quasars etc. In order to do this, we must calculate the relative populations in different atomic energy levels. As a first step, let's consider the simplest case: a 2-level atom. As is illustrated in Fig 2.5, there are a number of excitation and de-excitation mechanisms, and these mechanisms can be quantified by the *Einstein coefficients*. You will have already covered some of these mechanisms (i.e. the Einstein A and B coefficients), but some will be new to you (i.e. the C coefficients). Let's first summarise these mechanisms one by one.

2.3.1 Spontaneous radiative decay

An electron in level 2 has some probability of decaying to level 1 and emitting a photon with $h\nu$ equal to the energy difference between the two levels: $\nu_{12} = \Delta E_{12}/h$. The probability of decay per second is given by the *Einstein A coefficient*: A_{21}. Therefore, $n_2 A_{21}$ electrons transition from level 2 to level 1 per second per unit volume. This produces a spectral line with luminosity

$$L_{21} = h\nu_{12} \int_V n_2 \, A_{21} \, dV, \tag{2.10}$$

where n_2 is the number density of electrons in the second energy level (electrons per unit volume) and the integral is over the volume of the emitting region. The observed flux of the emission line for isotropic emission is therefore

$$F_{21} = \frac{h\nu_{12}}{4\pi d^2} \int_V n_2 \, A_{21} \, dV, \tag{2.11}$$

where d is the distance to the emitting region. During this course, it will be common to assume that the emitting region is homogeneous, dispensing with the need for the integral.

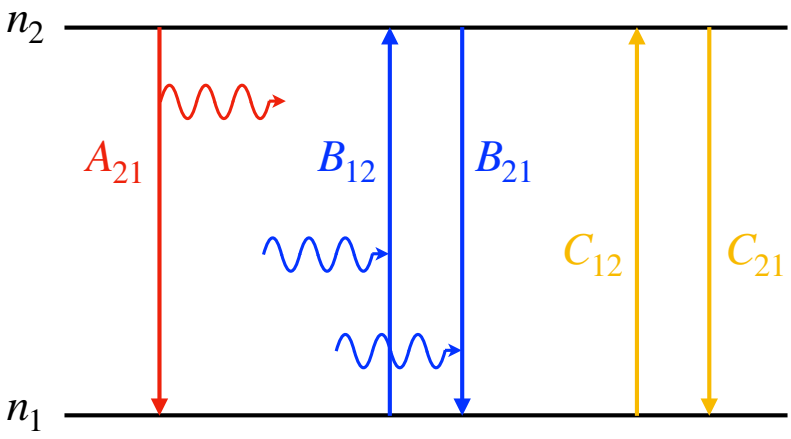

Figure 2.5: 2-level atom.

2.3.2 Absorption and stimulated emission

As already discussed, bound-bound absorption occurs when a photon with $\nu = \nu_{12}$ is absorbed and promotes an electron from level 1 to level 2. The probability of this happening is proportional to the density of incident photons with frequency ν_{12}. The *Einstein B coefficient* is defined such that the probability per unit time of excitation from level 1 to level 2 through photon absorption is

$$\text{Transition probability per second} = B_{12} \int_0^\infty u_\nu \, \phi(\nu) \, d\nu, \tag{2.12}$$

where the *line profile* $\phi(\nu)$ is a narrow function centred on ν_{12} and u_ν is the specific energy density defined last time. Since $\phi(\nu)$ is narrow, we can approximate it as a $\delta-$function so that the probability per unit time simply becomes $B_{12}u_{\nu_{12}}$.

An incident photon with frequency ν_{12} may, instead of being absorbed, increase the probability of an electron decaying from level 2 to level 1 though quantum mechanical effects. This is called *stimulated emission*: before the interaction, there is an incident photon with energy $h\nu_{12}$ and an electron with energy $E_1 + \Delta E_{12}$, after the transition there is still the initial photon, an electron with energy E_1 and a new photon with energy $h\nu_{12}$. Therefore, although the mechanism is rather counter-intuitive, we can at least appreciate that it conserves energy! The probability per second of stimulated emission is $B_{21}u_{\nu_{12}}$, where B_{12} is another Einstein coefficient (and we have again assumed a $\delta-$function line profile). The overall number density of electrons transitioning from level 1 to level 2 per second due to the incident photon field is therefore $u_{\nu_{12}}(n_1B_{12} - n_2B_{21})$, meaning that the luminosity *taken out* of the incident spectrum (i.e. the luminosity in the absorption line) is

$$L_{12} = h\nu_{12} \int_V u_{\nu_{12}} \left[n_1 B_{12} - n_2 \, B_{21} \right] \, dV. \tag{2.13}$$

2.3.3 Collisional Excitation and De-excitation

Bound electrons can also transition between energy levels when a free electron is *scattered* as it passes the atom. *Collisional excitation* occurs when the scattered electron gives up enough energy to excite an electron from level 1 to level 2, and *collisional de-excitation* occurs when the electron gains energy from the bound electron decaying from level 2 to level 1. Note, no photons are absorbed or emitted in this process, it is simply an exchange in energy between a free electron and a bound electron. The probability per second of collisional excitation or de-excitation is unsurprisingly proportional to the free electron density n_e – since the more free electrons there are, the greater the chance that one is going to scatter in the right way. The constants of proportionality are the *Einstein C coefficients*, C_{12} and C_{21}. Specifically, the rate of collisional de-excitations per unit volume is given by

$$R_{21} = n_e n_2 \int_0^\infty \sigma_{21}^{col}(v_e)\, v_e f(v_e)\, dv_e = n_e n_2 C_{21}, \tag{2.14}$$

where $\sigma_{21}^{col}(v_e)$ is the cross section and v_e is free electron velocity, which has a distribution given by the function $f(v_e)$. If the electrons are in thermal equilibrium (as will always be assumed to be the case in this course), then $f(v_e)$ is given by the Maxwellian distribution (Equation 1.14). It is useful to define the dimensionless *collision strength*, $\Omega_{21}(v_e)$:

$$\sigma_{21}^{col}(v_e) = \frac{h^2}{4\pi m_e^2 v_e^2} \frac{\Omega_{21}(v_e)}{g_2}, \tag{2.15}$$

where g_2 is the *statistical weight* of level 2 (you should have already covered this, but we will briefly summarise the most important atomic physics during the next lecture). Assuming a Maxwellian distribution, the C_{21} coefficient becomes

$$C_{21} = \left(\frac{2\pi\hbar^4}{k m_e^3}\right)^{1/2} \frac{T_e^{-1/2}}{g_2} \int_0^\infty \Omega_{21}(\Theta_e) \mathrm{e}^{-\Theta_e} d\Theta_e = 8.6 \times 10^{-12}\, \frac{\bar{\Omega}_{21}}{g_2}\, T_e^{-1/2}\ \mathrm{m}^3\ \mathrm{s}^{-1}, \tag{2.16}$$

where $\Theta_e \equiv m_e v_e^2/(2kT_e)$ is the kinetic energy of an electron as a fraction of kT_e. Here

$$\bar{\Omega}_{21} \equiv \int_0^\infty \Omega_{21}(\Theta_e) \mathrm{e}^{-\Theta_e} d\Theta_e \tag{2.17}$$

is the *Maxwellian averaged collision strength* – and this is a constant for a given transition.

Now what about the Einstein coefficient for collisional excitation, C_{12}? The equation for the excitation rate per unit volume has a similar form to that of the de-excitation rate, *except* only free electrons with kinetic energy $\geq \Delta E_{12}$ can excite bound electrons from level 1 to level 2. Therefore the rate per unit volume is

$$R_{12} = n_e n_1 \int_{\Delta E_{12}}^\infty \sigma_{12}^{col}(v_e)\, v_e f(v_e)\, dv_e = n_e n_1 C_{12}. \tag{2.18}$$

Again re-writing the cross section in terms of a collision strength

$$\sigma_{12}^{col}(v_e) = \frac{h^2}{4\pi m_e^2 v_e^2} \frac{\Omega_{12}(v_e)}{g_1}, \tag{2.19}$$

gives

$$C_{12} = 8.6 \times 10^{-12} \frac{\bar{\Omega}_{12}}{g_1} T_e^{-1/2} \, \mathrm{e}^{-\Delta E_{12}/kT_e} \, \mathrm{m}^3 \, \mathrm{s}^{-1}, \tag{2.20}$$

where the average collision strength is

$$\bar{\Omega}_{12} \equiv \int_0^\infty \Omega_{12}(\Theta_e + \Delta E_{12}/kTe) \, \mathrm{e}^{-\Theta_e} d\Theta_e. \tag{2.21}$$

Note that this is also a constant for a given transition.

2.4 Statistical Equilibrium

In statistical equilibrium, $dn_1/dt = 0 = dn_2/dt$. Therefore the number of electrons entering level 1 is equal to the number of electrons leaving level 1:

$$n_2 \, (A_{21} + u_{\nu_{12}} B_{21} + n_e C_{21}) = n_1 \, (u_{\nu_{12}} B_{12} + n_e C_{12}). \tag{2.22}$$

Statistical equilibrium will almost *always* hold – for example in stars and nebulae. From Equation (2.22), we can in principle calculate the relative populations of the two levels n_2/n_2, and from that ultimately calculate the luminosity of the emission line. In general this is fairly difficult, even for the two level atom, but in practice there are many situations in which we can make approximations and ignore terms in the above equation.

2.4.1 Thermodynamic equilibrium and Detailed balance

In *Thermodynamic equilibrium* (TE) (also known as *detailed balance*), all atomic processes (excitation vs de-excitation and ionisation vs recombination) are exactly balanced by their thermodynamically inverse process. This means that the rate of de-excitations via spontaneous decay is equal to that of excitations via absorption minus de-excitations via stimulated emission. For this condition to hold, the radiation field must be isotropic (i.e. in thermal equilibrium with itself). TE also means that the collisional excitation and de-excitation rates are balanced. For this condition to hold, the free electron population must be in thermal equilibrium, i.e. $v_e f(v_e)$ is a Maxwellian distribution. If both of these conditions are met, the radiation field is *also* in equilibrium with the particles so the radiation temperature is equal to the electron temperature, $T = T_e$. Therefore, in TE, the radiation field is a blackbody: $I_\nu = B_\nu$. This is a limit you have met before; for example it can be used to derive the Saha equation describing ionization balance in the core of stars.

From the above equation of statistical equilibrium (equation 2.22), we can see that in TE we have

$$n_2 \, (A_{21} + u_{\nu_{12}} B_{21}) = n_1 \, u_{\nu_{12}} B_{12} \tag{2.23}$$

and

$$n_2 \, C_{21} = n_1 \, C_{12}. \tag{2.24}$$

In previous courses, you have learned that the population of electron energy levels in TE is described by the *Boltzmann distribution*:

$$\frac{n_2}{n_1} = \frac{g_2}{g_1} \exp\left(-\frac{h\nu_{12}}{kT_e}\right), \tag{2.25}$$

where g_i is again the statistical weight – or *degeneracy* – of energy level i. We can use the limit of TE to derive the relation between the average collision strengths $\bar{\Omega}_{12}$ and $\bar{\Omega}_{21}$. From before (Equations 2.16 and 2.20), we know that

$$\frac{C_{12}}{C_{21}} = \frac{g_2}{g_1} \frac{\bar{\Omega}_{12}}{\bar{\Omega}_{21}} \exp\left(-\frac{h\nu_{12}}{kT_e}\right). \tag{2.26}$$

This equation is true in general. In the case of TE, since we have detailed balance and the electron levels are described by the Boltzmann distribution, we also have the relation:

$$\frac{C_{12}}{C_{21}} = \frac{n_2}{n_1} = \exp\left(-\frac{h\nu_{12}}{kT_e}\right), \tag{2.27}$$

therefore we see that $\bar{\Omega}_{12} = \bar{\Omega}_{21}$. Note that $\bar{\Omega}_{12}$ and $\bar{\Omega}_{21}$ are *constants*, and therefore they are equal to each other regardless of TE, we have just used the limit of TE to derive the relation between them. From now on, we will simply start referring to $\bar{\Omega}_{12}$ as the collision strength and drop the bar.

The conditions for TE are often not met. For example, the photosphere of a star is defined as the region where photons can first escape freely into space. Once photons can escape, the conditions for TE are not strictly met (since TE is achieved by every photon having many collisions before it leaves the medium and therefore sharing its energy with the electrons – in other words, the medium must be optically thick). However, the concept of local thermodynamic equilibrium (LTE) can be used. This holds providing the conditions in the absorbing/emitting medium do not change significantly over the course of the photon mean free path. There are many situations in which we cannot even use LTE: for instance the region above the photosphere in stars (the *chromosphere*), in which $T_e >> T$ (here T_e is the temperature of the electrons in the chromosphere, but T is the temperature of the photons streaming out of the photosphere – because the chromosphere is optically thin, photons from the photosphere do not have enough interactions in the photosphere to adjust to the new, higher electron temperature). We are very much interested in these situations in this course, since this is when we get emission and absorption lines in the spectrum!

2.4.2 Weak radiation field

If the radiation field is weak ($B_{21}u_\nu << n_eC_{21} + A_{21}$ and $B_{12}u_\nu << n_eC_{12}$), the equation of statistical equilibrium simplifies to

$$n_2 \left(A_{21} + n_eC_{21}\right) = n_1 \ + n_eC_{12}. \tag{2.28}$$

This is a very good approximation if we have strong emission lines (e.g. in nebulae), since in this case we know $L_{21} >> L_{12}$, and so

$$n_2 A_{21} >> [n_1 B_{12} - n_2 B_{21}] u_{\nu_{12}}. \tag{2.29}$$

Typically $n_1 B_{12} >> n_2 B_{21}$, and so the limit of weak radiation field is justified for an emission line region.

The Coronal Approximation

If the radiation field is weak and the density is not too high (e.g, in the upper chromosphere and corona in the sun where $n_e \lesssim 10^{18}\mathrm{m}^{-3}$, $n_e C_{21} << A_{21}$) we can make the *coronal approximation*:

$$\frac{n_2}{n_1} = C_{12} \frac{n_e}{A_{21}} \tag{2.30}$$

In the coronal approximation, the dominant processes are collisional excitation and spontaneous emission. This does not give detailed balance as $n_e C_{12}$ and A_{21} are not thermodynamically inverse processes. Note that in this case, n_2/n_1 is *not* given by the Boltzmann distribution (but we can still use $\Omega_{12} = \Omega_{21}$).

In the coronal approximation, the emission line luminosity L_{21} becomes

$$L_{21} = h\nu_{12} \int_V n_2 A_{21} dV = h\nu_{12} \int_V n_1 \, n_e \, C_{12} dV, \tag{2.31}$$

so that whenever the coronal approximation applies (most UV and X-ray lines as it turns out), the emitted line flux depends on the collision rate rather than the spontaneous emission coefficient.

Critical Density

The coronal approximation is applicable if $n_e C_{21} << A_{21}$. We can therefore define a *critical density*

$$n_e^* = \frac{A_{21}}{C_{21}}. \tag{2.32}$$

Therefore:

If $n_e << n_e^*$: collisional excitation is unimportant (coronal approximation)

If $n_e >> n_e^*$: the level populations are set by the C terms.

Adam Ingram

3 Emission Line diagnostics: 2 level atom

3.1 Introduction

In the last lecture, we solved the radiative transfer equation to see intuitively when we may expect emission or absorption lines in the spectrum, before studying statistical equilibrium in a two level atom. In this lecture, we will use our model of the two level atom to measure atomic abundances in astrophysical objects using emission line fluxes. In order to do this though, we must first quickly revise everything we need to know about atomic physics. There should be nothing new here, but it is important to summarise in the interest of being self-contained.

3.2 Atomic physics revision

3.2.1 Occupation rules

The occupation rules are set by the Pauli exclusion principle: no two electrons can be in exactly the same state. The electron state is set by quantum numbers: n = the principle quantum number, ℓ = the azimuthal quantum number, and s = the electron spin quantum number. The azimuthal quantum number can only take values

$$0 \leq \ell < n.$$

Therefore each *shell* (i.e. a given value of n) can have n *sub-shells* (i.e. given values of ℓ). A sub-shell contains electrons with different values of the *magnetic quantum number*, m_ℓ, which can take the values

$$|m_\ell| \leq \ell,$$

and different values of m_s, which is also called the spin quantum number and can take the values

$$|m_s| \leq s.$$

Therefore the number of electron states in a sub-shell is

$$\text{Sub} - \text{shell degeneracy} = (2s+1)(2\ell+1),$$

with each electron having a different combination of m_s and m_ℓ quantum numbers (a combination of the ℓ and s quantum numbers is also referred to as a *term*). Since there are n sub-shells in a shell, we know that the number of electron states in a shell must be

$$\text{Shell degeneracy} = \sum_{\ell=0}^{n-1}(2s+1)(2\ell+1) = (2s+1)\sum_{\ell=0}^{n-1}(2\ell+1) = (2s+1)n^2.$$

We can further split a sub-shell with the *total angular momentum* quantum number, j, which can take the values

$$|\ell - s| \leq j \leq |\ell + s|,$$

in integer steps. Similar to above, we can define a further quantum number m_j, which can take the values

$$|m_j| \leq j, \tag{3.1}$$

meaning that for a given value of j there are $(2j + 1)$ possible states. Therefore the number of states per term must be

$$\text{Sub} - \text{shell degeneracy} = \sum_{j=|\ell-s|}^{|\ell+s|} (2j + 1).$$

This *has* to be equal to $(2s + 1)(2\ell + 1)$ because we already showed that this is the degeneracy of a sub-shell (term). The easiest way to satisfy ourselves of this is by using an example; e.g. $\ell = 1$, $s = 1/2$. In this case, we see that $(2s + 1)(2\ell + 1) = 6$, and the same value of 6 is returned by the above equation.

3.2.2 Nomenclature

It is traditional (and, yes I know, not discernibly sensible) to symbolically represent $\ell = 0, 1, 2, 3, 4, \ldots$ sub-shells with the letters s, p, d, f, g, and so on in alphabetical order. For instance a sub-shell with $n = 1$ and $\ell = 0$ can be referred to as a $1s$ sub-shell. We can represent all of the possible states for a given element in this way. For instance, phosphorus (atomic number 15) is: 1s,2s,2p,3s,3p. From the above selection rules, and given that $s = 1/2$, we can calculate that these sub-shells respectively contain 2, 2, 6, 2 and 6 possible electron states. Altogether this is 18, but phosphorus only has 15 electrons. Therefore the final sub-shell only contains 3 electrons when the maximum would be 6. We can also label as a subscript how many electrons are actually *occupying* the levels. Again for the case of phosphorus, this gives $1s^2, 2s^2, 2p^6, 3s^2, 3p^3$.

Another way to label electron levels is using a *term symbol*:

$$n^{(2s+1)}L_j. \tag{3.2}$$

Here n, s and j are the same quantum numbers described above and L is replaced by a capital letter representing the quantum number ℓ; i.e. $\ell = 0, 1, 2, 3, 4$ is now represented by $L = S, P, D, F, G$. Therefore an electron with $n = 2$, $\ell = 1$, $s = 1/2$ and $j = 1/2$ would be labeled as $2^2P_{1/2}$. The n value is often missed from the start.

3.2.3 Energy levels

The ionization potential of a bound electron depends most sensitively on the principle quantum number. For example, in Hydrogen, the ionization potential energy is to a good approximation

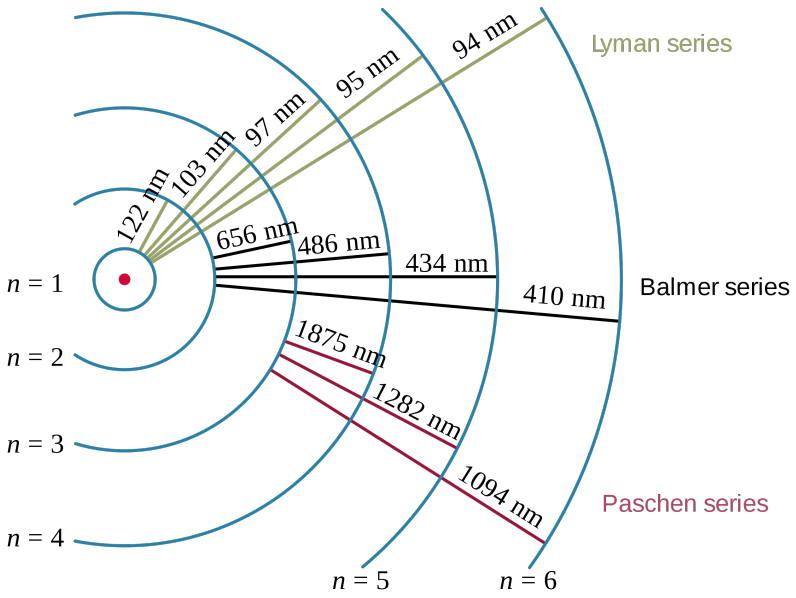

Figure 3.1: Energy levels of the hydrogen atom (from https://commons.wikimedia.org/w/index.php?curid=6273602).

$E_n \approx -13.6\ \text{eV}/n^2$. Fig 3.1 illustrates the $n = 1$ to $n = 6$ shells in a hydrogen atom. Transitions between two levels are all part of named series: transitions to or from $n = 1$ are part of the *Lyman series*, transitions to or from $n = 2$ are part of the *Balmer series* and transitions to or from $n = 3$ are part of the *Paschen series*. Not shown are the *Brackett* ($n = 4$), *Pfund* ($n = 5$) and *Humphreys* ($n = 6$) series. The wavelength of the emission line caused by electrons decaying from the higher level to the lower level is shown (this is of course also the wavelength of absorption lines due to electrons being excited from the lower to the higher level). All transitions in the Lyman series have their own names: the transitions between $n = 1$ and $n = 2$, 3 and 4 are called respectively Lyman α (L_α, line wavelength 122 nm), Lyman β (L_β, line wavelength 103 nm), and Lyman γ (L_γ, line wavelength 97 nm) – and so on alphabetically. Similarly for the Balmer series, the transitions between $n = 2$ and $n = 3$, 4 and 5 are respectively H_α (656 nm), H_β (486 nm), H_γ (434 nm), and again so on alphabetically.

However, spin-orbit coupling – an interaction between the electron orbital angular momentum and the electron spin angular momentum – means that the energy level associated with each value of n is split, such that the state with the higher j value has a slightly higher (less negative) energy. This is called *fine structure splitting*, and it is illustrated in Fig 3.2. Here we see that there is no fine structure splitting in the $n = 1$ level, because there is only one possible value of j according to the occupation rules: $j = 1/2$. However, there *is* splitting of the $n = 2$ level, between $j = 3/2$ and $j = 1/2$. The splitting is very small: whereas the L_α transition from $n = 2$ to $n = 1$ is 10.2 eV, the energy difference between $j = 3/2$ and $j = 1/2$ levels within the $n = 2$

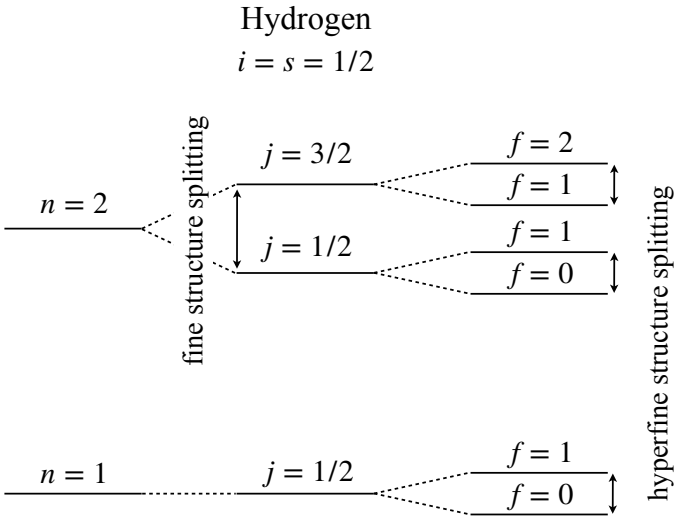

Figure 3.2: Fine and hyperfine structure splitting in the lowest two levels of the hydrogen atom.

shell is only $\sim 4.5 \times 10^{-5}$ eV. Still, this means that the Lyman α line is a very closely spaced doublet, although very good resolution is required to see this. As is also shown in Fig 3.2, these energy levels modified by fine structure splitting are further split themselves. This is known as *hyperfine structure splitting*, and it results from the interaction between the electron spin angular momentum and the nuclear spin angular momentum. Representing the nuclear spin angular momentum with the quantum number i, the hyperfine splitting level depends on the quantum number f, which can take the values $f = |j - i|$ to $|j + i|$ in integer steps. Hyperfine structure splitting is an even smaller effect than fine structure splitting, with the $n = 1$ transition from $f = 1$ to $f = 0$ having an energy difference of $\sim 5.9 \times 10^{-6}$ eV. This corresponds to a frequency of 1420 MHz and a wavelength of 21 cm. This 21 cm line can be seen both in emission and absorption by radio telescopes, and provides an important astrophysical diagnostic (although regrettably there will be no time to cover it in detail during this course).

3.2.4 Selection Rules

The selection rules determine which electric dipole transitions are possible (*allowed transitions*) and which are not (*forbidden transitions*). The physics of the selection rules is very much not our concern here, and so I will skip over a *lot* of detail to say that allowed transitions have: $\Delta j = 0, \pm 1$ (but no $j = 0$ to $j = 0$ transitions) and $\Delta m_j = 0, \pm 1$. There are also *semi-forbidden* transitions that obey the other selection rules but have $\Delta s \neq 0$. However, electric dipole interaction with light is merely a first-order approximation, and therefore forbidden transitions *may* be permitted

by higher order effects such as electric quadropole or magnetic dipole interactions. Because they are higher order, they are less likely than permitted transitions and therefore have much lower Einstein A coefficients. However, if a system is excited into a state whereby the only means of decaying is via a forbidden transition, this will eventually occur. For our purposes, all we really care about is that an allowed transition has a large Einstein A coefficient and a forbidden transition has a small Einstein A coefficient. As an example, the hyperfine structure transition is forbidden, and it's associated Einstein A coefficient is $\sim 3 \times 10^{-15} \mathrm{s}^{-1}$, compared to the A coefficient for the Lyman α line of $\sim 6.3 \times 10^{8} \mathrm{s}^{-1}$!

3.2.5 Nomenclature of spectral lines

As the final bit of nomenclature before going on to do something more interesting, we must define our labelling convention for spectral lines. Fig 3.3 shows a composite spectrum of 2,200 quasars, showing a number of lines. We see L_α and H_α here, but also a number of other lines. These lines are all labelled with the atomic symbol of the atom they originate from and a Roman numeral to denote the ionization state: I is neutral, II once ionized, III twice ionized and so on. Therefore OII is O^{1+} and OIII is O^{2+}. Note that the actual transition that caused the line is not labelled, only the ionic species of the element. Lines with no square brackets are allowed lines, lines with two square brackets are forbidden lines, and one bracket means semi-forbidden. Therefore, e.g., CIV is allowed, [OIII] forbidden and CIII] semi-forbidden.

3.3 Measuring Elemental Abundances with a 2 level Atom Model

An atom with a split ground state and a large interval to the next available energy level can be well approximated as a 2-level atom, providing the electron temperature is not so high that a significant number of electrons populate the next level (which is very reasonable since the temperature would have to be extremely high for this). The neutral halogens are good examples of such atoms: e.g. FI and ClI and ions in their isoelectronic sequence, e.g. NeII and ArII. Lines from the transition between the split ground state level are in the infrared (IR), and their flux is given by

$$F_{21} = \frac{h\nu_{12}}{4\pi d^2} \int_V n_2 A_{21} \, dV, \tag{3.3}$$

assuming isotropic emission. Assuming a uniform density, we can simplify to $F_{21} = h\nu_{12} \, V \, n_2 \, A_{21}/(4\pi d^2)$, which we can re-arrange to estimate the mass of ions in the upper fine structure level from a measured emission line flux:

$$M_2 = m_a \, n_2 \, V = \frac{m_a \, F_{21} \, 4\pi d^2}{h\nu_{12} \, A_{21}}, \tag{3.4}$$

where m_a is the mass of the atom.

In order to estimate the total mass of a given ionic species, we must also calculate the mass of ions in the lower state, M_1, and add to M_2 (i.e. we are assuming that, at this T_e, the number

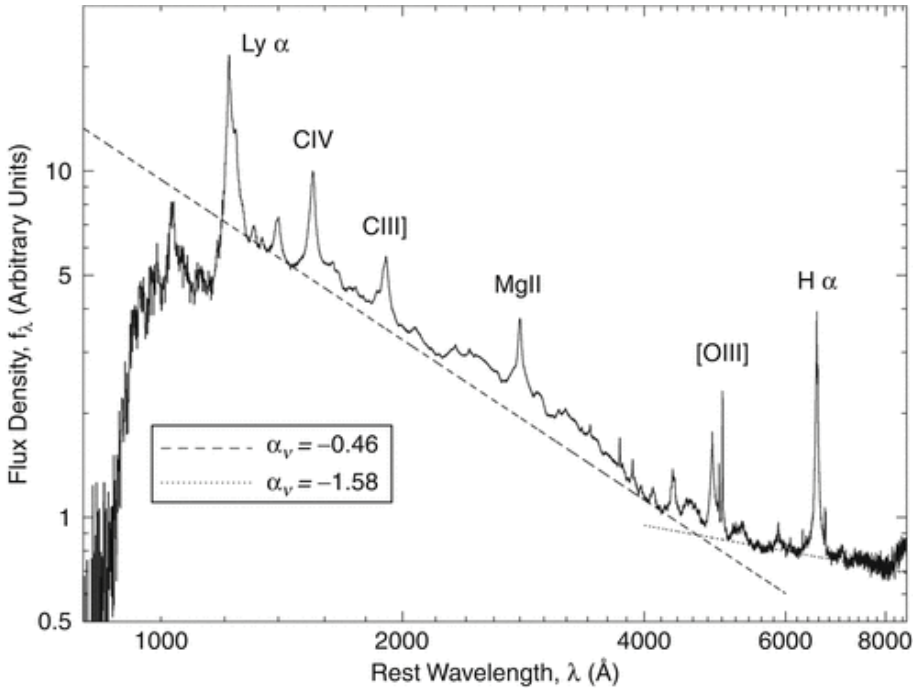

Figure 3.3: Composite quasar spectrum, constructed from over 2,200 quasars in the Sloan Digital Sky Survey data release 1. The dotted line indicates power law fits to the estimated continuum spectrum (From Perlman E.S. (2013) Active Galactic Nuclei; originally from Van den Berk et al. 2001).

of electrons in higher levels is negligible). In order to determine the fraction of electrons in the upper level, we must return to the equation of statistical equilibrium in a weak radiation field. The key question is: is the density above or below the critical density $n_e^* = A_{21}/C_{21}$? Well, fine structure transitions are forbidden and therefore A_{21} is small ($< 10^{-2}\mathrm{s}^{-1}$), meaning that the critical density can be quite low for electron temperatures typical of e.g. a planetary nebula, $n_e^* \sim 10^5 - 10^7\mathrm{cm}^{-3}$. Therefore, we can often assume that $n_e >> n_e^*$, and therefore that the equation of statistical equilibrium reduces to: $n_2 C_{21} = n_1 C_{21}$ – i.e. the population levels are set by the C coefficients, which we know are related by

$$\frac{C_{12}}{C_{21}} = \frac{g_2}{g_1} \exp\left(-\frac{h\nu_{12}}{kT_e}\right), \tag{3.5}$$

and therefore we know that:

$$\frac{n_2}{n_1} = \frac{g_2}{g_1} \exp\left(-\frac{h\nu_{12}}{kT_e}\right). \tag{3.6}$$

Now, we know that $h\nu_{12}$ is very small, and so we can either assume $h\nu_{12} << kT_e$, giving

$$\frac{n_2}{n_1} \approx \frac{g_2}{g_1}, \tag{3.7}$$

or use some reasonable estimate of T_e, safe in the knowledge that n_2/n_1 is only weakly dependent on T_e in this limit.

If we are instead in the low density limit ($n_e << n_e^*$), then statistical equilibrium becomes $n_2 A_{21} = n_1 n_e C_{12}$ and we can express C_{12} in therms of the collision strength to get

$$\frac{n_2}{n_1} = 8.6 \times 10^{12} \frac{n_e \Omega_{12}}{g_1 A_{21} T_e^{1/2}} \exp\left(-\frac{h\nu_{12}}{kT_e}\right). \tag{3.8}$$

Therefore, in the low density regime, the level populations depend on both electron density and temperature, whereas in the high density regime the level populations are independent of n_e and depend only weakly on T_e.

In general, IR lines are advantageous for a number of reasons:

- IR lines are relatively immune to the effects of interstellar extinction, which falls steeply as a function of wavelength, and so they can probe regions that are invisible at optical wavelengths or where only the front, lightly obscured regions are detected. They sample the whole volume of a nebula except for the densest, most obscured objects.
- They provide some diagnostics of species that usually have weak or nonexistent transitions at other wavelengths (e.g. Ne II).
- As we have just seen, the ground state fine-structure lines are insensitive to n_e.

However, IR observations have their challenges: ground based observations are hampered by the large thermal background and molecular absorption by the Earth's atmosphere. Space telescopes such as Spitzer, AKARI, Herschel and JWST circumvent these problems.

3.3.1 Example - Supernova 1987A

SN1987A exploded in the Large Magellanic Cloud (LMC) in February 1987. Because it was in the LMC, it's distance was well determined to 50 kpc. This was the first supernova visible to the naked eye in ~ 400 years! Because it was very bright and had a well determined distance, it could be studied in great detail. Roche, Aitken & Smith (1993), amongst other things, were able to estimate the mass of a number of ionic species of a number of elements in the ejecta using forbidden IR lines. Fig 3.4 shows the IR spectrum evolving in time. Early after the explosion, everything was completely optically thick and so no lines were seen. Eventually, lines became observable as the outer shell became optically thin. For example, very strong emission lines are observed on day 465 since the explosion, two of which are [Cl I] at 11.3 μm and [Ne II] at 12.8 μm. These are both the sort of IR fine structure lines that can be treat with our 2-level atom model in the $n_e > n_e^*$ regime. Starting from Equation (3.4), we can adopt a distance of $d = 50$ kpc in order to write a formula for the mass of ions in the upper state

$$\frac{M_2}{M_\odot} = 1.25 \times 10^{11}\ \mathrm{kg^{-1}m^{-1}s^2}\ F_{21}\ A_m\ \frac{\lambda_{21}}{A_{21}}, \tag{3.9}$$

where A_m is the mass number (i.e. $m_a = 1.66 \times 10^{-27} A_m$ kg). The day 465 12.8 μm [Ne II] line strength was $F_{21} = 4.1 \times 10^{-14}\mathrm{Wm^{-2}}$, the mass number of neon is $A_m = 20$ and the transition probability is $A_{21} = 9.5{\times}10^{-3}\ \mathrm{s^{-1}}$. Using an estimated electron temperature of $T_e = 3200$ K on day 456, and using the ratio of statistical weights $g_1/g_2 = 2$ gives $M_1/M_2 = g_1/g_2 \exp(h\nu/kT_e) = 2.84$. Therefore the total mass of singly ionized neon is $M_1 + M_2 = 5.3 \times 10^{-4}\ M_\odot$. Using exactly the same reasoning, the mass of neutral Chlorine can be estimated from: $A_{21} = 1.24 \times 10^{-2}\mathrm{s^{-1}}$, $A_m = 35.45$, $F_{21} = 2.7 \times 10^{-14}\mathrm{Wm^{-2}}$, $g_1/g_2 = 2$ to get $M = 3.6 \times 10^{-4}\ M_\odot$.

By tracking how the line strengths evolved with time, it was possible to see the evolution of the abundances of different ionic species of elements and compare with models for the ionization balance and radioactive decay of cobalt and Nickel as the supernova ejecta expanded and cooled.

3.3.2 Relative abundances

Often we don't know the distance and so we can't estimate the mass of different ionic species. We can however estimate *relative* abundances by comparing line strengths of different ions.

Adam Ingram

524 *P. F. Roche, D. K. Aitken and C. H. Smith*

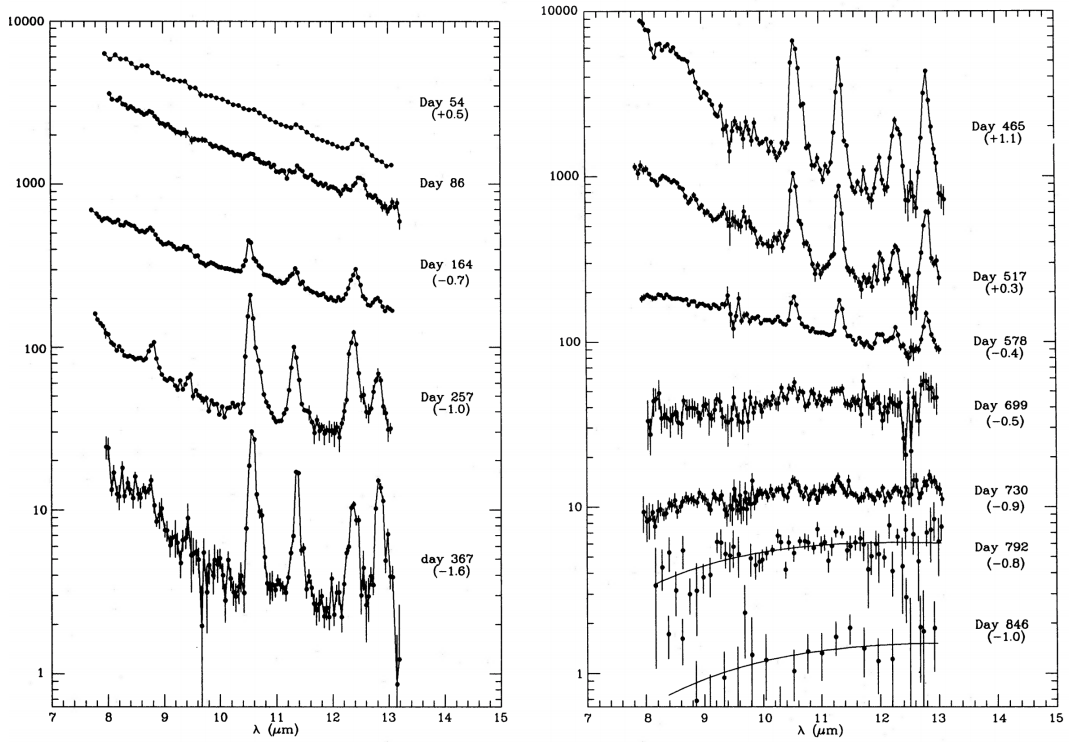

Figure 1. Spectra at 8–13 μm of SN 1987A. Error bars shown are 1 standard deviation of the mean and the flux is in units of 10^{-18} W cm^{-2} μm^{-1}. The logarithmic displacements of the spectra are given in brackets.

Figure 3.4: IR spectra of supernova 1987A.

4 Emission Line diagnostics: 3 level atom

4.1 Introduction

Last time we investigated the diagnostics accessible with a 2 level atom model. However, in a two level atom, there is only one emission line per atom/ion. Diagnostics of properties such as electron density and temperature rely on comparing fluxes of different lines from the *same* atom. In order for there to be more than one line, the atom needs to have at least three levels, and so we must extend our simple 2 level atom model to a three level model.

4.2 3 Level Atom

Fig 4.1 shows a sketch of a 3 level atom. Now statistical equilibrium becomes two equations:

$$\text{Electrons leaving level 3} = \text{Electrons entering level 3}, \tag{4.1}$$

and

$$\text{Electrons leaving level 2} = \text{Electrons entering level 2}. \tag{4.2}$$

In general, these equations are:

$$n_3[A_{32} + u_\nu B_{32} + n_e C_{32} + A_{31} + u_\nu B_{31} + n_e C_{31}] = n_1[u_\nu B_{13} + n_e C_{13}] + n_2[u_\nu B_{23} + n_e C_{23}], \tag{4.3}$$

and

$$n_2[A_{21} + u_\nu B_{21} + n_e C_{21} + u_\nu B_{23} + n_e C_{23}] = n_1[u_\nu B_{12} + n_e C_{12}] + n_3[A_{32} + u_\nu B_{32} + n_e C_{32}]. \tag{4.4}$$

By solving these equations, we can calculate line ratios, F_{32}/F_{31} or F_{31}/F_{21}. Clearly this is a fairly difficult problem in general, but we can often consider limits of the above equations in which a few terms dominate over the others. In particular, we will continue to consider cases with a weak radiation field (e.g. nebulae), in which we can ignore the B coefficients. The line ratio then depends on known quantities such as the A coefficients and the collision strengths, *and* two properties of the nebula: n_e and T_e. The trick is then to find particular atoms/ions in which the above equations are in a limit in which the dependence on n_e or T_e is weak for a typical nebula ($n_e \lesssim 10^{10}$ m^{-3} and $T_e \sim 10^4$ K). In this way, we can measure the temperature and density of nebulae from their emission lines.

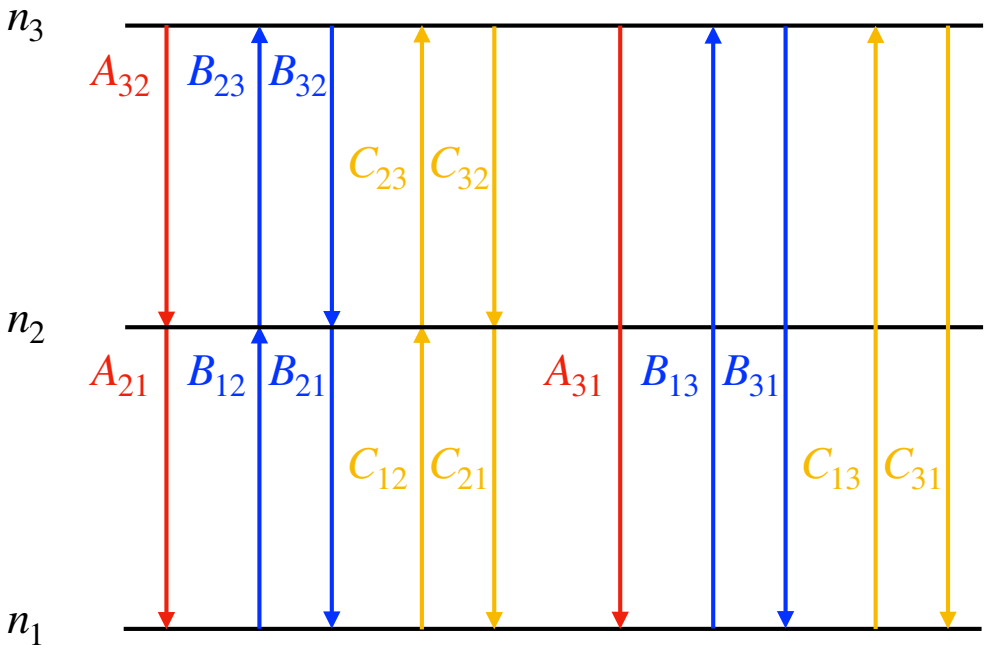

Figure 4.1: Sketch of a three level atom.

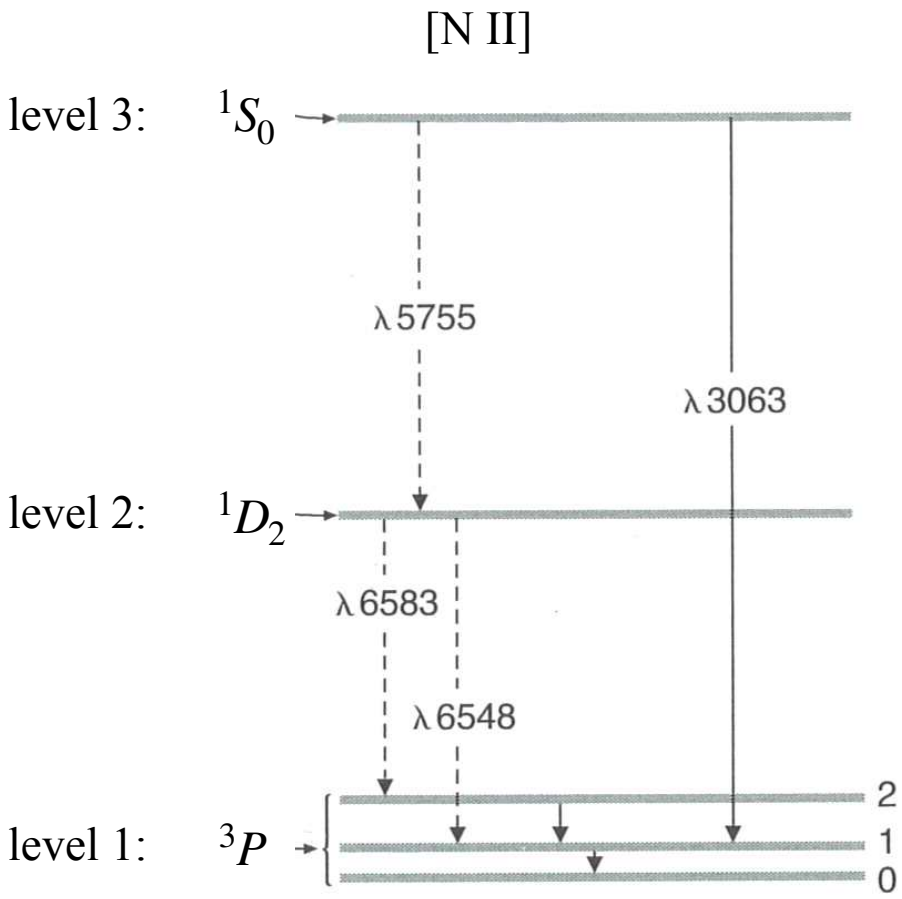

Figure 4.2: Energy levels of N II. The bottom level is split onto 3, but can be approximated as one level. Adapted from Osterbrock & Ferland, 'Astrophysics of Gaseous Nebulae and Active Galactic Nuclei' (Fig 3.1 on pg 59).

Table 3.12
Transition probabilities for C-like $2p^2$ and Si-like $3p^2$ ions

	[N II]		[O III]		[Ne V]		[S III]		[Ar V]	
Transition	A (s^{-1})	λ (Å)	A (s^{-1})	λ (Å)	A (s^{-1})	λ (Å)	A (s^{-1})	λ (Å)	A (s^{-1})	λ (Å)
$^1D_2$–$^1S_0$	1.0	5754.6	1.6	4363.2	2.8	2972.8	2.3	6312.0	3.5	4625.3
$^3P_2$–$^1S_0$	1.3×10^{-4}	3070.8	6.1×10^{-4}	2331.4	6.3×10^{-3}	1593.3	1.3×10^{-2}	3797.2	6.8×10^{-2}	2786.0
$^3P_1$–$^1S_0$	3.3×10^{-2}	3062.8	2.3×10^{-1}	2321.0	4.0	1574.6	8.4×10^{-1}	3721.7	6.7	2691.0
$^3P_2$–$^1D_2$	3.0×10^{-3}	6583.4	2.0×10^{-2}	5006.9	3.5×10^{-1}	3425.9	5.5×10^{-2}	9531.0	4.7×10^{-1}	7005.9
$^3P_1$–$^1D_2$	9.8×10^{-4}	6548.0	6.8×10^{-3}	4958.9	1.2×10^{-1}	3345.9	2.1×10^{-2}	9068.9	2.0×10^{-1}	6435.1
$^3P_0$–$^1D_2$	3.6×10^{-7}	6527.1	1.7×10^{-6}	4931.1	1.9×10^{-5}	3300.5	1.3×10^{-5}	8829.9	6.1×10^{-5}	6133.8
$^3P_1$–$^3P_2$	7.5×10^{-6}	121.89 μm	9.7×10^{-5}	51.814 μm	4.6×10^{-3}	14.32 μm	2.1×10^{-3}	18.713 μm	2.7×10^{-2}	7.9 μm
$^3P_0$–$^3P_2$	1.1×10^{-12}	76.5 μm	3.1×10^{-11}	32.661 μm	5.0×10^{-9}	9.01 μm	4.3×10^{-8}	12.00 μm	1.2×10^{-6}	4.9 μm
$^3P_0$–$^3P_1$	2.1×10^{-6}	205.5 μm	2.7×10^{-5}	88.356 μm	1.3×10^{-3}	24.28 μm	4.7×10^{-4}	33.47 μm	8.0×10^{-3}	13.1 μm
$^3P_2$–$^5S_2^o$	$1.3 \times 10^{+2}$	2142.8	$5.8 \times 10^{+2}$	1666.2	$6.0 \times 10^{+3}$	1146.1	1.2×10^{4}	1728.9	—	—
$^3P_1$–$^5S_2^o$	$5.5 \times 10^{+1}$	2139.0	$2.4 \times 10^{+2}$	1660.8	2.4×10^{3}	1137.0	4.4×10^{3}	1713.1		

C-like: Galavis, M. E., Mendoza, C., & Zeippen, C. J. 1997, A&AS, 123, 159; Mendoza, C., Zeippen, C. J., & Storey, P. J. 1999, A&AS, 135, 159; Storey, P. J. & Zeippen, C. J. 2000, MNRAS, 312, 813; Si-like: Tayal, S. S. 1997, ADNDT, 67, 331; Biemont, E., & Bromage, G. E. 1983, MNRAS, 205, 1085.

Figure 4.3: Transitional probabilities of N II and other similar ions. From Osterbrock & Ferland, 'Astrophysics of Gaseous Nebulae and Active Galactic Nuclei' (Table 3.12 on pg 56).

4.3 Temperature diagnostics

Ions that can be modelled as a 3 level atom, emit optical/UV lines and have very high critical densities for all transitions turn out to have F_{32}/F_{31} line ratios that only really depend on T_e and not on n_e. [OIII] and [NII] lines are classic examples. Fig 4.2 shows the energy levels of [NII]. The most prominent transitions are shown. Any transitions not labelled have very low Einstein A coefficients (see the table in Fig 4.3). We see that there are actually 5 levels here, but we can treat the split ^3P level as a single level. In order to do this, we just need to sum up all the spontaneous emission coefficients of transitions that end up in the ^3P level to get A_{31} and A_{21}. The statistical weight of the ^3P level is just given by $g = (2s + 1)(2\ell + 1)$. Alternatively, we can add up the degeneracy of each of the three sub-levels, $(2j + 1)$. Of course we get the same answer either way: $g_1 = 9$. Instead of a single F_{21} line, we will see a doublet if we can resolve it: one at 658.3 nm and the other at 654.8 nm. We simply need to sum up the fluxes from these lines: $F_{21} = F_{658.3\text{nm}} + F_{654.8\text{nm}}$. The flux ratio is:

$$\frac{F_{32}}{F_{21}} = \frac{F_{575.5\text{nm}}}{F_{658.3\text{nm}} + F_{654.8\text{nm}}} = \frac{n_3 A_{32} h\nu_{23}}{n_2 A_{21} h\nu_{12}} = \frac{n_3 A_{32} \lambda_{12}}{n_2 A_{21} \lambda_{23}}. \tag{4.5}$$

Since the radiation field is weak, the equations of statistical equilibrium are:

$$n_3[A_{31} + A_{32} + n_e C_{31} + n_e C_{32}] = n_e[n_1 C_{13} + n_2 C_{23}], \tag{4.6}$$

and:

$$n_2[A_{21} + n_e C_{23} + n_e C_{21}] = n_e[n_1 C_{12} + n_2 C_{32}]. \tag{4.7}$$

The gaps between energy levels are fairly large compared with kT_e, so $n_3 << n_2 << n_1$, and we can simplify to:

$$n_3[A_{31} + A_{32} + n_e C_{31} + n_e C_{32}] = n_e n_1 C_{13}, \tag{4.8}$$

Collision strengths Υ for C-like $2p^2$, O-like $2p^4$, Si-like $3p^2$ and S-like $3p^4$ ions

Ion	^3P, ^1D	^3P, ^1S	^1D, ^1S	$^3P_0$, $^3P_1$	$^3P_0$, $^3P_2$	$^3P_1$, $^3P_2$	^3P, $^5S^o$
N^+	2.64	0.29	0.83	0.41	0.27	1.12	1.27
O^{+2}	2.29	0.29	0.58	0.55	0.27	1.29	0.18
Ne^{+4}	2.09	0.25	0.58	1.41	1.81	5.83	1.51
Ne^{+2}	1.36	0.15	0.27	0.24	0.21	0.77	—
S^{+2}	6.95	1.18	1.38	3.98	1.31	7.87	2.85
Ar^{+4}	3.21	0.56	1.65	2.94	1.84	7.81	—
Ar^{+2}	4.83	0.84	1.22	1.26	0.67	3.09	—

N^+, O^{+2}, and Ne^{+4} from Lennon, D. J., & Burke, V. M. 1994, A&AS, 103, 273; Ne^{+2} from Butler, K., &

Figure 4.4: Collision strengths of N II and other similar ions. From Osterbrock & Ferland, 'Astrophysics of Gaseous Nebulae and Active Galactic Nuclei' (Table 3.6 on pg 53).

and:

$$n_2[A_{21} + n_e C_{21}] = n_e n_1 C_{12}. \tag{4.9}$$

I said that the critical density is large, meaning that we will be able to use the coronal approximation. In order to show that, we need the values for the spontaneous emission coefficients (Fig 4.3) and the collision strengths (Fig 4.4). From this, we can see that for [NII]:

$$A_{32} = A(^1S_0 \rightarrow ^1D_2) = 1 \text{ s}^{-1}, \tag{4.10}$$
$$A_{31} = A(^1S_0 \rightarrow ^3P_0) + A(^1S_0 \rightarrow ^3P_1) + A(^1S_0 \rightarrow ^3P_2) \approx 3.3 \times 10^{-2} \text{ s}^{-1} \tag{4.11}$$
$$A_{21} = A(^1D_2 \rightarrow ^3P_0) + A(^1D_2 \rightarrow ^3P_1) + A(^1D_2 \rightarrow ^3P_2) \approx 4 \times 10^{-3} \text{ s}^{-1}, \tag{4.12}$$

and:

$$\Omega_{23} = \Omega(^1D, ^1S) = 0.83 \tag{4.13}$$
$$\Omega_{13} = \Omega(^3P, ^1S) = 0.29 \tag{4.14}$$
$$\Omega_{12} = \Omega(^3P, ^1D) = 2.64. \tag{4.15}$$

Finally, note that the statistical weights are $g_1 = 9$, $g_2 = 5$, $g_3 = 1$. As an example, the critical density for the $2 \rightarrow 1$ transition is:

$$n_e^* = \frac{A_{21}}{C_{21}} = \frac{4 \times 10^{-3}}{8.6 \times 10^{-12}(\Omega_{12}/g_2)T_e^{-1/2}}. \tag{4.16}$$

For $T_e = 10^4$ K, this gives $n_e^* \approx 9 \times 10^{10}$ m^{-3}. This is larger than the density of a typical nebula and so we can indeed employ the coronal approximation to get:

$$n_3[A_{31} + A_{32}] = n_e\, n_1\, C_{13}, \tag{4.17}$$
$$n_2 A_{21} = n_e n_1 C_{12}. \tag{4.18}$$

Therefore the energy level population ratio is

$$\frac{n_3}{n_2} = \frac{C_{13}A_{21}}{C_{12}[A_{31} + A_{32}]}, \tag{4.19}$$

which we see is independent of n_e. The line ratio is

$$\frac{F_{575.5\text{nm}}}{F_{658.3\text{nm}} + F_{654.8\text{nm}}} = \frac{\lambda_{12}}{\lambda_{23}} \frac{C_{13}A_{32}}{C_{12}[A_{31} + A_{32}]}. \tag{4.20}$$

Now, we know that

$$\frac{C_{13}}{C_{12}} = \frac{\Omega_{13}}{\Omega_{12}} \exp\left[-\frac{\Delta E_{12} - \Delta E_{13}}{kT_e}\right] = \frac{\Omega_{13}}{\Omega_{12}} \exp\left[-\frac{h\nu_{23}}{kT_e}\right]. \tag{4.21}$$

Subbing this in, we get

$$\frac{F_{575.5\text{nm}}}{F_{658.3\text{nm}} + F_{654.8\text{nm}}} = \frac{\Omega_{13}}{\Omega_{12}} \frac{\lambda_{12}}{\lambda_{23}} \frac{A_{32}}{[A_{31} + A_{32}]} \exp\left[-\frac{h\nu_{23}}{kT_e}\right] = 0.13 \exp\left[-\frac{2.5 \times 10^4\ \text{K}}{T_e}\right], \tag{4.22}$$

which we can re-arrange to measure the temperature of a nebula from the observed line ratio.

4.4 Density diagnostics

To estimate density, we again consider a 3-level atom, but now we want a configuration sensitive to n_e and insensitive to T_e. For this, the following properties turn out to be useful:

- A very forbidden $3 \rightarrow 2$ transition ($A_{32} \sim 0$),
- $n_3 << n_2 << n_1$ for the full range of typical nebula temperatures and densities,
- Collisional transitions between levels 3 and 2 can be ignored,
- The energy gap between levels 2 and 3 is very small.

In this regime, level 3 and level 2 balance become respectively

$$n_3[A_{31} + n_e C_{31}] = n_1 n_e C_{13} \tag{4.23}$$
$$n_2[A_{21} + n_e C_{21}] = n_1 n_e C_{12}. \tag{4.24}$$

The line ratio is therefore:

$$\frac{F_{31}}{F_{12}} = \frac{\lambda_{12}}{\lambda_{13}} \frac{A_{31}}{A_{21}} \frac{n_3}{n_2} = \frac{\lambda_{12}}{\lambda_{13}} \frac{A_{31}}{A_{21}} \frac{C_{13}}{C_{12}} \frac{A_{21} + n_e C_{21}}{A_{31} + n_e C_{31}}. \tag{4.25}$$

The prime examples of density diagnostics are [O II] and [S II], and other examples are [N I], [Cl III], [Ar IV], [K V] and [Ne IV].

Let's take a look at one of the prime examples: [O II]. Fig 4.5 shows the energy levels for [O II] and [S II]. The two transitions shown are both forbidden lines: $A_{31} = 1.8 \times 10^{-4}\ \text{s}^{-1}$,

$A_{21} = 3.6 \times 10^{-5}$ s^{-1}, and their wavelengths are very similar ($\lambda_{12} = 372.9$ nm and $\lambda_{13} = 372.6$ nm, converting from Angstroms to nanometers). The statistical weights are: $g_1 = 4$, $g_2 = 6$, $g_3 = 4$. The collision strength for transitions from ^4S to ^2D is $\Omega = 1.34$, and the exact energy level that electrons end up in when they are collisionally excited to the ^2D sub-shell depends on the relative statistical weights of the two sub-sub-shells in that sub-shell. We can therefore assign effective collision strengths of $\Omega_{12} = 1.34 \times\ g_2/(g_2 + g_3) = 0.804$ and $\Omega_{13} = 1.34 \times\ g_3/(g_2 + g_3) = 0.536$.

Now, the line ratio is given by Equation (4.25). The first thing we can do is show that the ratio C_{13}/C_{12} is more or less independent of temperature because the energy gap between levels 2 and 3 is so small:

$$\frac{C_{13}}{C_{12}} = \frac{\Omega_{13}}{g_1} e^{-h\nu_{13}/kT_e} \frac{g_1}{\Omega_{12}} e^{h\nu_{12}/kT_e} = \frac{\Omega_{13}}{\Omega_{12}} e^{-h\nu_{23}/kT_e} \approx \frac{\Omega_{13}}{\Omega_{12}} = \frac{g_3}{g_2}. \tag{4.26}$$

We can then evaluate the line ratio in low and high density regimes. For $n_e << n_e^*$, the collisional de-excitation terms are much less important than the spontaneous emission terms and the line ratio becomes

$$\frac{F_{31}}{F_{12}} = \frac{\lambda_{12}}{\lambda_{13}} \frac{A_{31}}{A_{21}} \frac{C_{13}}{C_{12}} \frac{A_{21}}{A_{31}} = \frac{\lambda_{12}}{\lambda_{13}} \frac{C_{13}}{C_{12}} \approx \frac{\Omega_{13}}{\Omega_{12}} = \frac{2}{3}, \tag{4.27}$$

where we have used $\lambda_{13} \approx \lambda_{12}$. For $n_e >> n_e^*$, the collisional de-excitation terms are dominant and so Equation (4.25) instead becomes

$$\frac{F_{31}}{F_{12}} = \frac{\lambda_{12}}{\lambda_{13}} \frac{A_{31}}{A_{21}} \frac{C_{13}}{C_{31}} \frac{C_{21}}{C_{12}} = \frac{\lambda_{12}}{\lambda_{13}} \frac{A_{31}}{A_{21}} \frac{g_3}{g_1} e^{-h\nu_{13}/kT_e} \frac{g_1}{g_2} e^{h\nu_{12}/kT_e} = \frac{\lambda_{12}}{\lambda_{13}} \frac{A_{31}}{A_{21}} \frac{g_3}{g_2} e^{-h\nu_{23}/kT_e} \approx \frac{A_{31}}{A_{21}} \frac{g_3}{g_2} = \frac{10}{3}. \tag{4.28}$$

Therefore the line ratio is constant at very low and high densities with a transition for $n_e \sim n_e^*$, as is shown in Fig 4.6. For [O II] and [S II], the critical density happens to be $n_e \sim 10^{9-10}$ m^{-3} for typical nebula temperatures making them very good density diagnostics for nebulae. Fig 4.7 shows real examples of [O II] line doublets, with one near the low density limit and the other near the high density limit.

4.5 Diagnostic diagrams

In reality, we don't actually need line ratios that depend only on temperature or only on density. All we need is to measure line ratios for different atoms, for which the dependence on temperature and density is *different*. Fig 4.8 shows a sketch of a *diagnostic diagram*. Here, we have measured line ratios for [N II], [O II] and some other ion. The ratio for [N II] is more or less independent of density and [O II] is more or less independent of temperature. The line ratio for the other ion depends on both – but this doesn't matter because we can just compare all of our line diagnostics from the same spectrum and see where they cross.

Fig 4.9 shows an example of a diagnostic diagram constructed for a real planetary nebula. In this case, we see that the principle doesn't pan out – the lines do not intersect at one point, or in one small region of the diagram. This indicates that different lines are predominantly emitted from regions of different density and/or temperature. We can see this directly with

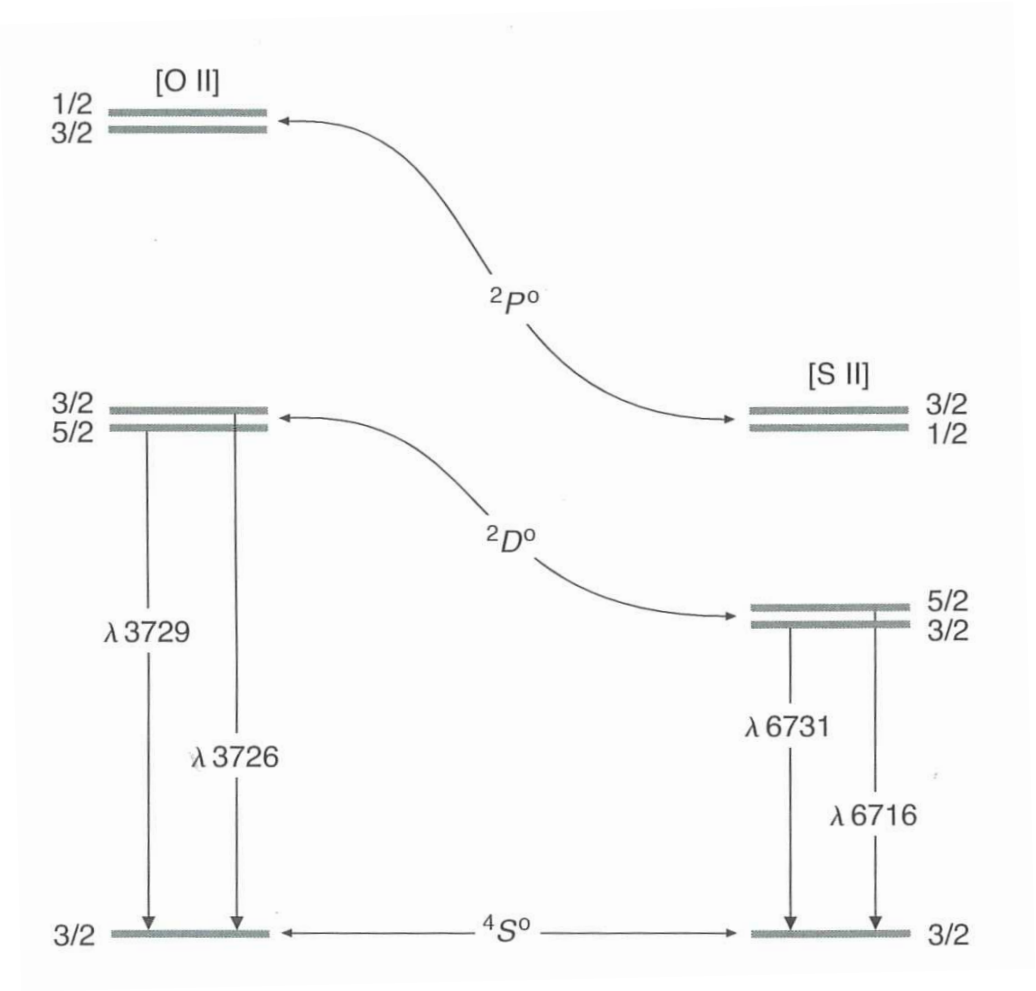

Figure 4.5: Energy levels of O II and S II. From Osterbrock & Ferland, 'Astrophysics of Gaseous Nebulae and Active Galactic Nuclei' (Fig 5.7 on pg 122).

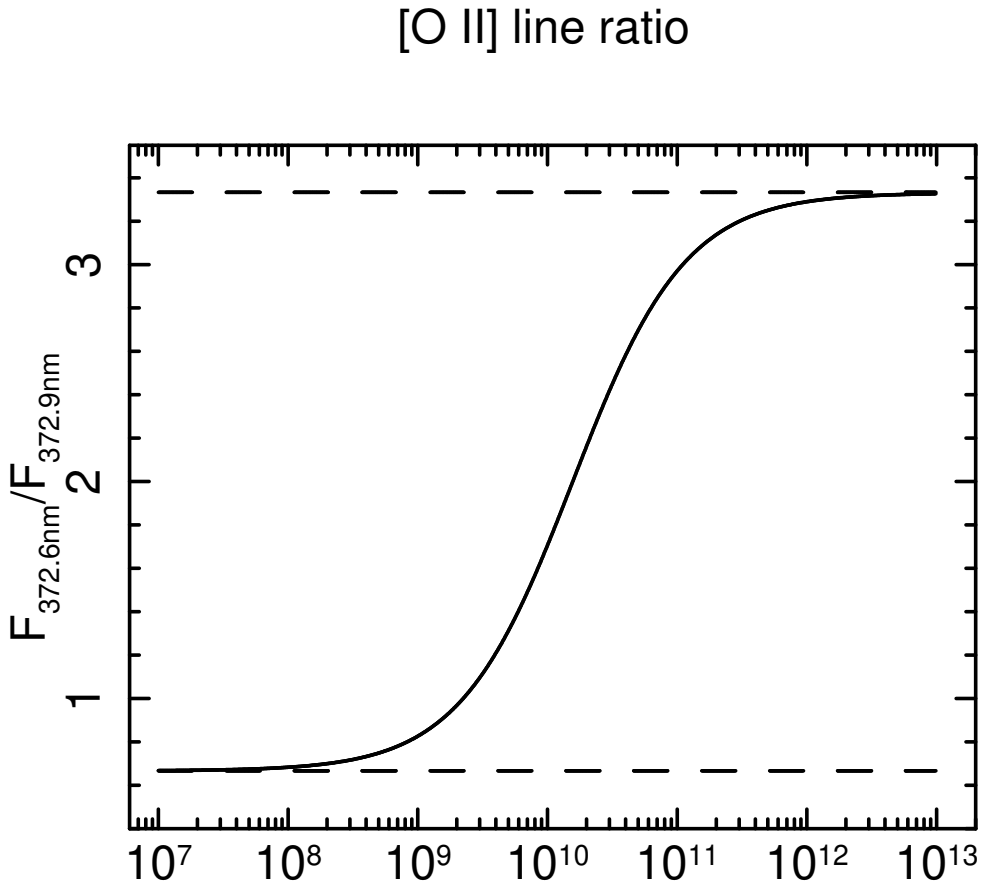

Figure 4.6: Line ratio as a function of electron density for [OII] at $T_e = 10^4$ K (although the temperature dependence is weak). Dashed lines show the low and high density limits of 2/3 and 10/3.

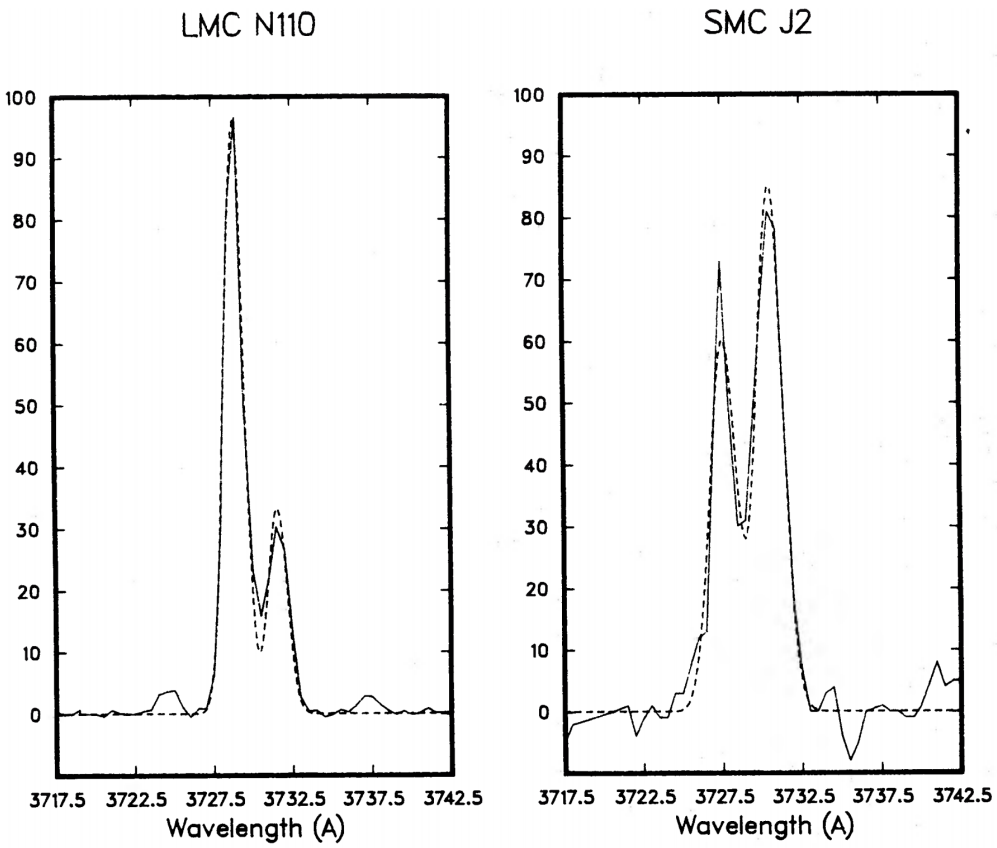

Figure 4.7: [O II] doublets in two planetary nebulae. Solid lines are observed and dashed lines are a fitted double Gaussian model. LMC N110 is near the high density limit (line ratio $\sim$ 2.6), and SMC J2 is near the low density limit (line ratio $\sim$ 0.68). From Barlow et al (1987).

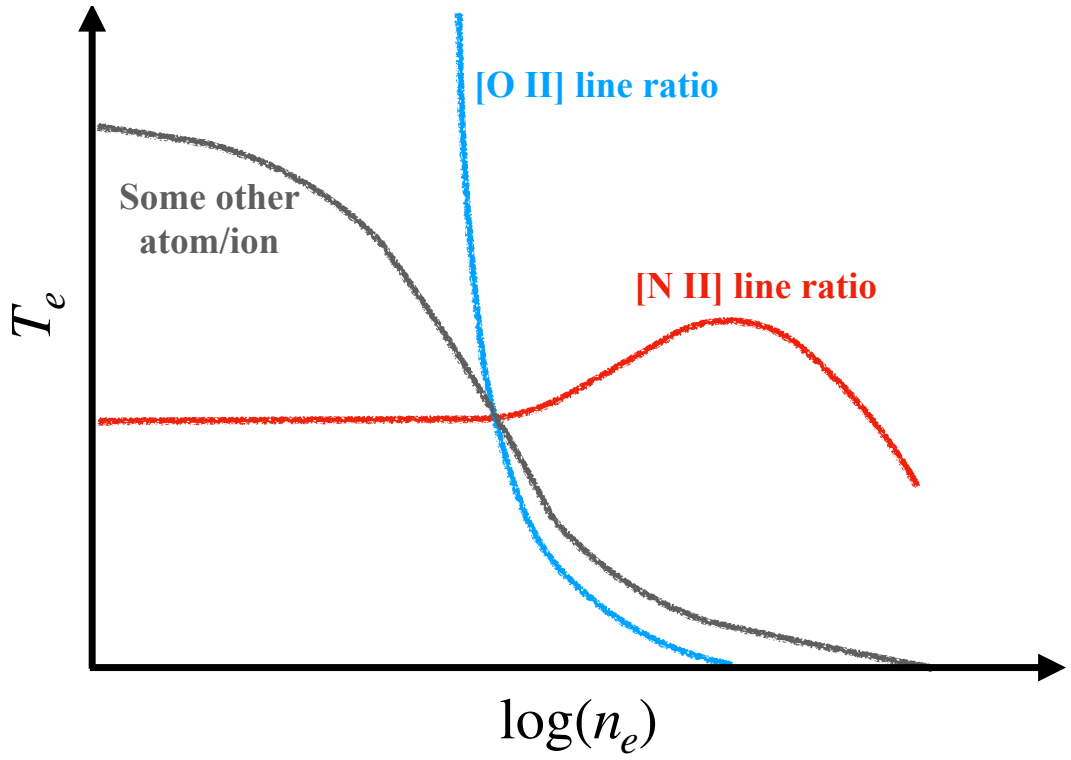

Figure 4.8: Sketch of a diagnostic diagram showing how line ratios from a region can in principle be combined to constrain the density and temperature of that region.

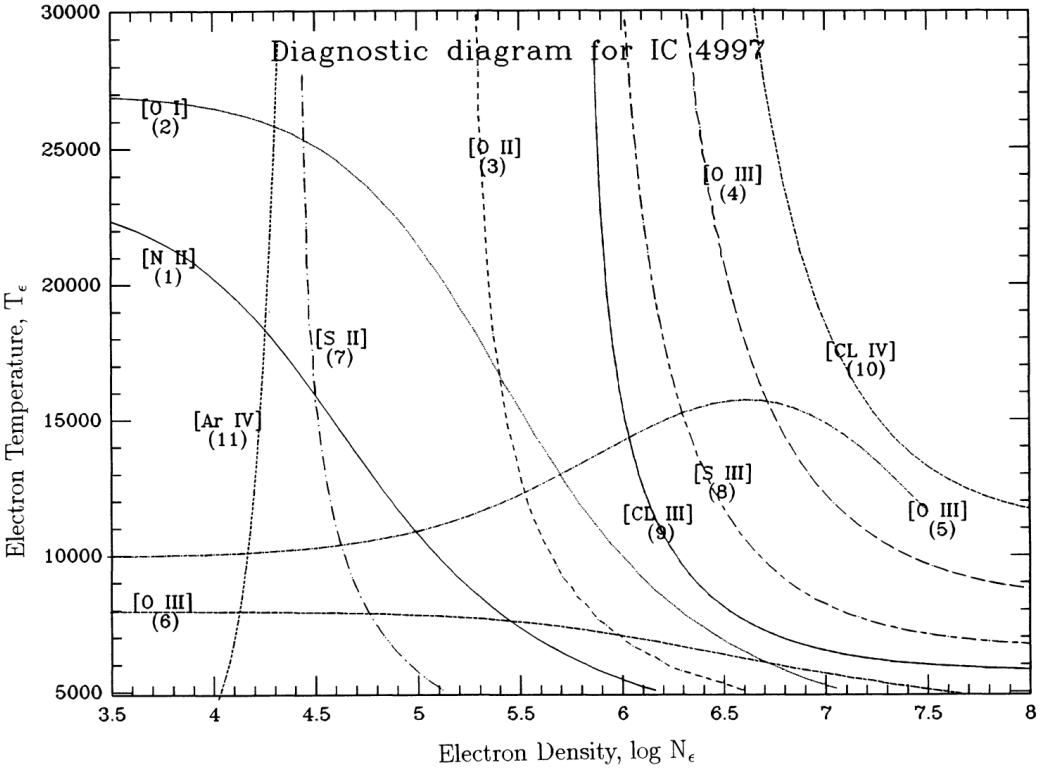

Figure 4.9: Diagnostic diagram for the planetary nebula IC 4997. From Hyung, Aller & Feibelman (1994).

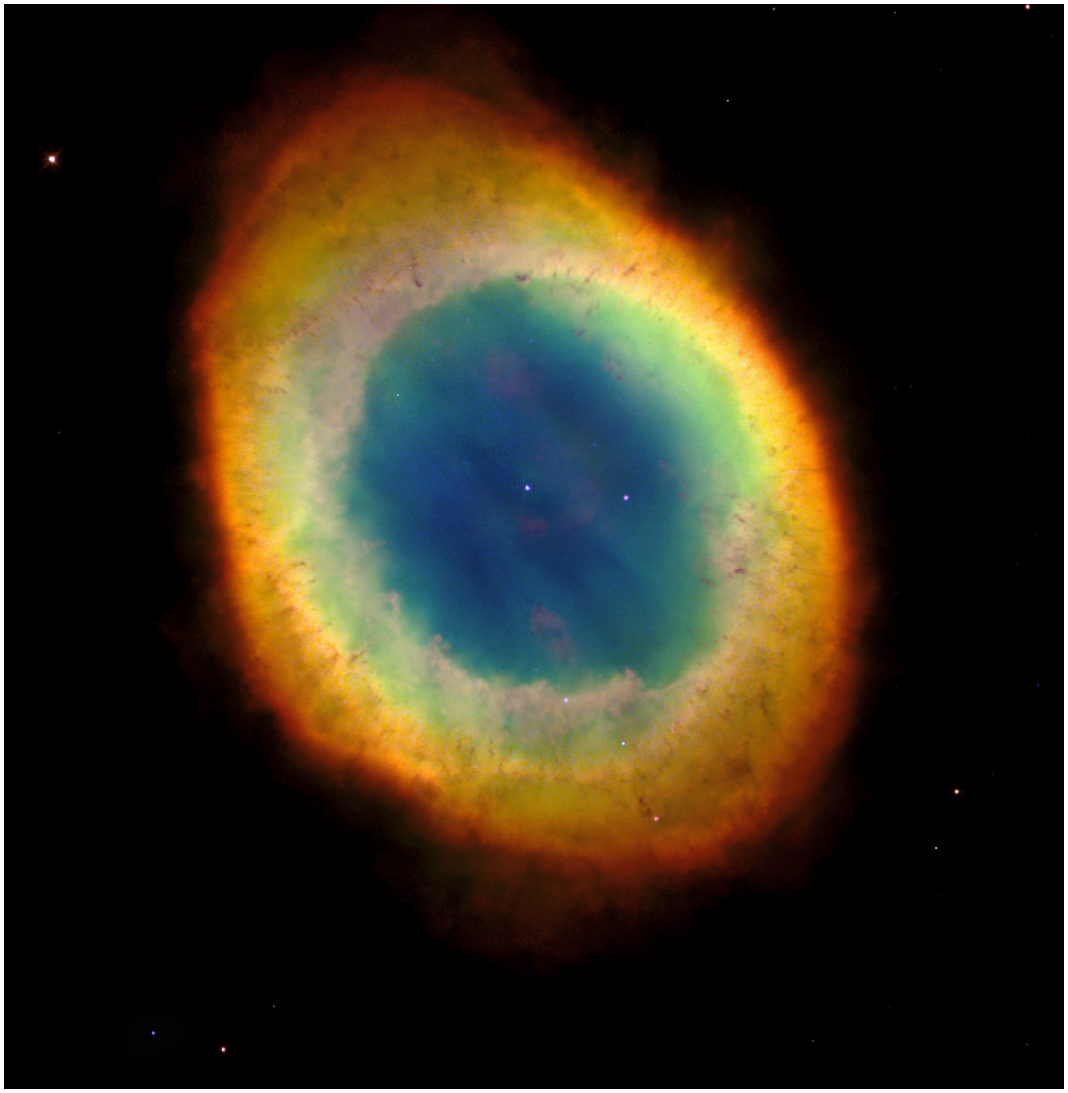

Figure 4.10: M57, the Ring Nebula. Red: [N II] 658.4 nm, Green: [O III] 500.7 nm, Blue: Helium 468.6 nm.

good enough spatial resolution. Fig 4.10 is a particularly spectacular example – the Ring Nebula. We see that the collisionally excited [N II], [O III] and He II lines are emitted predominantly from different regions of the nebula. We can understand this a little more quantitatively by writing out the equation for the flux of an emission line from a given ion without making the usual assumption of everything being uniform within the entire emitting volume:

$$F_{21} = \frac{hc}{\lambda_{12}} \frac{A_{21}}{4\pi d^2} \int n_2 \, dV. \tag{4.29}$$

Remember that this is for a given *ion* of a particular element, so we can express this in terms of the fraction of atoms of the element that are in this particular ionization state:

$$F_{21} = \frac{hc}{\lambda_{12}} \frac{A_{21}}{4\pi d^2} \int \frac{n_2}{n_{ion}} \frac{n_{ion}}{n_E} \, n_E \, dV. \tag{4.30}$$

Here, n_E is the number density of element E and n_{ion} is the number density of a particular ionic species of element E. Modelling the nebula as spherical and defining the *ionization fraction* $\zeta \equiv n_{ion}/n_E$ gives

$$F_{21} = \frac{hc}{\lambda_{12}} \frac{A_{21}}{d^2} \int_0^{r_{out}} \frac{n_2}{n_{ion}}(r) \, \zeta(r) \, n_E \, r^2 \, dr. \tag{4.31}$$

Therefore, if the nebula is radially stratified in terms of ionization fraction, or in terms of energy level populations (e.g. if the temperature is not uniform), this will effect the line strengths. We in particular expect the ionization fraction to be radially stratified. As we will see next time, the central star of the nebula is more easily able to ionize the inner regions. Radial stratification is also present in stars, as the density and temperature change dramatically with distance from the core. To bring this back to the Ring Nebula, we can for example understand why the [N II] lines are only present in the outskirts of the nebula: maybe the inner regions are hot enough for N III and higher ionization species to be more common there than N II.

Finally, we can also use the relative line strengths from different elements to measure relative abundances. We can manipulate the above equation to become

$$F_{21} = \frac{hc}{\lambda_{12}} X \frac{A_{21}}{d^2} \int_0^{r_{out}} \frac{n_2}{n_{ion}}(r) \, \zeta(r) \, n_H \, r^2 \, dr, \tag{4.32}$$

where $X \equiv n_E/n_H$ is the *chemical abundance* of element E relative to hydrogen and n_H is the number density of hydrogen. If we can solve for ionization balance in the nebula, we can then use line ratios from different elements in order to measure elemental abundances.

5 Ionization and Recombination

5.1 Introduction

So far, we have calculated the expected emission line strengths for various transitions in various ionic species of various elements. Now we will think about the balance between ionization and recombination, which governs the relative populations of different ionic species for each element. Similarly to excitation and de-excitation, we will consider two different types of ionization and recombination: photo- and collisional.

5.2 Photo-ionization and Photo-recombination

5.2.1 Photoionization

Photo-ionization is simply a photon with energy greater than the ionization potential being absorbed to liberate an electron. The process can be written as

$$X^i + h\nu \rightarrow X^{i+1} + e, \tag{5.1}$$

where X^i is the atom (or ion) being ionized, $h\nu$ is the incident photon, X^{i+1} is the resulting ion and e is the liberated electron. The free electron now has the energy that the absorbed photon had, minus the ionization potential of the atomic level it has been liberated from; e.g. $E_\gamma = 15$ eV, $E_{\rm bound} = -13.6$ eV gives $E_{\rm free} = E_\gamma + E_{\rm bound} = 1.4$ eV. The free electron may then have collisions with other free electrons, leading to the electron energy distribution becoming Maxwellian. The photoionization rate for ionization of X^i

$$\Phi_i = \int_{\nu_0}^{\infty} 4\pi\sigma_i^{bf}(\nu)\frac{J_\nu}{h\nu}\,d\nu, \tag{5.2}$$

where $\sigma_i^{bf}(\nu)$ is the bound-free absorption cross-section, $h\nu_0$ is the ionization potential of X^i and J_ν is the average specific intensity

$$J_\nu = \frac{1}{4\pi}\int I_\nu d\Omega. \tag{5.3}$$

The number of ionizations of X^i per unit volume per unit volume per unit second is then $n_i\Phi_i$, where n_i is the number density of X^i ions.

5.2.2 Radiative recombination

This is the thermodynamic inverse of photoionization, so the process can be described by reversing the arrow in Equation (5.1):

$$X^{i+1} + e \rightarrow X^i + h\nu. \tag{5.4}$$

Therefore, a free electron (energy E_{free}) recombines with an ion. It now has (negative) energy E_{bound} in its new bound state, and a photon is emitted with energy $E_\gamma = E_{\text{free}} - E_{\text{bound}}$. For example, we can exactly reverse the previous example: $E_{\text{bound}} = -13.6$ eV, $E_{\text{free}} = 1.4$ eV means that the produced photon has $E_\gamma = E_{\text{free}} - E_{\text{bound}} = 1.4 + 13.6\text{eV} = 15$ eV. The number of recombinations to a given energy level per unit volume per unit time is then

$$\text{Recombination rate density} = n_{I+1}\, n_e \int_0^\infty \sigma_{fb}(v_e)\, f(v_e) v_e \, dv_e = n_{I+1}\, n_e\, \alpha_r, \tag{5.5}$$

where $\sigma_{fb}(v_e)$ is the free-bound cross-section for capture to a given energy level of a given ion and α_r is the *recombination rate coefficient*. If $f(v_e)$ is Maxwellian, then $\alpha_r \propto T_e^{-1/2}$.

5.3 Collisional ionization and recombination

Collisional ionization takes place when an electron is scattered as it passes an ion, giving up sufficient energy to liberate a bound electron; i.e.:

$$X^i + e \rightarrow X^{i+1} + e + e. \tag{5.6}$$

The rate of collisional ionizations of X^i from energy level E_j is $n_i n_e Q_i(j)$, where n_i is again the number density of X^i and $Q_i(j)$ is the *collisional ionization rate coefficient*:

$$Q_i(j) = 2 \times 10^{-14} \frac{\xi_j}{E_j^2} T_e^{1/2} \mathrm{e}^{-E_j/kT_e}, \tag{5.7}$$

where ξ_j is the number density of electrons in the j^{th} bound energy level. We therefore see that Q_i is only important for high temperatures: $kT_e > |E_j|$.

Collisional recombination is the thermodynamic inverse of collisional ionization:

$$X^{i+1} + e + e \rightarrow X^i + e. \tag{5.8}$$

Since this only happens when two free electrons scatter off X^{i+1} at the same time, it is only relevant in very dense environments. We will not need to consider collisional recombination in this course; although, as an aside, it *is* probably important in accretion discs around stellar-mass black holes, which can be very dense (as we will see in the High Energy Astrophysics course). This is currently a bit of a headache for accretion disc models.

The ionization state of a population of ions can be calculated by balancing the ionization and recombination rates.

5.4 Hydrogen Recombination

In the case of hydrogen, free electrons recombine with ions and rapidly cascade down from whatever energy level they first recombined to down to the ground state, radiating emission lines at each step of the cascade. The flux ratio of emission line $i \rightarrow k$ to emission line $k \rightarrow m$ is simply

$$\frac{F_{ik}}{F_{km}} = \frac{n_i A_{ik} h\nu_{ki}}{n_k A_{km} h\nu_{mk}}, \tag{5.9}$$

where $i > k$ and $k > m$. Therefore this ratio depends on the ratio of the level populations, which is determined by excitations and de-excitations within each H atom (as before with our 2 level atom) *and* ionizations and recombinations. We therefore need to write down a steady state equation in which the number of electrons leaving each energy level is equal to the number of electrons entering that level (exactly the same as the statistical equilibrium we have already considered, but only now we also must account for ionization and recombination!).

In general, this is an extremely difficult problem, but it simplifies enormously for hydrogen when $n_e \lesssim 10^{16}\text{m}^{-3}$ and $T_e \lesssim 10^4$ K because:

- Collisional de-excitations can be ignored in hydrogen for $n_e \lesssim 10^{16}\text{m}^{-3}$ because the spontaneous emission coefficients are so large ($A > 10^6\text{s}^{-1}$),
- Collisional excitations are unimportant for $T_e \lesssim 10^4$ K because the energy difference between the ground state and level 2 is high ($\Delta E = 10.2\text{eV} >> kT_e$),
- Collisional ionization and recombination are also unimportant for the same reasons,
- Electrons can cascade all the way down to the ground state before they are photo-ionized, again because the A coefficients are so large.

The energy level balance can therefore be calculated by considering only radiative recombination and spontaneous emission. Therefore, we can write down the following equation between electrons entering level k and electrons leaving level k:

$$n_e\, n_H\, \alpha_k^r + n_i \sum_{i>k} A_{ik} = n_k \sum_{m<k} A_{km}, \tag{5.10}$$

where n_H is the number density of hydrogen atoms. The first term on the LHS is electrons recombining to level k, the second is electrons decaying to level k from a higher bound level, and the RHS is electrons decaying from level k to a lower level. This forms a set of coupled equations (i.e. one equation for each value of k) called the *capture-cascade equations*. To solve them, we can pick some high energy level I and assume that the electron population above that level is zero:

$$n_e\, n_H\, \alpha_I^r = n_I \sum_{m=1}^{I-1} A_{Im}, \tag{5.11}$$

and re-arrange to get

$$n_I = \frac{n_e\, n_H\, \alpha_I^r}{\sum_{m=1}^{I-1} A_{Im}} \propto n_e\, n_h T_e^{-1/2}, \tag{5.12}$$

where the final step comes from $\alpha_I^r \propto T_e^{-1/2}$, which as we saw earlier comes from assuming a Maxwell distribution of electron velocities. We can then move on to level $I-1$:

$$n_e\ n_H\ \alpha_{I-1}^r + n_I A_{I(I-1)} = n_{I-1} \sum_{m=1}^{I-2} A_{(I-1)m}. \tag{5.13}$$

Re-arranging gives

$$\begin{aligned} n_{I-1} &= \frac{n_e\ n_H\ \alpha_{I-1}^r + n_I A_{I(I-1)}}{\sum_{m=1}^{I-2} A_{(I-1)m}} \\ &= \frac{\alpha_{I-1}^r/\alpha_I^r + A_{I(I-1)}/\sum_{m=1}^{I-1} A_{Im}}{\sum_{m=1}^{I-2} A_{(I-1)m}}\ n_e\ n_H\ \alpha_I^r. \end{aligned} \tag{5.14}$$

We could stay here all day working through all the other levels, but hopefully you can already see that we will get expressions with more and more ratios of recombination coefficients and a final factor of $n_e\ n_H\ \alpha_I^r$. Now, the ratio of recombination coefficients α_m^r/α_k^r is only weakly dependent on n_e and T_e. If we assumed for illustration that every α_m^r/α_k^r is constant, then we would end up with $n_k \propto n_e\ n_H\ T_e^{-1/2}$ for each level k, and the flux ratio between any two lines would be constant. The relative flux of two Balmer lines (e.g. H_α flux / H_β flux) is called the *Balmer decrement* and is only weakly dependent on electron temperature. More accurately:

$$\frac{F(H_\alpha)}{F(H_\beta)} = 2.86 \left(\frac{T_e}{10^4\mathrm{K}}\right)^{-0.07}, \tag{5.15}$$

which is accurate to within 1% over the range $10^8 \lesssim n_e \lesssim 10^{10}\mathrm{m}^{-3}$ and $5\times10^3 \lesssim T_e \lesssim 1.2\times10^4$ K – and can therefore be used for most planetary nebulae. Simple relations between Brackett and Balmer lines can also be used in the same limit

$$\frac{F(Br_\alpha)}{F(H_\beta)} = 0.079 \left(\frac{T_e}{10^4\mathrm{K}}\right)^{-0.36}, \tag{5.16}$$

$$\frac{F(Br_\gamma)}{F(H_\beta)} = 0.028 \left(\frac{T_e}{10^4\mathrm{K}}\right)^{-0.24}. \tag{5.17}$$

Another useful relation that is valid in the same range of density and temperature is that the ratio of ionizing photons $\dot{N}_\gamma$ to photons in the H_α line is $\dot{N}_\gamma/\dot{N}_{H\alpha} = 2.2$. You will use this ratio in one of the problem sets in order to calculate the rate of ionizing photons from the flux in the H_α emission line, and the distance to the nebula emitting the line. Note that, if we can measure the bolometric luminosity by integrating the spectrum over a wide range of wavelengths, we can compare it with the inferred $\dot{N}_\gamma$ in order to constrain an effective temperature of the star; i.e. $\dot{N}_\gamma$ depends on both the bolometric luminosity *and* spectral shape of the star. Assuming that the star's spectrum is a Planck function with temperature T_{eff}, this temperature T_{eff} can be constrained by comparing the inferred values of $\dot{N}_\gamma$ and L_{bol}.

Note: ($hc = 1.99\times10^{-25}$Jm $= 1.24\times10^{-6}$ eV m)

5.5 Stromgren Sphere

The Stromgren sphere is a very simple model for ionization balance. Imagine we have a nebula made of pure hydrogen gas with a central star. The star radiates ionizing photons, which are absorbed by HI atoms to create HII ions and free electrons. These HII ions in time recombine with free electrons. The nebula is in equilibrium, so the number of ionizations is equal to the number of recombinations. The Stromgren sphere is the spherical region in which nearly *all* of the hydrogen is ionized. This is called an HII region.

To calculate the radius of the Stromgren sphere, we start off by setting the ionization rate equal to the recombination rate. The recombination rate per unit volume is $\alpha^r n_e n_{HII}$. For a spherical region of radius R with a uniform density across its volume, the recombination rate is therefore

$$\text{Recombination rate} = \alpha^r n_e n_{HII} \frac{4}{3}\pi R^3 \tag{5.18}$$

If the rate of ionizing photons per second being radiated by the central star is $\dot{N}_\gamma$, and if every photon from the star is eventually absorbed by an HI atom, then the ionization rate is simply $\dot{N}_\gamma$. Therefore, in equilibrium we have:

$$\alpha^r n_e n_{HII} \frac{4}{3}\pi R^3 = \dot{N}_\gamma . \tag{5.19}$$

Now, we want to define the size of the region in which the HII content approaches 100%. In this limit, we have $n_e = n_{HII}$. Subbing this into the above equation and re-arranging gives the radius of the HII region (the Stromgren sphere):

$$R_s^3 = \left(\frac{3\dot{N}_\gamma}{4\pi\alpha^r n_e^2} \right)^{1/3} . \tag{5.20}$$

The emission rate of ionized photons can then be calculated e.g. from the flux of the H_α line measured from the nebula using the $\dot{N}_\gamma / \dot{N}_{H\alpha} = 2.2$ relation, providing the distance to the nebula is known.

The above is very simplified. In reality, the photo-ionization rate (from earlier on in the lecture) for isotropic radiation (so that $J_\nu = I_\nu$) is:

$$\Phi_{HI} = \int_{\nu_0}^{\infty} \frac{4\pi I_\nu}{h\nu} \sigma^{bf}(\nu)\, d\nu . \tag{5.21}$$

Now, the Einstein A coefficients are very large for hydrogen, and so if a hydrogen atom recombines to an excited state, the electron will very quickly cascade down to the ground state, usually before there is time for the atom to be once more ionized. We can therefore assume that the bound free cross section is only the cross-section for photoionization from the ground state. This also means that photons must all have energy ≥ 13.6 eV to ionize HI, and therefore in the above integral $\nu_0 = 13.6\text{eV}/h$. Before, we just simply assumed that the ionization rate is $\Phi_{HI} = \dot{N}_\gamma$. We can make this approximation because the absorption cross section is large

Spectral Type	$\dot{N}_\gamma$ (s^{-1})	R (pc)
G2V	10^{39}	6.7×10^{-5}
B0V	4×10^{46}	1.6×10^{-2}
O6V	10^{49}	0.1

Table 5.1: Typical Stromgren sphere radii for a $n_e = 10^{10}\text{m}^{-3}$ nebulae with central star of different spectral type.

(note that $4\pi I_\nu \sigma(\nu) d\nu$ is a photon rate). By setting $\Phi_{HI} = \dot{N}_\gamma$, we are simply assuming that *all* photons ionize HI atoms, and *none* fly out of the nebula. The above equation is therefore more accurate and we see we will get $\Phi_{HI} < \dot{N}_\gamma$.

There is also a subtlety with recombination. That is, any time a HI atom recombines directly to the ground state, an ionizing photon will be emitted. Note that the energy of the emitted photon (called a *Lyman α continuum photon*) in this case will be equal to the energy that the captured electron had plus 13.6 eV, and therefore *all* photons emitted due to recombination to the ground state will be energetic enough to ionize another HI atom. This photon will be quickly absorbed, and so recombinations directly to the ground state contribute no net recombinations! This means that the recombination coefficient for recombinations to the ground state must be ignored, and the α^r we must use in our formula for the radius of the Stromgren sphere is the sum of the recombination coefficients for all other levels: $\alpha^r(T_e) = \sum_{k=2}^{\infty} \alpha_k^r(T_e)$. At $T_e = 10^4$ K, $\alpha^r = 2.6 \times 10^{-19}$ m^3s^{-1}.

Table 5.1 shows some typical values for the Stromgren sphere radius assuming central stars of different spectral type. We see that for a very hot central star, the HII region may be resolvable if the nebula is close enough to us. Fig 5.1 shows a particularly spectacular example of a resolvable HII region: the Rosetta nebula. The hole in the centre of the red emission is the HII region and is almost 1 degree across (note that, instead of a central star, here there is a central star cluster).

5.5.1 Ionization Timescales

Now let us consider how the HII region formed. In the simplest case, we had a nebula made up entirely of bound H atoms, when suddenly a star formed at the centre and began to emit ionizing photons. This leads to an ionization front moving out from the star as the newly formed HII region gets bigger until it eventually becomes the size of the Stromgren sphere and stops expanding. To calculate the expansion rate, we can imagine the HII region at a given point in time to be a sphere (radius R) and consider a shell (width ΔR) of neutral H atoms immediately outside of that sphere. In the ionized sphere, we have $n_e(R) = n_{HII}(R)$, $n_H(R) = 0$ and in the neutral shell we have $n_{HII}(R) = n_e(R) = 0$, and $n_H(R)$ in the shell is equal to $n_{HII}(R)$ in the sphere. The number of H atoms in the shell is

$$\text{H atoms in the shell} = 4\pi R^2 n_H(R) \Delta R. \tag{5.22}$$

The number of ionizing photons being provided by the star in a time interval Δt is $\dot{N}_\gamma \Delta t$. Not all of these photons are available to ionized H atoms in the shell though, because some ionize H

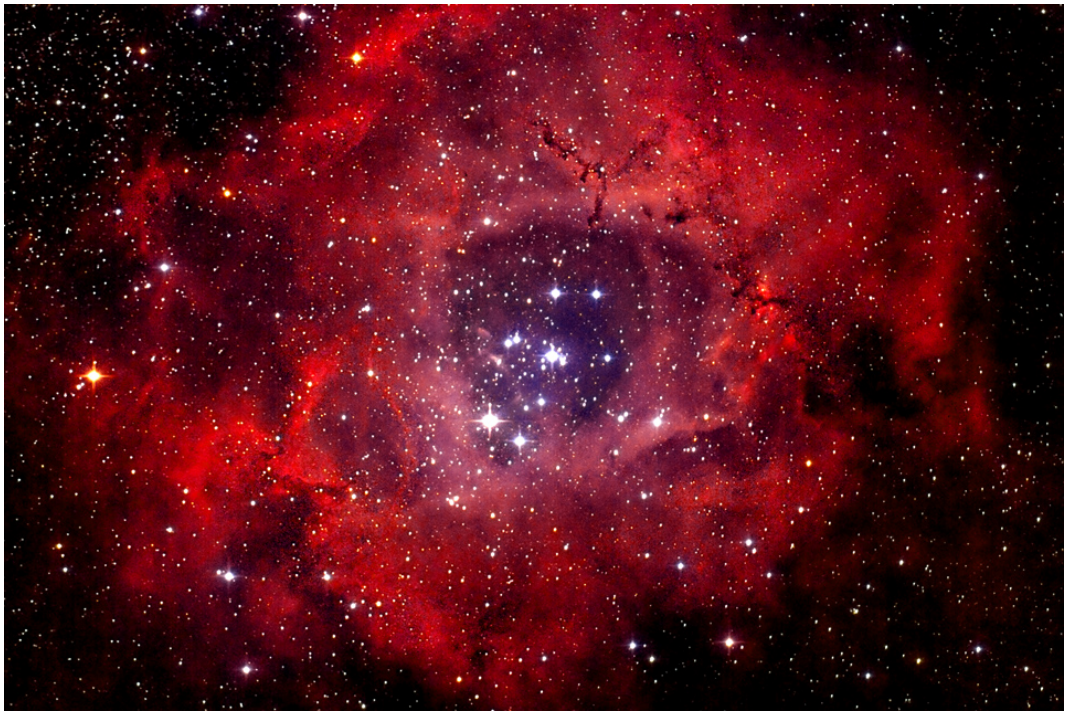

Figure 5.1: The Rosetta nebula.

atoms within the sphere. The only photons that are available to ionize H atoms in the shell are the ones that escape the sphere. In other words, the number of ionizing photons in the shell is $\dot{N}_\gamma \Delta t$ *minus* the number of ionizations within the sphere in time interval Δt. The sphere is in equilibrium, so the number of ionizations in the HII region equals the number of recombinations. We therefore have that the number of ionizing photons available to the shell is

$$\text{Ionizing photons in the shell} = \dot{N}_\gamma \Delta t - \frac{4}{3}\pi R^3 \alpha^r n_{HII}^2(R)\Delta t. \tag{5.23}$$

If each photon in the shell ionizes an H atom, we have:

$$\begin{aligned} 4\pi R^2 n_H(R+\Delta R)\Delta R &= \dot{N}_\gamma \Delta t - \frac{4}{3}\pi R^3 \alpha^r n_{HII}^2(R)\Delta t \\ 4\pi R^2 n_H(R)\frac{dR}{dt} &= \dot{N}_\gamma - \frac{4}{3}\pi R^3 \alpha^r n_H^2(R), \end{aligned} \tag{5.24}$$

Where $n_H(R)$ refers to the density of H atoms in the *shell* (= number of HII atoms in the sphere). We can simplify this equation by subbing in the variables $\lambda = R/R_s$ and $\tau = t/t_{rec}$, where $t_{rec} = 1/(\alpha^r n_H)$ and R_s is the Stromgren sphere radius. This gives

$$4\pi n_h \lambda^2 \frac{R_s^3}{t_{rec}}\frac{d\lambda}{d\tau} = \dot{N}_\gamma - \frac{4}{3}\pi\lambda^3 R_s^3 \alpha^r n_h^2. \tag{5.25}$$

Multiplying by t_{rec}/R_s^3 gives

$$3\lambda^2 \frac{d\lambda}{d\tau} = 1 - \lambda^3. \tag{5.26}$$

We can solve this with the substitution $y = \lambda^3$, which simplifies the equation to $dy/d\tau = 1 - y$. Since $\lambda = 0$ when $\tau = 0$, the solution becomes

$$\lambda^3(t) = 1 - \mathrm{e}^{-\tau}. \tag{5.27}$$

Assuming uniform density, we can convert λ back to R to get

$$R(t) = R_s \left[1 - \mathrm{e}^{-t/t_{rec}}\right]^{1/3}. \tag{5.28}$$

This makes sense: the ionization front moves out with some characteristic e-folding recombination timescale, $t_{rec} = 1/(\alpha^r n_H)$, and asymptotes at $R = R_s$. Fig 5.2 shows a particularly dramatic example of a propagating ioization front in the 'pillars of creation'.

5.6 Electron temperature from balance of heating and cooling

We can now appreciate that the electron temperature of a nebula or star, or basically anything in statistical equilibrium, is set by a balance of heating and cooling. Heating is set by the photoionization rate and cooling is set by the rate of photons leaving the nebula. Fig 5.3 shows the electron temperature dependence of the heating rate (dashed line) for different temperatures of the central star, T_*, and of the overall cooling rate (solid line).

Since most emission from a nebula is in the form of lines, line emission dominates the cooling rate. The plot also shows contributions from various lines to the cooling rate. We see that they all increase rapidly with temperature. This is because they are all collisionally excited lines, and so higher temperature means that more electrons are in the excited states required for these lines to form.

The heating rate, on the other hand, decreases fairly slowly with electron temperature. This is because 1) the photo-recombination rate decreases with temperature, and 2) collisional ionizations become more important for high T_e, and they ionize neutral hydrogen, leaving less neutral hydrogen to be photo-ionized.

This thermostatic process gives most H II regions temperatures of around 10^4 K.

Adam Ingram

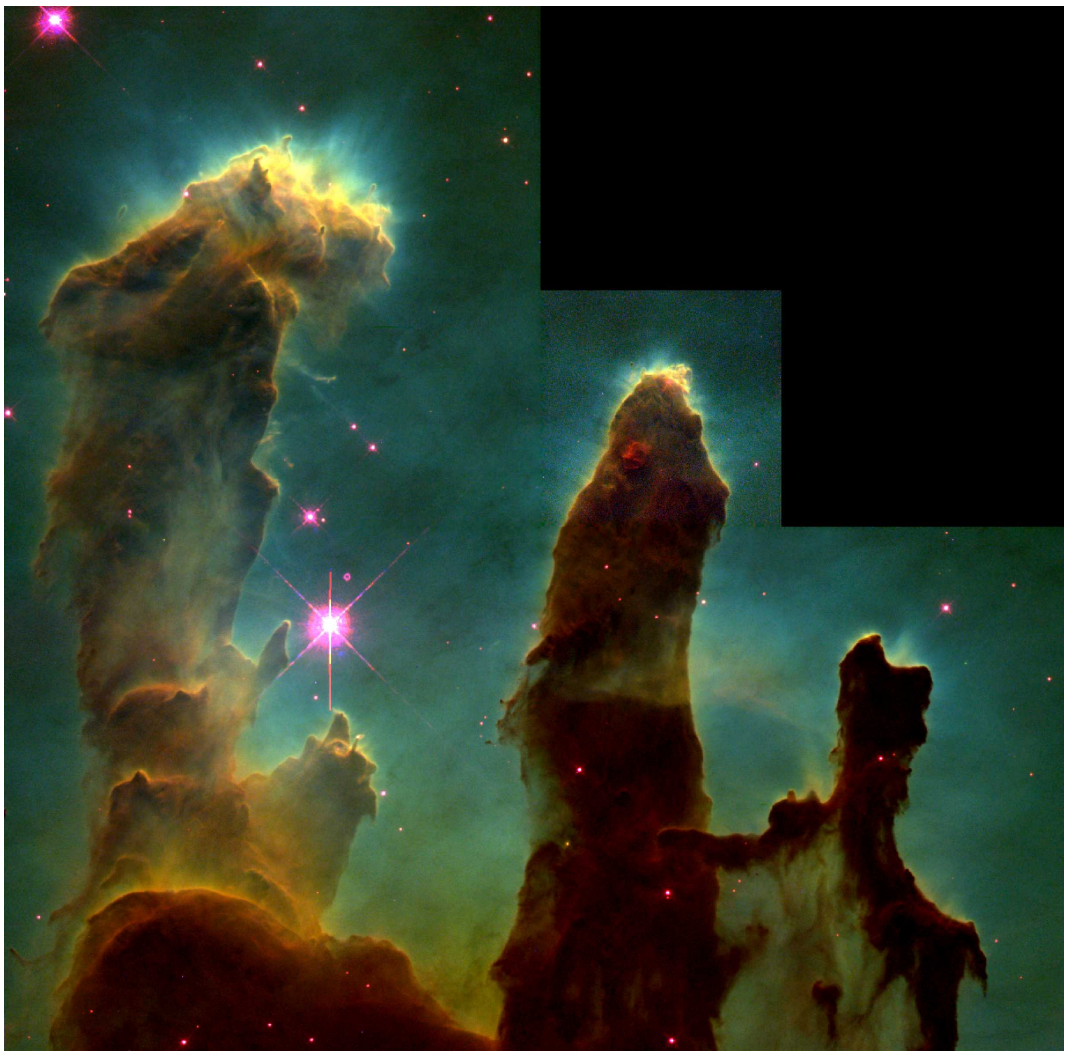

Figure 5.2: The Pillars of creation in the Eagle Nebula. Image taken by the Hubble Space Telescope in 1995.

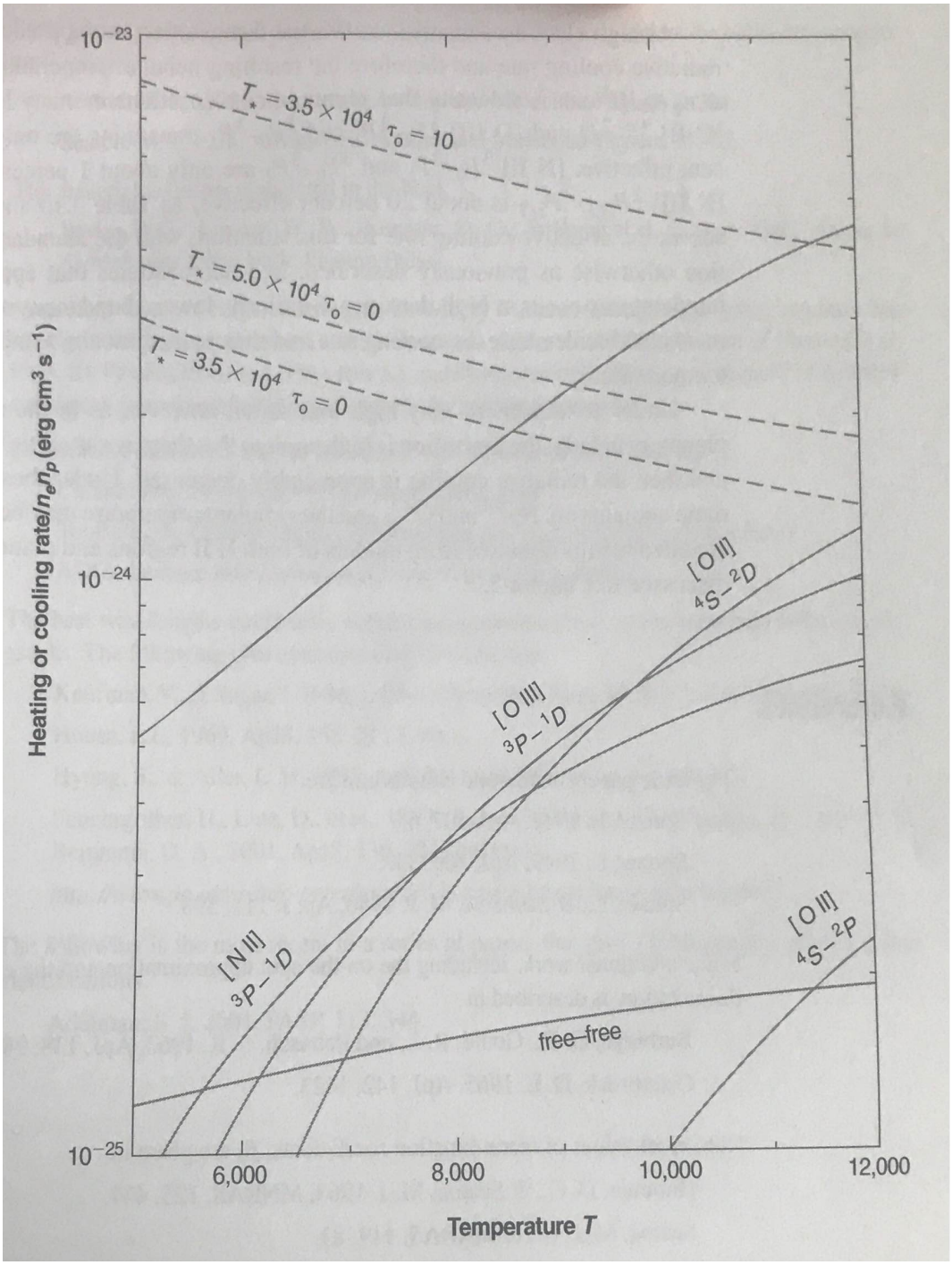

Figure 5.3: Balance of heating from photo-ionization and cooling from line emission in a nebula. From Osterbrock & Ferland, 'Astrophysics of Gaseous Nebulae and Active Galactic Nuclei' (Fig 3.3 on pg 63).

6 Absorption Lines

6.1 Introduction

We have spent the last few lectures thinking about emission lines, which happen when $S_\nu > I_\nu(\tau = 0)$; i.e. the medium in our line of sight to a light source is hotter than the source itself. Now we're going to think about the opposite case of $S_\nu < I_\nu(\tau = 0)$; i.e. the medium in our line of sight is *colder* than the source. This can happen when cool gas lies between the observer and a hot source such as a quasar or a star. This is the context we will consider for the this lecture, but note that absorption lines also occur in stars from the outer layers absorbing radiation from the optically thick core.

In the cool absorbing gas, the atoms (or ions) will typically be in a low-lying state (precisely because the gas is cool), such that absorption occurs predominantly from the ground state. For hydrogen, almost all atoms are in $n = 1$, so we only see Lyman series absorption from interstellar matter (although note that this may not be the case in e.g. stellar atmospheres). Since absorbing atoms tend to be in their ground state, we will be able to model absorption lines due to the level $1 \longrightarrow 2$ transition in a 2-level atom.

6.2 Equivalent width

When we see an absorption line in an observed spectrum, the first thing we will want to do is measure its strength. A useful measurement of the line strength is the *equivalent width* (EW), W_λ. Fig 6.1 shows that the EW is the width that the line would have if it had the same area as the observed line, but only it saturates to have a purely rectangular line profile. One useful property of the equivalent width is that it is normalized to the continuum flux, and so we do not need to know the exact level of the continuum in order to define the strength of the line (therefore we do not need good absolute flux calibration for example). The equivalent width is typically defined to be a wavelength:

$$W_\lambda = \int_{\lambda=0}^{\lambda=\infty} \frac{I_\lambda^{cont} - I_\lambda}{I_\lambda^{cont}}\, d\lambda, \tag{6.1}$$

where I_λ^{cont} is the continuum level, which can be determined either by measuring the flux in a region with no lines or fitting a model etc. Obviously, it is also possible to define an analogous expression for the EW in frequency units W_ν. Here, we will use W_λ, but we can still work with photon frequencies instead of wavelengths by using the relations $c = \nu\lambda$ and $I_\nu = (\lambda/\nu)I_\lambda$ from

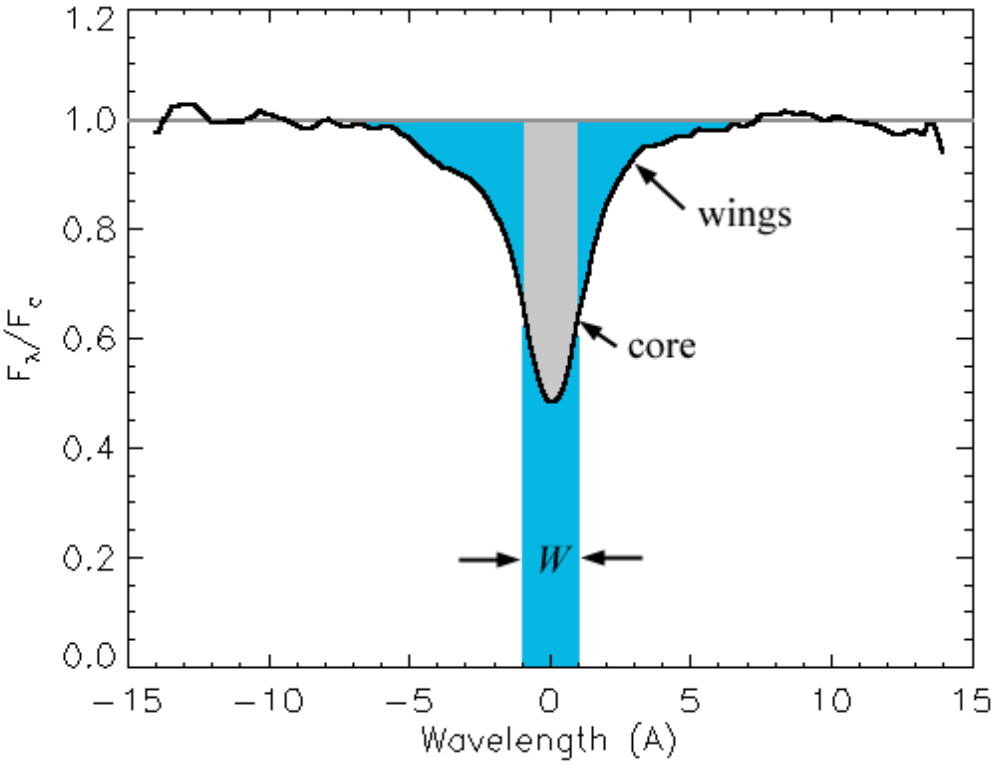

Figure 6.1: Illustration of the equivalent width of an absorption line.

Lecture 1. This gives

$$W_\lambda = \int_{\nu=0}^{\nu=\infty} \frac{I_\nu^{cont} - I_\nu}{I_\nu^{cont}} \frac{\lambda}{\nu}\, d\nu. \tag{6.2}$$

We can then use the formal solution of the radiative transfer equation, $I_\nu = I_\nu^{cont} \exp(-\tau_\nu)$, to find

$$W_\lambda = \int_{\nu=0}^{\nu=\infty} \left[1 - \mathrm{e}^{-\tau_\nu}\right] \frac{c}{\nu^2}\, d\nu. \tag{6.3}$$

Note that this is the optical depth of the $1 \longrightarrow 2$ transition, and so τ_ν here is a narrow function centered on $\nu = \nu_{12}$.

Since the optical depth governs the strength of the line, it is convenient to define the integrated optical depth of the line:

$$\tau_{12} = \int_{\nu=0}^{\nu=\infty} \tau_\nu\, d\nu. \tag{6.4}$$

From the definition of the optical depth in terms of the absorption coefficient, this becomes

$$\tau_{12} = \int_{\nu=0}^{\nu=\infty} \int_s \alpha_\nu\, ds\, d\nu = \int_s n_1 \left[\int_{\nu=0}^{\nu=\infty} \frac{\alpha_\nu}{n_1} d\nu\right] ds = \sigma_{12} \int_s n_1 ds = N_1\, \sigma_{12}, \tag{6.5}$$

where

$$\sigma_{12} = \int_{\nu=0}^{\nu=\infty} \sigma_\nu\, d\nu = \int_{\nu=0}^{\nu=\infty} \frac{\alpha_\nu}{n_1}\, d\nu, \tag{6.6}$$

is the cross-section of the line and N_1 is the *column density*. This is the number of absorbing particles along the path length per unit area. For example, if a beam from a background source passes a distance s through an absorbing cloud, and the $1 \longrightarrow 2$ transition refers to hydrogen, then N_1 is the number of ground state hydrogen atoms per unit area in the cloud along a path length s.

From the above equations, we see that if we measure the EW of an absorption line, we can use this to measure the column density of the absorbing atom/ion – but only if we know the cross-section of the line. We therefore need to calculate the theoretically expected line cross section.

6.3 Line cross section

In order to calculate the line cross section, let's return to our model for the 2-level atom. Recall that the net rate of electrons per unit volume being excited from level 1 to level 2 due to absorption is

$$\text{Excitation rate per unit volume} = \left[n_1 B_{12} - n_2 B_{21}\right] \int u_\nu \phi(\nu) d\nu, \tag{6.7}$$

where B_{12} represents absorption, B_{21} represents stimulated emission the energy density is related to the specific intensity as

$$u_\nu = \frac{1}{c} \int I_\nu d\Omega, \tag{6.8}$$

and $\phi(\nu)$ is the line profile – a narrow function centered at $\nu = \nu_{12}$. Most of the time we've been thinking about this as a $\delta-$function, but let's keep things nice and general for the time being.

Since each excitation leads to photons transferring energy $h\nu$ to a ground state electron, the energy taken out of the beam by a volume dV of absorbing material in a time interval dt and frequency interval $d\nu$, is:

$$dE = h\nu \; u_\nu \; [n_1 B_{12} - n_2 B_{21}]\phi(\nu) dt \; dV \; d\nu. \tag{6.9}$$

Subbing in the above expression for u_ν gives

$$\frac{dE}{d\Omega} = h\nu \; \frac{I_\nu}{c} \; [n_1 B_{12} - n_2 B_{21}]\phi(\nu) dt \; dV \; d\nu, \tag{6.10}$$

and expressing the volume element in terms of an area element and a path length element, $dV = dA \; ds$, allows us to calculate the reduction in the specific intensity of the beam due to absorption

$$-dI_\nu = \frac{dE}{dA dt d\nu d\Omega} = h\nu \; \frac{I_\nu}{c} \; [n_1 B_{12} - n_2 B_{21}]\phi(\nu) \; ds. \tag{6.11}$$

We can then calculate the absorption coefficient, α_ν, from $dI_\nu = -\alpha_\nu \; I_\nu \; ds$:

$$\alpha_\nu = \frac{h\nu}{c} \; [n_1 B_{12} - n_2 B_{21}]\phi(\nu). \tag{6.12}$$

Finally, we can calculate the line cross section

$$\sigma_{12} = \int \frac{h\nu}{c} \; [B_{12} - \frac{n_2}{n_1} B_{21}]\phi(\nu) d\nu \approx \frac{h\nu_{12}}{c} \; [B_{12} - \frac{n_2}{n_1} B_{21}], \tag{6.13}$$

and the line optical depth trivially follows: $\tau_{12} = N_1 \sigma_{12}$.

So we can calculate the line cross section in terms of the Einstein B coefficients, but now we need to know how to calculate the B coefficients from quantum mechanics!

6.4 Einstein B coefficients: oscillator strength

First, we can derive the relationship between B_{12} and B_{21} by looking at the limit of TE (just as we did for the C coefficients). This gives:

$$B_{21} = \frac{g_1}{g_2} B_{12}, \tag{6.14}$$

(see Appendix for the derivation). The line cross section therefore becomes

$$\sigma_{12} = \sigma_{abs} \left[1 - \frac{n_2}{n_1} \frac{g_1}{g_2} \right], \tag{6.15}$$

where the integrated atomic absorption cross section is

$$\sigma_{abs} = \int \frac{h\nu}{c} B_{12} \phi(\nu) \; d\nu \approx \frac{h\nu_{12}}{c} B_{12}. \tag{6.16}$$

We therefore need to know the level populations in order to calculate σ_{12}. In general though, we don't know n_2/n_1. One regime in which we *do* know n_2/n_1 is in TE – in that case, n_2/n_1 is simply given by the Boltzmann distribution:

$$\frac{n_1}{n_2} = \frac{g_1}{g_2} \exp\left[\frac{h\nu_{12}}{kT_e}\right]. \tag{6.17}$$

It is therefore useful to express the energy levels in terms of *departure coefficients*, such that

$$\frac{n_2}{n_1} = \frac{b_2}{b_1}\frac{g_1}{g_2} \exp\left[\frac{h\nu_{12}}{kT_e}\right]. \tag{6.18}$$

Clearly in TE, $b_2/b_1 = 1$, and out of TE, $b_2/b_1 \neq 1$. We can now write out our expression for the line cross section

$$\sigma_{12} = \sigma_{abs}\left[1 - \frac{b_2}{b_1}\mathrm{e}^{-h\nu_{12}/kT_e}\right]. \tag{6.19}$$

Now we only need to know how to calculate σ_{abs} from quantum mechanics! It is useful to express the absorption coefficient in terms of the absorption *oscillator strength*, f_{12}:

$$B_{12} = \frac{\pi e^2}{m_e h\nu_{12}} f_{12} \tag{6.20}$$

where e is the electron charge and m_e is the electron mass. Therefore

$$\sigma_{abs} = \frac{\pi e^2}{m_e c} f_{12}, \tag{6.21}$$

and we can simply look up the oscillation strength for a given excitation in a book (e.g. Astrophysical Quantities by C W Allen or the NIST database).

6.5 Limiting cases

We can now calculate the line EW in terms of the column density N_1, the absorption oscillator strength, f_{12}, and the departure coefficients, b_2/b_1. As always, it is instructive to look at a few limiting cases.

Optically thin (weak) lines at short wavelengths

In this case, $\tau_\nu << 1$, and therefore we can Taylor expand the exponential in the expression for the EW,

$$W_\lambda = \int_{\nu=0}^{\nu=\infty} \left[1 - \mathrm{e}^{-\tau_\nu}\right] \frac{c}{\nu^2}\, d\nu, \tag{6.22}$$

to get

$$W_\lambda \approx \int_{\nu=0}^{\nu=\infty} \tau_\nu \frac{c}{\nu^2}\, d\nu \approx \frac{\lambda_{12}^2}{c}\,\tau_{12} = \frac{\lambda_{12}^2}{c}\, N_1\sigma_{12}. \tag{6.23}$$

For lines at optical / UV (or even shorter) wavelengths, we have $h\nu_{12} >> kT_e$, and so the exponential in the expression for σ_{12} becomes very small. We can therefore simply write

$$\sigma_{12} = \sigma_{abs}. \tag{6.24}$$

Therefore, in the case of weak (i.e. not saturated) optical lines, the EW is *linearly* related to the column density

$$W_\lambda = \frac{\lambda_{12}^2}{c} N_1 \frac{\pi e^2}{m_e c} f_{12}. \tag{6.25}$$

We can therefore measure the column density of, say, hydrogen by measuring the equivalent width of hydrogen absorption lines (recall we should only really see Lyman series lines in absorption because cold hydrogen is mostly in the ground state) and applying the formula

$$N_1 = \frac{m_e c^2}{\pi e^2} \frac{W_\lambda}{f_{12}\lambda_{12}^2}, \tag{6.26}$$

which becomes

$$\left(\frac{N_1}{\mathrm{cm}^{-2}}\right) = 1.13 \times 10^{17} \frac{(W_\lambda/\mathrm{m\mathring{A}})}{f_{12}(\lambda_{12}/\mathring{A})^2}. \tag{6.27}$$

Lines at long wavelengths

For IR - radio lines, which have $h\nu_{12} << kT_e$, $\sigma_{12} \neq \sigma_{abs}$, but we can instead Taylor expand the exponential in our equation for σ_{12} to get

$$\sigma_{12} \approx \sigma_{abs} \left[1 - \frac{b_2}{b_1}\left(1 - \frac{h\nu_{12}}{kT_e}\right)\right]. \tag{6.28}$$

Therefore, stimulated emission can reduce the strength of absorption lines with long wavelengths. In fact, in some extreme cases we can get *population inversion*, whereby

$$\frac{b_2}{b_1} > \frac{1}{1 - h\nu_{12}/kT_e}. \tag{6.29}$$

In this case, we actually have $n_2/n_1 > 1$, leading to net *negative* absorption! So in this case, the absorption line is actually an emission line. Such anti-absorption lines occur in the microwave and radio spectra of masers, mostly in diatomic molecules such as OH and SIO. We will not be covering molecular lines in this course, but the concept is the same: population inversion leads to the absorption line actually being in emission.

Masers can be extremely useful astrophysically because the produce very strong emission lines. Fig 6.2 shows an example of OH maser lines in the galaxy Arp 220. The rest frame frequencies of these lines are 1665 MHz and 1667 MHz, but they have been redshifted by bulk velocity of the gas, and also broadened by the velocity dispersion of the gas. These strong lines can be used to accurately map out the velocity of gas in galaxies.

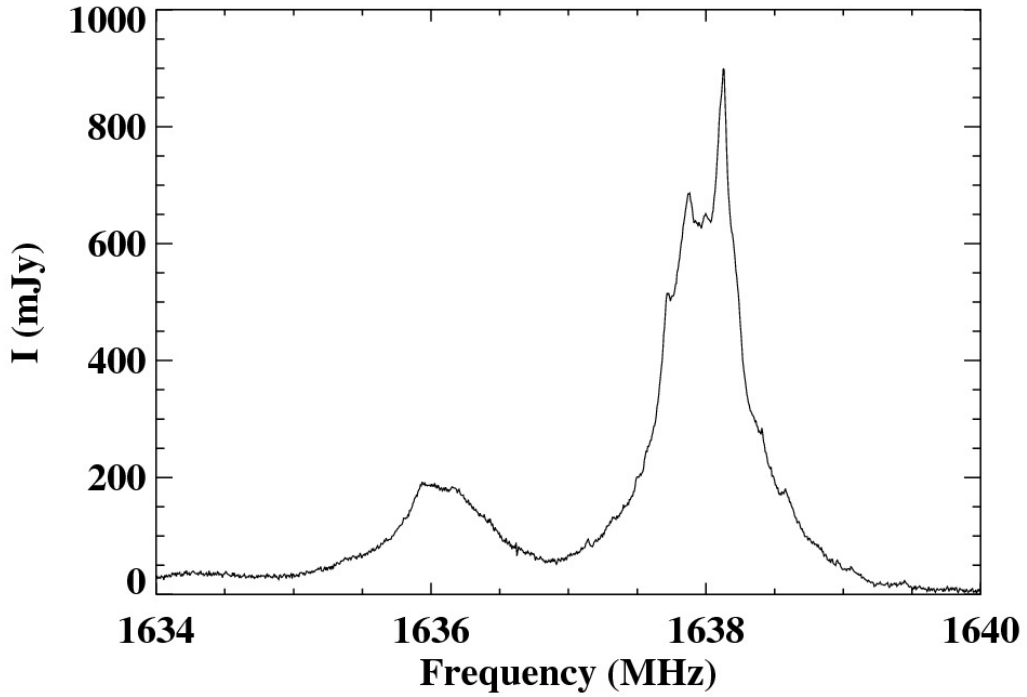

Figure 6.2: OH maser emission from Arp 220. The lines shown are the 1665 and 1667 MHz transitions, which have been redshifted to lower frequency. The data shown here were acquired using the Arecibo observatory.

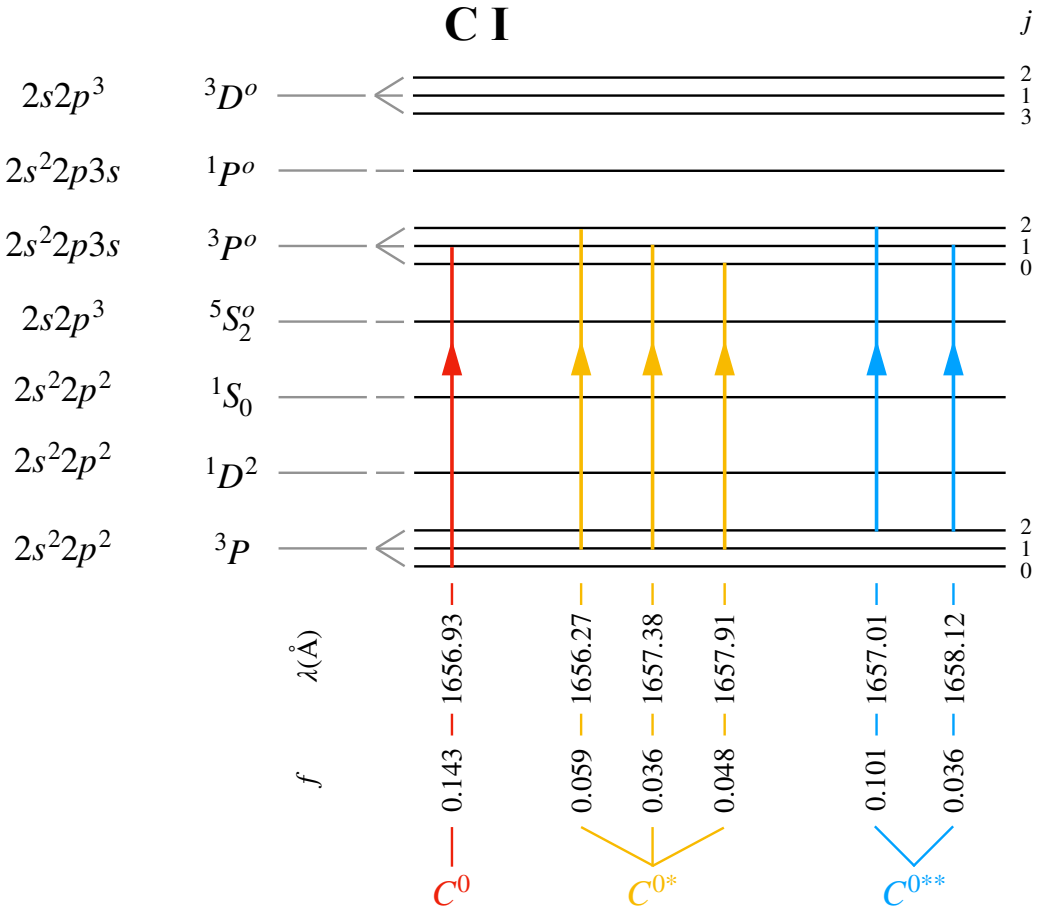

Figure 6.3: Energy levels of a neutral carbon atom.

6.6 Excitation temperature

We can estimate the temperature of the gas imprinting absorption lines onto an observed spectrum by comparing the EWs of different lines from the same atom/ion. Since most absorbing atoms are in their ground state, atoms in which multiple lines originate from a split ground state are particularly useful. If these lines are at optical/UV rest frame wavelengths and are optically thin, then even better: we can use Equation 6.25 to calculate the EWs of lines from the lower / upper ground state (level 1 / 2) to the excited state (level 3), and approximate the level populations with the Boltzmann formula, to get:

$$\frac{W_{\lambda_{23}}}{W_{\lambda_{13}}} = \left(\frac{\lambda_{23}}{\lambda_{13}}\right)^2 \frac{f_{23}}{f_{13}} \frac{g_2}{g_1} e^{-\Delta E_{12}/kT_e}. \tag{6.30}$$

The resulting temperature estimate is called the *excitation temperature*.

A good example of an atom with a split lower level is neutral carbon (CI). Fig 6.3 shows the energy levels of CI. The ground state ^3P is a triplet, and there are multiple transitions up to the $^3P^o$ level (the "o" meaning odd parity – note the $^3P \rightarrow ^3P^o$ transition is essentially one electron transitioning from $n = 2$, $\ell = 1$ to $n = 3$, $\ell = 0$), all with very similar wavelengths and fairly similar oscillator strengths (see the figure). Transitions from the $^3P_0$, $^3P_1$ and $^3P_2$ states are called C^0, C^{0*} and C^{0**} respectively. If we can measure the equivalent widths of all of these different lines in the $\lambda \approx 1657\mathring{A}$ region, then we can use the above formula to get two estimates of the excitation temperature by comparing the EW of the C^0 line with the combined EWs of the C^{0*} lines, and also with the combined EWs of the C^{0**} lines.

An example of an observed spectrum with CI absorption lines is shown in Fig 6.4. The continuum is from a distant quasar PKS 1232+0815, at redshift $z = 2.33771$, and the lines are imprinted by a cool cloud of gas in the line of sight, in this case fairly close to the quasar itself. The original measurement of the excitation temperature of these lines in 2000 was very important because it provided the first direct observational confirmation of a very fundamental cosmological prediction: that the cosmic microwave background (CMB) cools over time as the Universe expands. This is possible because the gas in the ISM is excited by CMB photons, and so the excitation temperature gives an estimate of the CMB temperature at the redshift of the gas. Specifically, we expect the CMB temperature to go as $T_{CMB}(z) = (1 + z)T_{CMB}(z = 0)$, where $T_{CMB}(z = 0) = 2.726$ K is the CMB temperature today. For one of the homework problems, you will use the column densities of the C^0, C^{0*} and C^{0**} lines measured by Srianand et al (2000) et al from the spectrum shown in Fig 6.4 to estimate $T_{CMB}(z = 2.3)$.

6.7 Curve of Growth

We already know that for optically thin lines, $W_\lambda \propto N_1$. To extend this relation to intermediate and large optical depths, we must appreciate that the observed line can be broadened by two main mechanisms:

1. By Doppler shifts due to motions of the absorbing atoms/ions,

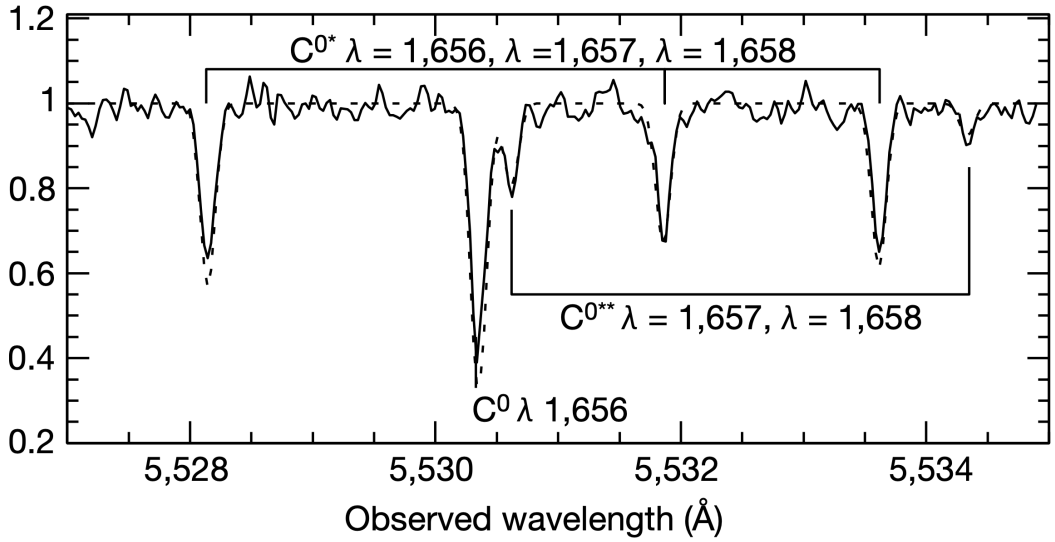

Figure 6.4: C^0, C^{0*} and C^{0**} absorption lines seen in the spectrum of the $z = 2.33771$ quasar PKS 1232+0815. From Srianand, Petitjean & Ledoux (2000), Nature.

2. 'Natural' broadening due to the Heisenberg uncertainty principle.

As for the first process: if the ion is travelling with a velocity v towards the observer, then the observed frequency of the line from that ion will be shifted by the Doppler effect:

$$\nu_{obs} = \nu_{em}\left(1 + \frac{v}{c}\right). \tag{6.31}$$

The ions are all travelling in different directions with different speeds and so we will see a distribution of different Doppler shifts. If the variance of line of sight velocities is σ^2 (the *velocity dispersion*), then the line profile is

$$I_\nu = I_\nu^{cont} \exp\left[-\tau_{12} g(\nu)\right], \tag{6.32}$$

where

$$g(\nu) = \exp\left(-\frac{(\nu - \nu_{12})^2}{2(\sigma\nu_{12})^2}\right), \tag{6.33}$$

is a Gaussian function and ν_{12} is the rest frame frequency of the line. The velocity dispersion can be a combination of thermal motions and turbulence, $\sigma^2 = kT_{ion}/(m_{ion}c^2) + \sigma^2_{turb}$.

Fig 6.5 shows how the resulting line profile changes as the optical depth increases (here, τ_{12} is increasing from 1 to 10 in steps of 1 and I arbitrarily assumed $\sigma = 10^{-2}$). We see that the line EW, as expected, grows linearly for low optical depth, but at $\tau_{12} \sim 5$ the line core saturates, and so doubling the number of ions in the line of sight suddenly doesn't double the equivalent width of the line anymore (note how close e.g. the $\tau_{12} = 9$ and $\tau_{12} = 10$ lines are to each other). The line EW can only grow by the flux in the wings getting lower.

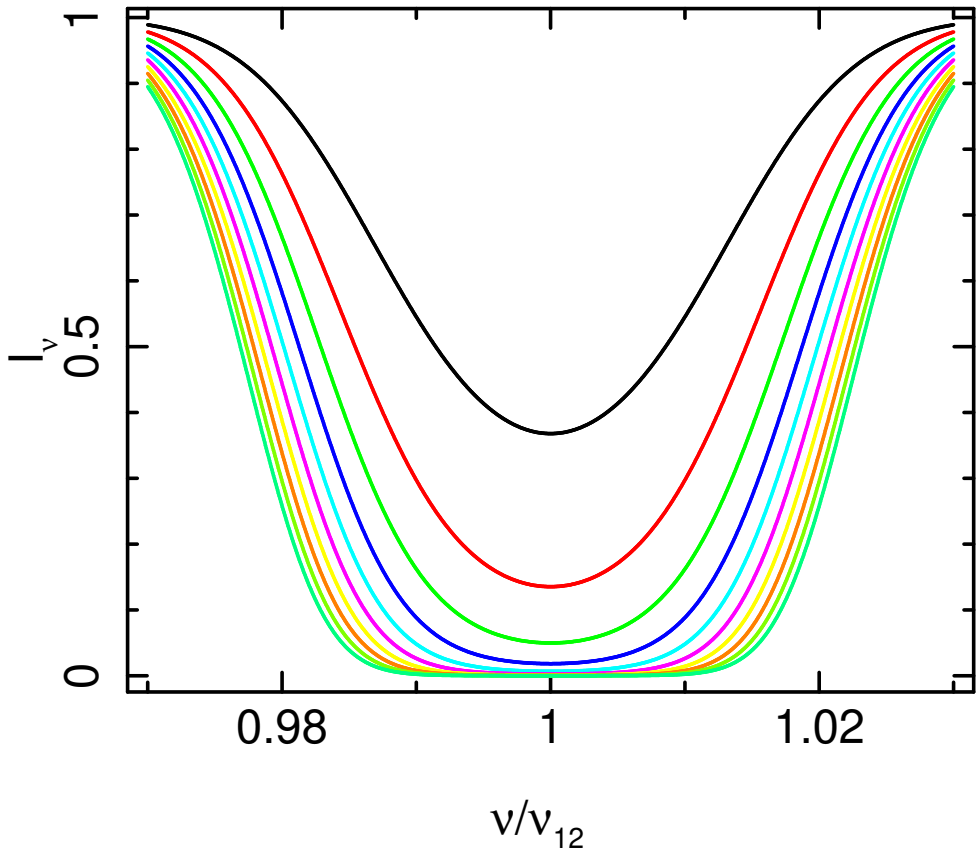

Figure 6.5: Absorption line profile broadened by Gaussian mechanisms ($\sigma = 10^{-2}$) for 10 different optical depths: $\tau_{12} = 1$ (top), $\tau_{12} = 10$ (bottom), intermediate lines are in steps of $\Delta\tau_{12} = 1$.

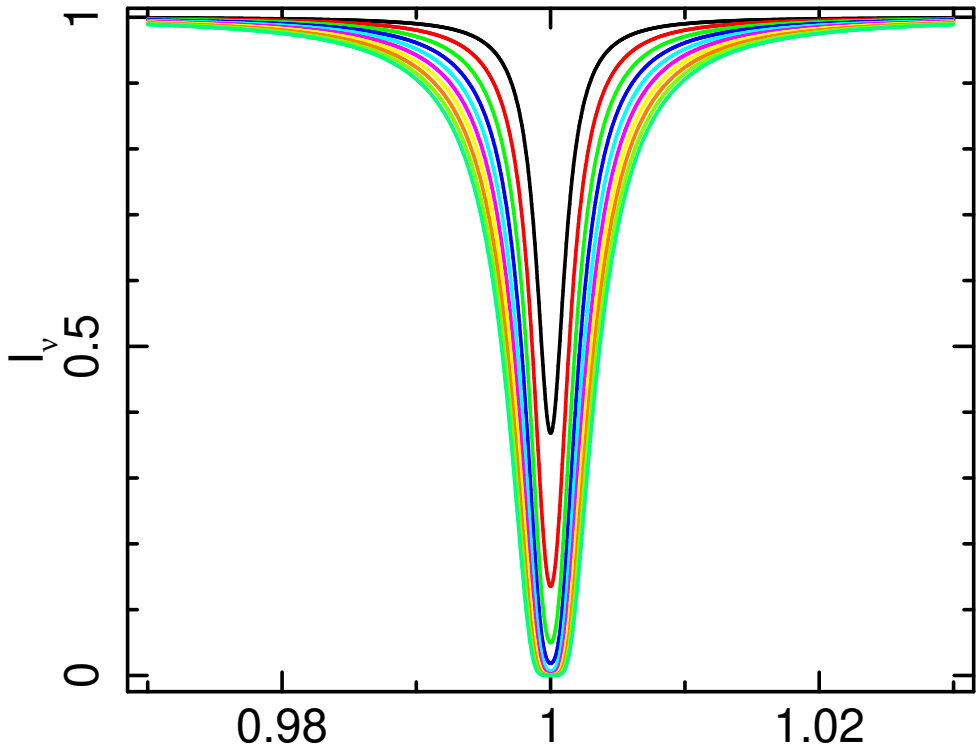

Figure 6.6: Absorption line profile broadened by Lorentzian mechanisms ($\Delta = 10^{-3}\nu_{12}$) for 10 different optical depths: $\tau_{12} = 1$ (top), $\tau_{12} = 10$ (bottom), intermediate lines are in steps of $\Delta\tau_{12} = 1$.

The uncertainty principle does not broaden the line into a Gaussian profile, but into a *Lorentzian* profile:

$$\ell(\nu) = \frac{\Delta^2}{(\nu - \nu_0)^2 + \Delta^2}, \tag{6.34}$$

where Δ is the half width at half maximum. The line profile in the absence of any Doppler broadening is therefore $I_\nu \propto \exp[-\tau_{12}\ell(\nu)]$. Fig 6.6 shows the resulting line profile for the same 10 values of optical depth as before (I arbitrarily assumed $\Delta = 10^{-3}\nu_0$). We see that the Lorentzian function has a narrow core and broad lines. This means that it does not saturate until the optical depth is huge, and when it does saturate, the broad wings means that the EW keeps on growing as τ_{12} increases.

These two processes combine via a convolution (Voigt profile). The relation between column density and line EW for this combined profile, known as the *curve of growth*, is shown in Fig 6.7. We see 3 regimes:

Low optical depths: $W_\lambda \propto N_1$, as expected.

Intermediate optical depths: $W_\lambda \propto \sqrt{\ln(N_1)}$, as the core of the Gaussian component becomes saturated and so it is difficult to grow the EW by adding more column density.

High optical depths: $W_\lambda \propto \sqrt{N_1}$. Eventually, the line becomes so saturated that the wings of the Lorentzian become important, and the EW grows as a steeper function of N_1.

6.8 The ISM and IGM

Gas associated with galaxies is called the interstellar medium (ISM), and gas outside of galaxies is called the intergalactic medium (IGM). Absorption lines imprinted on the spectra of background light sources can be used to measure the properties of the ISM and IGM.

6.8.1 The Lyman alpha forest

The Lyman α forest is a huge number of absorption lines seen in the spectra of very distant galaxies and quasars. Fig 6.8 shows an example: The spectrum of a $z = 3.63$ quasar has many absorption lines imprinted onto it by gas at lower redshifts. The broad emission lines, including Lyman α at $\lambda = 3.63 \times 1216\mathring{A} = 6562.8\mathring{A}$, are from the quasar itself. The vast majority of these absorption lines are Lyman α lines (rest frame wavelength $\lambda_{Ly\alpha} = 1216\mathring{A}$) imprinted by clouds of H I gas at different redshifts, and the higher column density clouds also imprint higher order Lyman series lines at shorter wavelengths. Fig 6.9 demonstrates that we can in principle use the number of lines and the column density of each line to reconstruct the number and density of clouds as a function of redshift. The observations show that the number of clouds increases as a function of redshift, which is nicely explained by the expansion of the Universe. The number of clouds at redshifts approaching that of the quasar is actually seen to drop off (*the proximity effect*). This is because the quasar ionizes the gas in its direct vicinity, thus reducing the H I column density of these clouds. In cosmological models, these clouds are actually sheets and filaments in the cosmic web (see Fig 6.10), either associated with galaxies (ISM) or not (IGM).

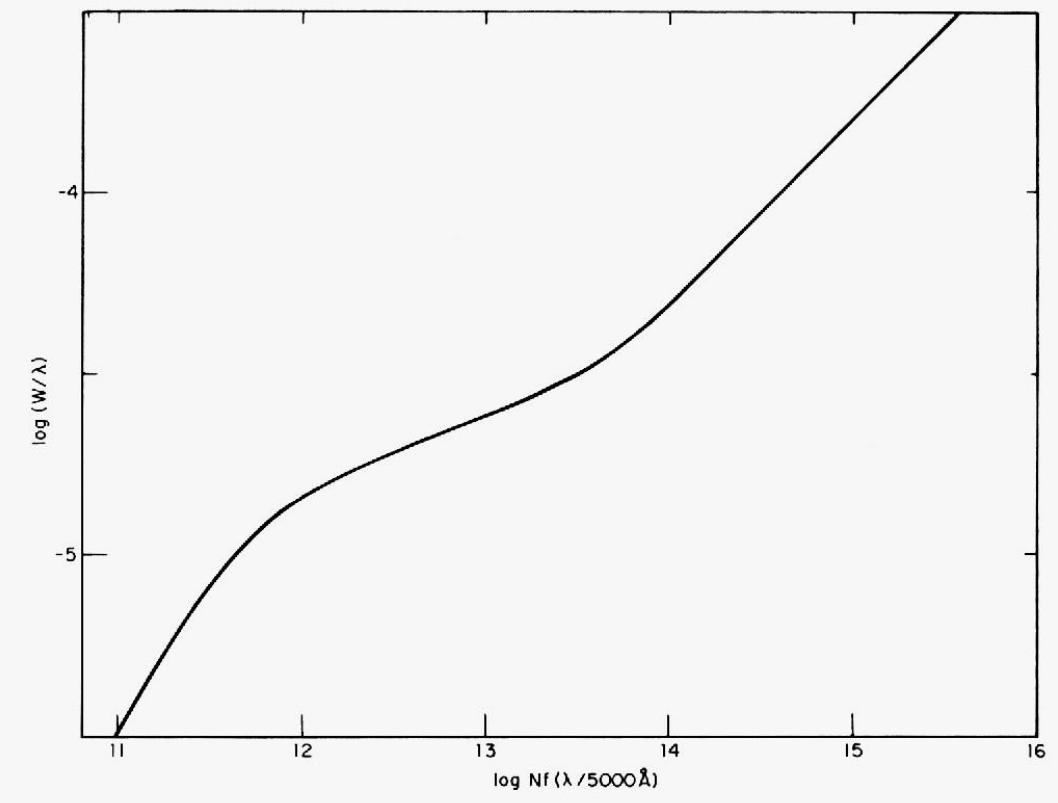

Figure 6.7: Curve of growth: EW as a function of column density. From Aller, 'Atoms, Stars and Nebulae' (1971).

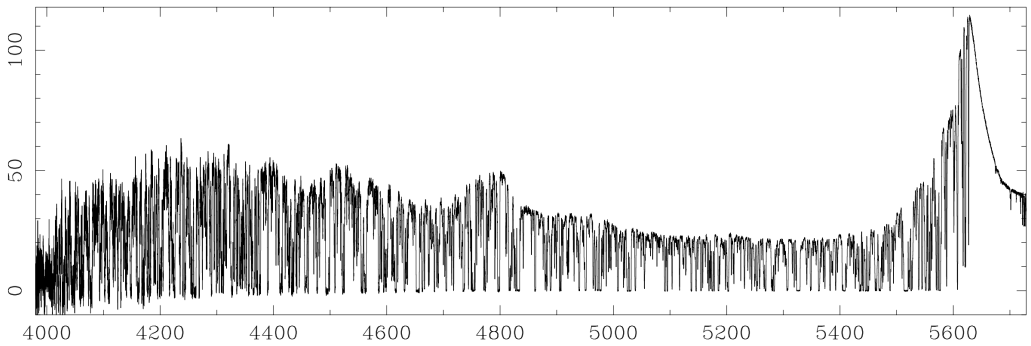

Figure 6.8: Spectrum of a $z = 3.63$ quasar (x-axis is wavelength in Angstroms) with a 'forest' of Lyman series of absorption lines imprinted by gas clouds at a range of redshifts, all lower than the redshift of the background quasar.

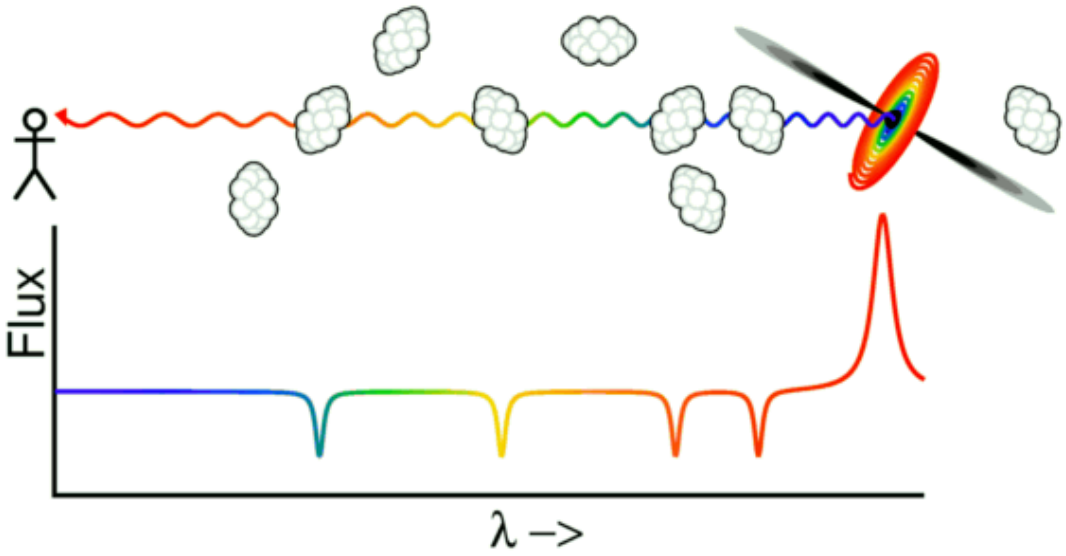

Figure 6.9: Schematic representation of the Lyman α forest: clouds at different distances from us imprint Lyman series absorption lines on the spectrum with different redshifts.

Figure 6.10: A computer simulation of a possible Lyman α forest configuration at $z = 3$ (Shalf et al 2000).

In addition to Lyman series absorption lines, the observed spectrum also drops-off sharply at a rest frame wavelength of 912$\mathring{A}$. This is called the Lyman limit, and photons at this or shorter wavelengths can ionize neutral hydrogen (i.e. $hc/\lambda > 13.6$ eV). Since the ionization cross-section of hydrogen is so high, the Universe is opaque to photons just bluer than the Lyman limit (recall that the cross-section drops off as ν^{-3}, so the Universe is transparent to soft X-rays and even shorter wavelengths).

6.8.2 The Gunn-Peterson Trough

Since the epoch of reionization, most of the hydrogen in the Universe has been ionized. This means that the H I column density of clouds intercepted after reionization is quite low (i.e. most of the hydrogen is H II). We still see the Lyman α forest absorption lines though because the cross section of Lyman α is huge – and so only a small column density of material is needed for a line to be observable. If we were to see photons that were emitted from a quasar *before* the end of the epoch of reionization, those photons would have travelled through a *huge* H I column on their way to us, since the ionization fraction of hydrogen back then was so much lower. The Lyman α lines imprinted on the spectrum at this time would therefore be so saturated that they would completely blend together, leaving no flux at all in the portion of the spectrum covered by the lines. If the portion of the spectrum covered by these lines stretches all the way down to the Lyman limit at the redshift of the quasar, then we would see no flux at all blueward of the most redshifted Lyman α absorption line. This is called the *Gunn-Peterson trough*.

The first observational confirmation of the Gunn-Peterson trough is shown in Fig 6.11. This is from Becker et al (2001) using data from the Sloan Digital Sky Survey (SDSS). The three quasars at $z < 6$ show strong absorption lines blueward of $\lambda = z\lambda_{Ly\alpha}$, but there are still some spikes in flux. For the $z > 6$ quasar, however, the flux at wavelengths shorter than $\lambda = z\lambda_{Ly\alpha}$ is ~zero. This confirms that the epoch of reionization ended at $z \sim 6$.

The sharp drop-off in flux caused by the Lyman limit and/or Gunn-Peterson trough provides a way to search for high redshift galaxies and quasars. The *drop-out technique* consists of searching for sources that are visible at longer wavelengths but suddenly disappear at shorter wavelengths (see Fig 6.12). Typically, candidates are identified using photometry and then later confirmed by spectroscopic follow up.

6.9 Appendix: relation between Einstein coefficients

In TE, there is detailed balance:

$$n_1 B_{12} u_{\nu_{12}} = n_2 A_{21} + n_2 B_{21} u_{\nu_{12}}, \tag{6.35}$$

where we have gone back to approximating $\phi(\nu) = \delta(\nu - \nu_{12})$ because life is too short! Re-arranging the above equation, we find

$$u_{\nu_{12}} = \frac{A_{21}/B_{21}}{(n_1/n_2)(B_{12}/B_{21}) - 1}. \tag{6.36}$$

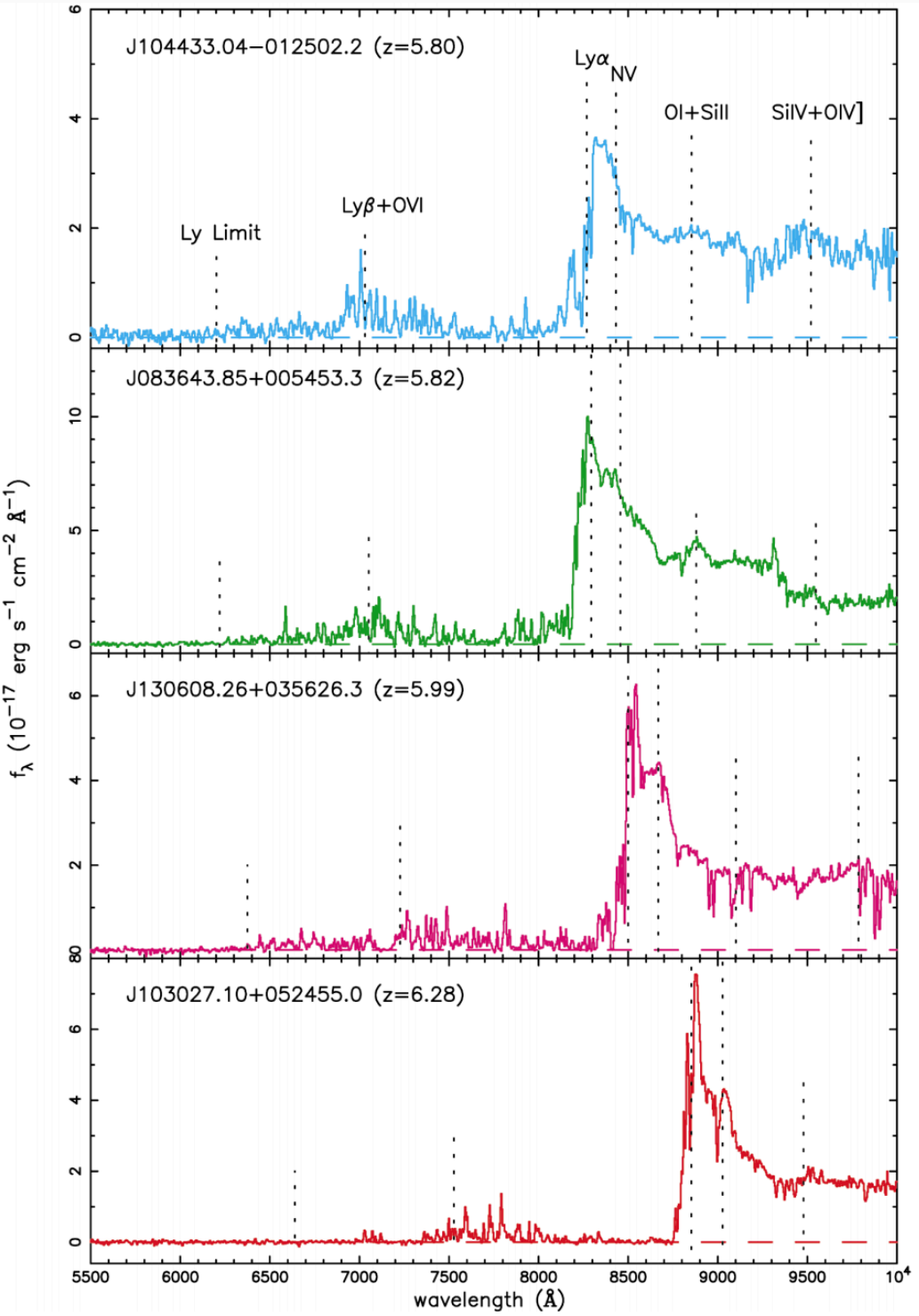

Figure 6.11: Spectra of four SDSS quasars from Becker et al (2001). The highest redshift quasar has essentially no flux at wavelengths below that of the highly redshifted Lyman α line (marked by a dashed line). This is the first observational confirmation of the Gunn-Peterson trough.

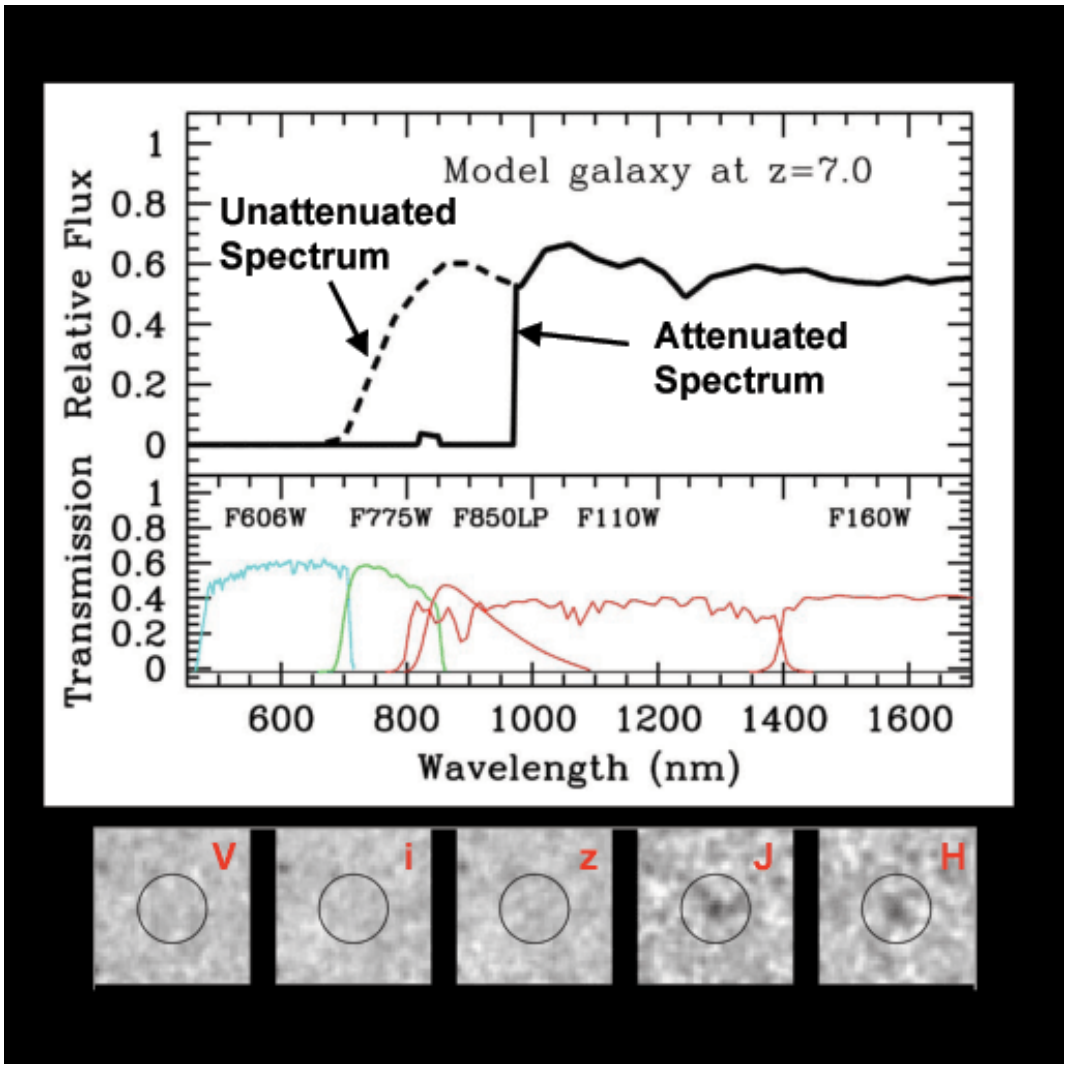

Figure 6.12: Illustration of the drop-out technique to discover distant galaxies and quasars. A high redshift galaxy can be seen in some photometry filters but not in others.

In TE, the levels follow the Boltzmann distribution:

$$\frac{n_1}{n_2} = \frac{g_1}{g_2} \exp\left[\frac{h\nu_{12}}{kT_e}\right], \tag{6.37}$$

giving

$$u_{\nu_{12}} = \frac{A_{21}/B_{21}}{(g_1/g_2)(B_{12}/B_{21})\exp(h\nu_{12}/kT_e) - 1}. \tag{6.38}$$

In thermal equilibrium, we also have $I_\nu = B_\nu$, meaning that

$$u_{\nu_{12}} = 4\pi \frac{2h\nu_{12}^3/c^3}{\exp(h\nu_{12}/kT_e) - 1} \tag{6.39}$$

for isotropic emission. The above two equations need to equal each other for *all* values of T_e, meaning

$$(g_1/g_2)(B_{12}/B_{21}) = 1, \tag{6.40}$$

and

$$\frac{A_{21}}{B_{21}} = \frac{8\pi h\nu_{12}^3}{c^3}. \tag{6.41}$$

We therefore have our desired relation between the absorption and stimulated emission coefficients

$$B_{21} = \frac{g_1}{g_2} B_{12}. \tag{6.42}$$

7 Stellar Spectroscopy

7.1 Introduction

In this Lecture we will learn about radiative transfer in stars, using a lot of what we've learned so far about the radiative transfer equation, blackbody radiation, and absorption lines.

7.2 Stars

7.2.1 Basic Properties

Stars are extremely optically thick objects: a photon emitted in the core will be scattered / absorbed and re-emitted *many* times before finally leaving the star. For example, the mean free path of photons in the Sun is $\ell \sim 1$ cm (i.e. $\alpha \sim 1\text{cm}^{-1}$), and the radius of the Sun is $R_\odot = 6.957 \times 10^5$ km. A photon emitted in the core will follow a random walk to get out of the Sun, and so after N interactions it will cover a distance $R = \ell N^{1/2}$. Plugging the numbers in for the Sun gives $N \sim 10^{20}$.

The density and temperature peak in the core and drop off towards the surface (see Fig 7.1 and Fig 7.2). Since there is a temperature gradient, stars are not formally in TE, but the temperature gradient is small over a distance of ℓ and so the conditions of LTE are met. This means that the electron temperature is equal to the photon temperature throughout the stellar interior. The surface layer is called the *photosphere*: this is defined as the region where photons can stream freely out of the star and is $\sim 10 - 100$ km thick in the Sun (note that ℓ is much longer at $R \sim R_\odot$ than at $R \sim 0$ because the density is so much lower). Since photons can now escape, the photosphere is not in LTE; and since the photosphere is cooler than the interior, it imprints absorption lines onto the thermal spectrum. Outside of the photosphere is a thin atmosphere (Fig 7.2, right). In the atmosphere, the electron temperature increases, but the photon temperature is the same as it was when the photons were emitted in the photosphere – i.e. the atmosphere is *far* from LTE. We see in the figure that the atmosphere consists of the *chromosphere* and the much hotter *corona*.

7.2.2 Spectral Classifications

Stars have a quasi-blackbody spectrum with absorption lines. Fig 7.3 shows the spectrum of the Sun: it has an effective temperature of $T_{\text{eff}} = 5,777$ K, with absorption lines imprinted onto it. The absorption lines are called Fraunhofer lines (after Joseph von Fraunhofer). Early on, it was noted that different stars had different patterns of absorption lines, and so stars were classified

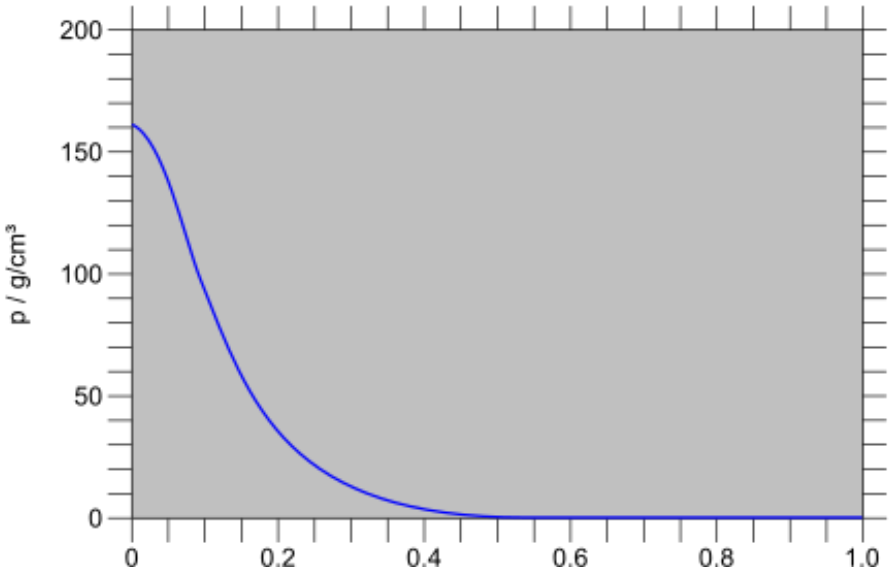

Figure 7.1: Density of the Sun as a function of radius. $R_s = R_\odot = 6.957 \times 10^5$ km.

by these patterns of lines. The spectra were not understood, so the names of the classification system are rather arbitrary. The spectral types are: O, B, A, F, G, K, M. The traditional mnemonic to remember this is Oh Be A Fine Girl Kiss Me, although this sounds very dated so perhaps we need a new one. We now know that the effective temperature (and therefore mass) decreases from class O to class M: T_{eff} goes from $\sim 40,000$ K in O stars to $\sim 1,500$ K in M stars.

There are further sub-divisions. Numbers 0-9 are appended as sub-divisions of effective temperature with 0 as the hottest, therefore the hottest type is O0 and the coolest is M9. Finally, a third Roman numeral, I-VII is appended to convey compactness, with I being the least dense and VII being the most dense. Compactness is often expressed in terms of surface gravity, $g = GM/R^2$, and we see from the definition that denser stars clearly have a higher surface gravity. Main sequence stars – otherwise known as dwarf stars – are of class V, whereas evolved giants and supergiants have a lower Roman numeral, and sub-dwarfs and white dwarfs are respectively VI and VII. The Sun is of spectral type G2V, in that its effective temperature falls in the G2 class, and it is a main sequence star.

7.3 Emergent Flux

Now let's use the radiative transfer equation to calculate the flux that we will see from different parts of a star's surface.

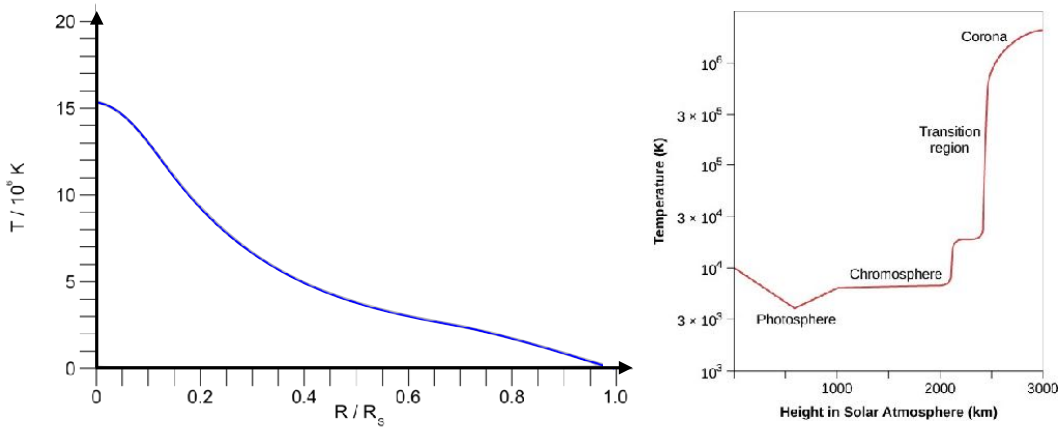

Figure 7.2: *Left:* Temperature of the Sun as a function of radius ($R_s = R_\odot = 6.957 \times 10^5$ km). The electron temperature is equal to the photon temperature because the interior of the Sun is in LTE. *Right:* Electron temperature of the Sun's atmosphere as a function of distance from the surface. The photon temperature is the same as that in the photosphere ($T \sim 5,800$ K).

7.3.1 Radial optical depth

Fig 7.4 illustrates that we observe light from a star along rays. These rays travel in straight lines that intersect the star, as shown. Until now, we have been defining the optical depth along the ray: the path for a given ray is $s' = 0$ at the back of the star to $s' = s$ at the front of the star, such that the ray goes from $\tau'_\nu = 0$ to $\tau'_\nu = \tau_\nu$. Even though this definition of the optical depth is very convenient for a plane-parallel geometry with the light ray travelling perpendicular to the surface, it is not very convenient for a star. This is because in a star we have spherical symmetry, and therefore α_ν and j_ν are both functions of R. It is therefore more convenient to re-define the optical depth as a *radial* optical depth:

$$d\tau_\nu = -\alpha_\nu dR, \tag{7.1}$$

such that the optical depth for a ray that travels from $R' = R$ to $R' = R_*$ is:

$$\tau_\nu(R) = -\int_{R_*}^{R} \alpha_\nu(R')\, dR' = \int_{R}^{R_*} \alpha_\nu(R')\, dR'. \tag{7.2}$$

Note that, as well as the new definition being radial, it also differs from the old definition in another way: it is defined *backwards*, such that $\tau_\nu = 0$ at the *surface* of the star. I will use this new definition of the optical depth for the entire lecture. It is a very useful quantity because it makes it easy to think about how far into a star we are looking.

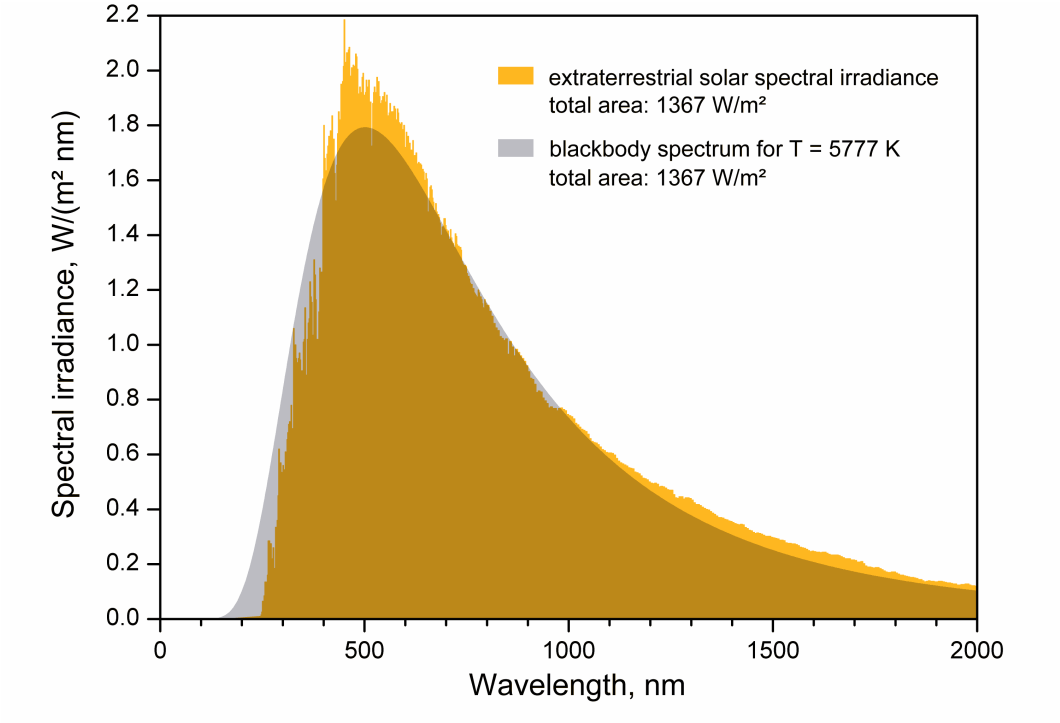

Figure 7.3: Spectrum of the Sun: a quasi-blackbody spectrum with $T_{\text{eff}} = 5,777$ K and absorption lines.

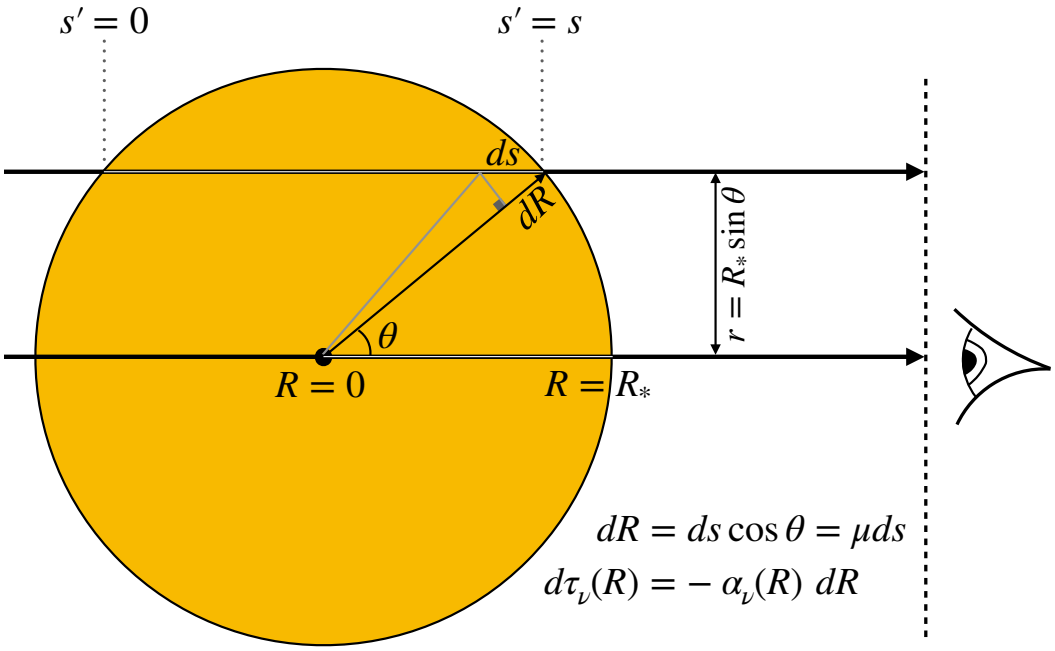

Figure 7.4: Schematic of light rays from a star travelling to the observer. The radial optical depth τ_ν tells us how far into the star we are seeing, so $\tau_\nu(R_*) = 0$.

We can now take the radiative transfer equation:

$$\frac{dI_\nu}{ds}(\mu, R) = j_\nu(R) - \alpha_\nu(R) I_\nu(\mu, R), \tag{7.3}$$

and re-express it in terms of our new definition of τ_ν. From the figure, we see that $ds = dR/\mu$, and so:

$$\mu\frac{dI_\nu}{dR}(\mu, R) = j_\nu(R) - \alpha_\nu(R) I_\nu(\mu, R). \tag{7.4}$$

Subbing in $d\tau_\nu = -\alpha_\nu dR$ then gives:

$$\mu\frac{dI_\nu}{d\tau_\nu}(\mu, \tau_\nu) = I_\nu(\mu, \tau_\nu) - S_\nu(\tau_\nu). \tag{7.5}$$

This is the version of the radiative transfer equation that we will solve for a star.

7.3.2 Formal solution

We already solved the radiative transfer equation in Lecture 2 using the old definition of optical depth. We can use the same method to solve with the new definition of optical depth. First, multiply Equation (7.5) by $e^{-\tau_\nu/\mu}$ to get:

$$e^{-\tau_\nu/\mu}\mu\frac{dI_\nu}{d\tau_\nu}(\mu, \tau_\nu) = e^{-\tau_\nu/\mu}\left[I_\nu(\mu, \tau_\nu) - S_\nu(\tau_\nu)\right]. \tag{7.6}$$

We can then use the product rule to show that:

$$\frac{d}{d\tau_\nu}\left[e^{-\tau_\nu/\mu} I_\nu(\mu, \tau_\nu)\right] = -\frac{S_\nu}{\mu} e^{-\tau_\nu/\mu}. \tag{7.7}$$

To solve, we now need to integrate *backwards* down the ray; i.e. following back from the observer to the star. To keep things general, let us integrate from τ_{out} to τ_{in}, such that $\tau_{in} > \tau_{out}$ because τ_{in} is deeper inside of the star than τ_{out}. This gives:

$$\left[I_\nu(t_\nu) e^{-t_\nu/\mu}\right]_{t_\nu=\tau_{out}}^{t_\nu=\tau_{in}} = -\int_{\tau_{out}}^{\tau_{in}} S_\nu(t_\nu) e^{-t_\nu/\mu} \frac{dt_\nu}{\mu}, \tag{7.8}$$

where t_ν is the dummy integration variable for optical depth. Re-arranging, we get:

$$I_\nu(\tau_{out}, \mu) = I_\nu(\tau_{in}, \mu) e^{-(\tau_{in}-\tau_{out})/\mu} + \int_{\tau_{out}}^{\tau_{in}} S_\nu(t_\nu) e^{-(t_\nu-\tau_{out})/\mu} \frac{dt_\nu}{\mu}. \tag{7.9}$$

Here, the two terms of the RHS can be interpreted as before. The first term is the intensity originating from inside of τ_{in}, decreased by absorption along the path of the ray from τ_{in} to τ_{out}. The second term is the contribution from emission along the path, also decreased by absorption.

7.3.3 Eddington-Barbier Relation

Let's take our formal solution to the radiative transfer equation and apply it to a star. For a ray that travels from deep within the star, $\tau_{in} = \infty$, all the way to the surface, $\tau_{out} = 0$, to then be measured by the observer, the solution becomes:

$$I_\nu(0, \mu) = \int_0^\infty S_\nu(t_\nu) e^{-t_\nu/\mu} \frac{dt_\nu}{\mu}. \tag{7.10}$$

We see that the emergent intensity, perhaps unsurprisingly, depends critically on the source function $S_\nu(\tau_\nu)$. We do not know *a priori* what the τ_ν dependence of the source function is, but we know that it increases with τ_ν because we know that the temperature increases as we go deeper into the star. We can approximate the source function by Taylor expanding around $\tau_\nu = 0$ and only keeping linear terms to get

$$S_\nu(\tau_\nu) = a_\nu + b_\nu \tau_\nu. \tag{7.11}$$

I will justify this assumption a little more later, but for now we can look at our equation for the emergent intensity and realize that it is a weighted average of the source function at different optical depths. This weighted average is *dominated* by the small optical depths. Another way of putting it is that we don't expect to be able to see far into the star, in that the photons that we detect were very likely emitted from $\tau \lesssim 1$ (recall that $\tau \sim 1$ corresponds to the mean free path of photons in the medium). It is therefore a good approximation to consider S_ν in the small τ_ν limit.

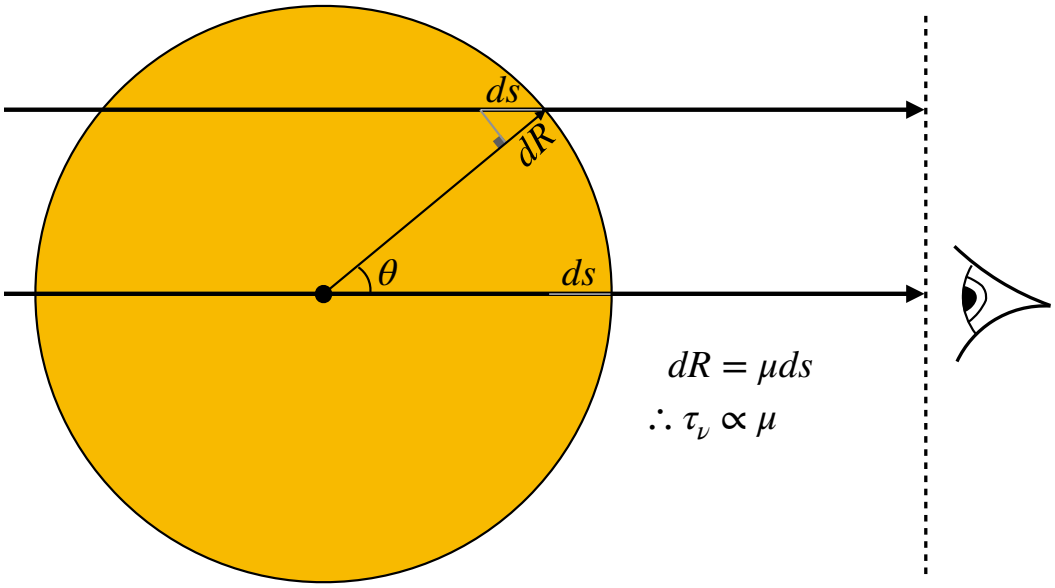

Figure 7.5: Schematic demonstrating that we always see the same path length into a star, therefore we the depth we see into the star depends on θ.

Subbing our linear approximation of the source function into the equation for the emergent specific intensity gives:

$$I_\nu(0,\mu) = \int_0^\infty [a_\nu + b_\nu t_\nu]\, \mathrm{e}^{-t_\nu/\mu} \frac{dt_\nu}{\mu}, \tag{7.12}$$

which becomes

$$I_\nu(0,\mu) = a_\nu + b_\nu \mu. \tag{7.13}$$

We therefore see that:

$$I_\nu(0,\mu) = S_\nu(\tau_\nu = \mu). \tag{7.14}$$

This is the *Eddington-Barbier relation*. It says that the specific intensity we see is just the source function at an optical depth of $\tau_\nu = \mu$. Therefore, for the sight line that intersects the centre of the star, we see the source function at $\tau_\nu = 1$. On the other hand, sight lines that intersect the limb (i.e. the very outside of the star) only see down to $\tau_\nu = 0$. This is demonstrated schematically in Fig 7.5: if we always see the same path length ds into the star, then the depth dR we see into the star is $dR = \mu ds$. This means that we always see down to a depth of $\tau_\nu/\mu = 1$.

For most stars, we just see the integrated flux and therefore cannot resolve out the specific intensity at different angular separations from the centre. It therefore makes sense to calculate

the integrated emergent flux from the entire surface of the star by integrating over solid angle:

$$F_\nu = 2\pi \int_0^1 I_\nu(0,\mu)\mu d\mu \tag{7.15}$$

$$= 2\pi \int_0^1 \left[a_\nu \mu + b_\nu \mu^2\right] d\mu \tag{7.16}$$

$$= 2\pi \left\{ a_\nu \left[\frac{\mu^2}{2}\right]_0^1 + b_\nu \left[\frac{\mu^3}{3}\right]_0^1 \right\} \tag{7.17}$$

$$F_\nu = \pi \left\{ a_\nu + \frac{2}{3} b_\nu \right\}. \tag{7.18}$$

Therefore the *average* emergent specific intensity is $I_\nu = F_\nu/\pi = a_\nu + 2b_\nu/3$, and so

$$I_\nu = S_\nu(\tau_\nu = 2/3). \tag{7.19}$$

Therefore, on average we see down to an optical depth of $\tau_\nu = 2/3$.

7.3.4 The Grey Atmosphere

Further intuition can be gained from a simplifying case in which we ignore the frequency dependence of α_ν. This is called the *grey atmosphere approximation*. The solution to the radiative transfer equation for a ray in the star travelling from $t = \infty$ to $t = \tau$ now becomes

$$I(\tau,\mu) = \int_\tau^\infty S(t) \mathrm{e}^{-(t-\tau)/\mu} \frac{dt}{\mu}. \tag{7.20}$$

In the grey atmosphere approximation, we can derive a simple form for the source function, provided we appreciate that the star is in LTE everywhere, and make one more approximation called the *Eddington Approximation*. That is, we will approximate the star as an ideal isotropic gas. In this case, the radiation pressure P is related to the total radiation density, u, (this is just the integral over all frequencies of u_ν) as $P = u/3$. Recalling that $u = 4\pi J/c$, where J is the mean intensity gives

$$P(\tau) = \frac{4\pi}{3c} J(\tau). \tag{7.21}$$

The mean intensity and the radiation pressure are defined as:

$$J(\tau) = \frac{1}{2} \int_{-1}^{+1} I(\tau,\mu) d\mu \tag{7.22}$$

$$P(\tau) = \frac{2\pi}{c} \int_{-1}^{+1} I(\tau,\mu)\mu^2 d\mu, \tag{7.23}$$

where the integral runs from $\mu = -1$ to $\mu = +1$ because we are *inside* of the star, so photons can move inwards as well as outwards. It is useful to also define the total radiative flux

$$F(\tau) = 2\pi \int_{-1}^{+1} I(\tau,\mu)\mu d\mu. \tag{7.24}$$

Because the star is in LTE everywhere, F must be *constant*. This comes from equilibrium and energy conservation considerations: all regions are in LTE and so the energy flux must be uniform across the entire system. We therefore know that $dF/d\tau = 0$. Differentiating our expression for $F(\tau)$ and inserting our definition of $\mu dI/d\tau$ gives

$$\frac{dF}{d\tau} = 0 = 2\pi \int_{-1}^{+1} (I - S) d\mu = 2\pi \left[\int_{-1}^{+1} I d\mu - \int_{-1}^{+1} S d\mu \right] = 4\pi (J - S). \tag{7.25}$$

We therefore see that $J = S$, which we expected because the star is in LTE.

We can use the same trick on the radiation pressure to get

$$\frac{dP}{d\tau} = \frac{F}{c}. \tag{7.26}$$

Integrating this (indefinite integral) gives

$$P(\tau) = \frac{F}{c} \left[\tau + A \right], \tag{7.27}$$

where A is an integration constant. Combining our two expressions for the radiation pressure gives

$$S(\tau) = \frac{3F}{4\pi} (\tau + A), \tag{7.28}$$

which is the promised further justification of the linear form we assumed for the source function earlier in the lecture.

All that remains now is to find the value of the integration constant. To do this, we can first calculate the emergent intensity by integrating down the ray from $\tau = 0$ to $\tau = \infty$:

$$\begin{aligned} I(0, \mu) &= \frac{3F}{4\pi} \int_0^\infty (t + A) \mathrm{e}^{-t/\mu} dt & (7.29) \\ &= \frac{3F}{4\pi} \left[\mu \int_0^\infty (t/\mu) \mathrm{e}^{-t/\mu} d(t/\mu) + A \int_0^\infty \mathrm{e}^{-t/\mu} d(t/\mu) \right] & (7.30) \\ &= \frac{3F}{4\pi} (\mu + A). & (7.31) \end{aligned}$$

From this, we can calculate the radiative flux escaping the star:

$$\begin{aligned} F(\tau = 0) &= 2\pi \int_0^1 I(0, \mu) \mu d\mu & (7.32) \\ &= \frac{3F}{2} \int_0^1 (\mu^2 + A\mu) d\mu & (7.33) \\ &= \frac{3F}{2} \left[\frac{\mu^3}{3} + A \frac{\mu^2}{2} \right]_0^1 & (7.34) \\ &= \frac{3F}{2} \left[\frac{1}{3} + \frac{A}{2} \right]. & (7.35) \end{aligned}$$

Since, F is a constant, we can set $F(\tau = 0) = F$ to find that:

$$A = \frac{2}{3}. \tag{7.36}$$

The source function, under the grey atmosphere approximation and the Eddington approximation, is therefore

$$S(\tau) = \frac{3F}{4\pi}\left(\tau + \frac{2}{3}\right). \tag{7.37}$$

Therefore, our assumption that S is linear in τ from before is justified. From this relation, it is fairly straightforward to see that, on average, we see an optical depth of $\tau = 2/3$ into the star. This is because we know that the intensity integrated over the entire star must follow $I = F/\pi$ (by definition), and must be equal to the source function at some optical depth. The above equation therefore tells us that $I = F/\pi = (3F/4\pi)(\tau + 2/3)$, and re-arranging we see that $\tau = 2/3$.

7.3.5 Limb Darkening

Now we have calculated a form for the source function, we can use the Eddington-Barbier relation [$I(0, \mu) = S(\tau = \mu)$] to calculate how the intensity varies as a function of the angle θ. This is the *limb darkening* law:

$$\frac{I(0,\mu)}{I(0,1)} = \frac{S(\tau = \mu)}{S(\tau = 1)} = \frac{3}{5}\left[\mu + \frac{2}{3}\right]. \tag{7.38}$$

Fig 7.6 shows how the intensity of the star is expected to vary as a function of projected distance on the sky from the centre of the star, r. The projected distance is $r = R_* \sin\theta$, R_* is the stellar radius, and I have simply used the limb darkening law above. We can see limb darkening in images of the Sun: see Fig 7.7

This is the limb darkening law for the frequency integrated intensity. Breaking down into narrow frequency ranges, we expect limb darkening to be more extreme for blue light than for red light. This is because the spectrum is a blackbody function, $I_\nu(0, \mu) = B_\nu(T(\mu))$, and so the intensity dropping off towards the limbs of the star means that the temperature also drops off towards the limbs (as you will explore in the second problem set). Fig 7.8 shows how the temperature dropping off with projected distance from the centre leads to limb darkening becoming more extreme for higher frequencies. Another way we can think of limb darkening is that the temperature of the star decreases with radius, and so we see a hotter spectrum for sight lines that penetrate further into the star.

It has long been possible to observe this wavelength dependent limb darkening effect for the sun. It is now even possible to detect limb darkening for unresolved stars, because the limb darkening law shows up in the profile of exoplanet transits. Fig 7.9 shows the expected flux from the star as the exoplanet transits across our line of sight (from Knutson et al 2007). Bluer light has deeper and narrower transits due to the wavelength dependence of the limb darkening law. This is actually seen in observational data: Fig 7.10 shows transits of the exoplanet HD 209458b

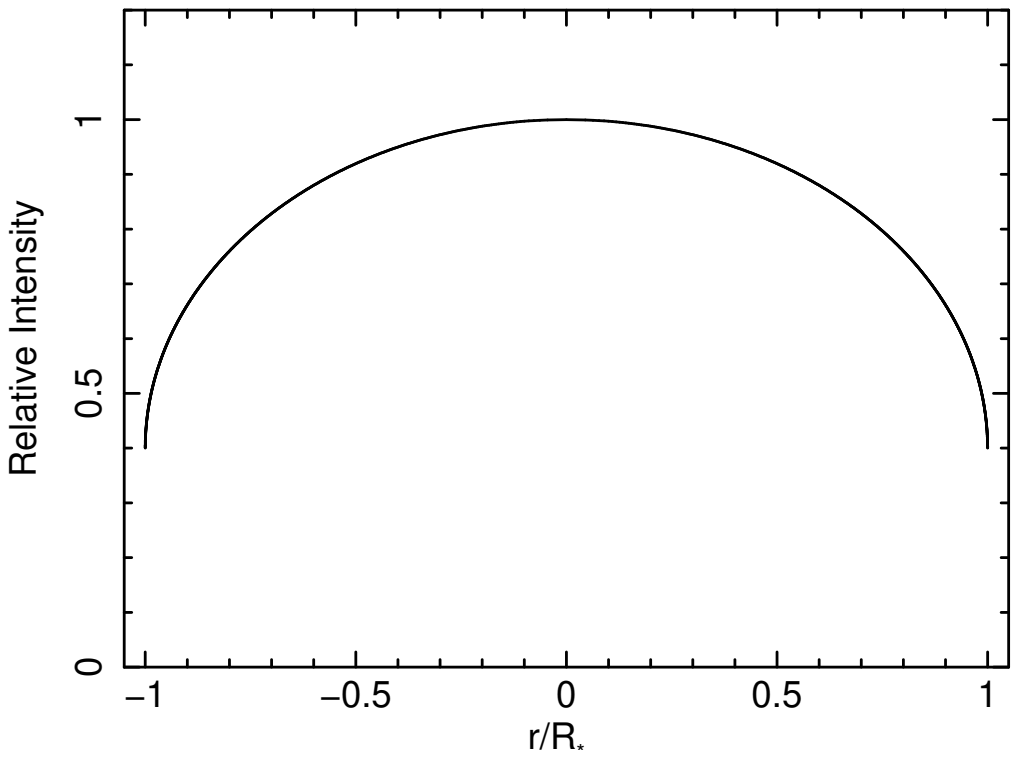

Figure 7.6: Limb darkening law derived from the grey atmosphere approximation.

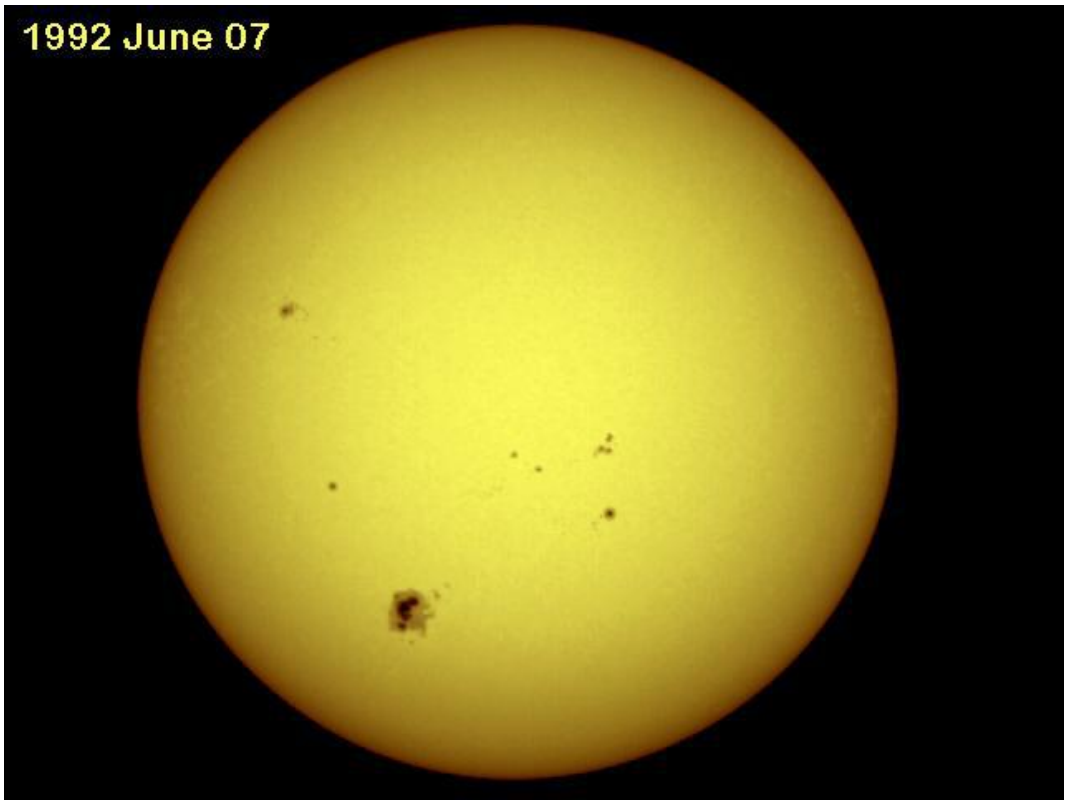

Figure 7.7: Image of the sun. Note the limb darkening.

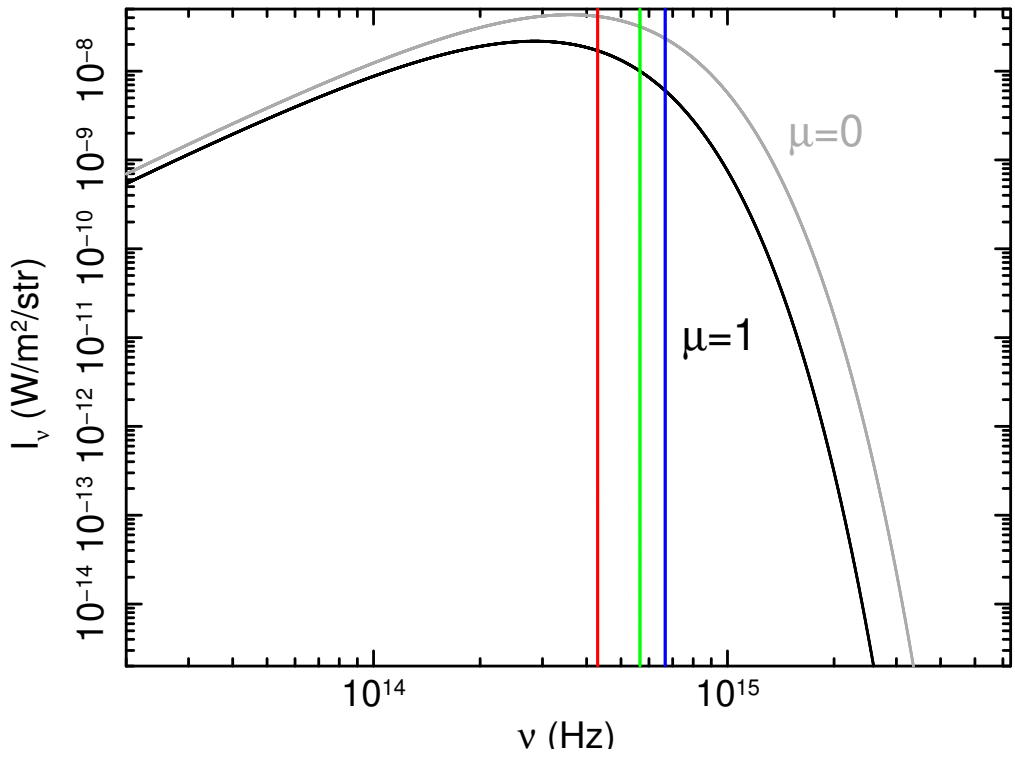

Figure 7.8: Spectrum from the centre (black) and limb (grey) of the sun. The red, green and blue lines mark the frequencies of red, green and blue light. We see that limb darkening is more extreme for higher frequencies, since the Planck functions diverge at high ν.

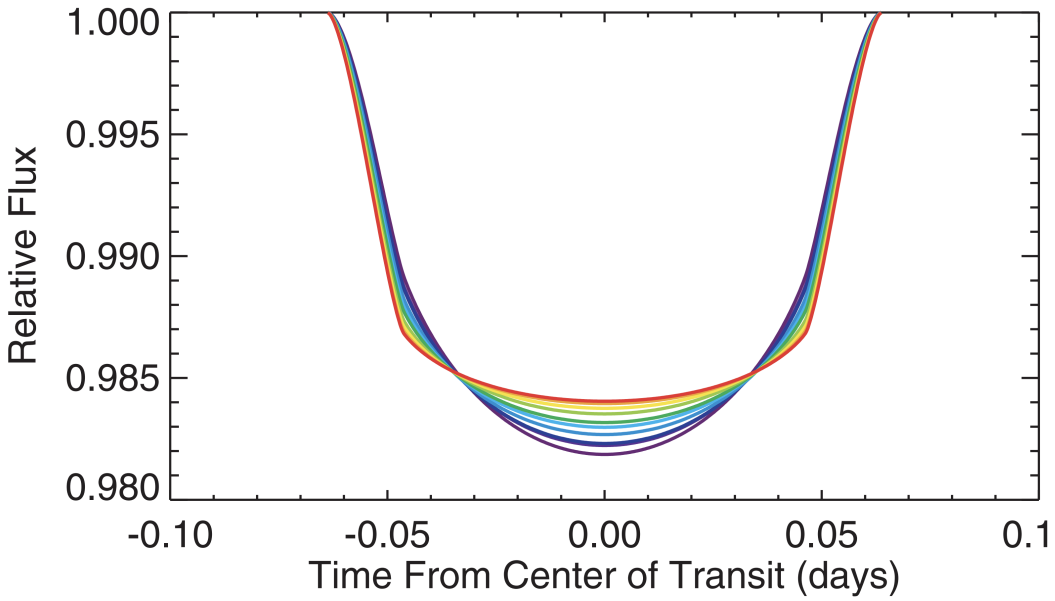

Figure 7.9: Model expolanet transit profiles for different wavelengths of visible light, taking stellar limb darkening into account.

in front of the star HD 209458, taken with the Hubble Space Telescope (Knutson et al 2007). The out-of-transit flux level has been shifted for clarity, but we can see that the wavelength dependence of the transits is exactly as expected from the simple limb darkening model.

7.4 The Emergent Spectrum

From what we've discussed so far, it is clear that the spectrum of a star is a sum of blackbody functions, since different sight lines each see a black body spectrum with a slightly different temperature, depending on how far into the star that sight line sees. Specifically, the overall (continuum) specific intensity is:

$$I_\nu = \frac{1}{\pi} 2\pi \int_0^1 B_\nu[T(\mu)]\mu d\mu. \tag{7.39}$$

This would be the whole story if the *entire* star were in LTE, but the atmosphere is not in LTE. It cannot be in LTE because photons can freely escape instead of staying in the star to share their energy. Since the photosphere is out of LTE and it is cooler than the rest of the star, it imprints absorption lines and edges onto the spectrum. Fig 7.11 illustrates the formation of absorption lines schematically. For a given μ, we always see down to the same *optical depth*, but for frequencies with an enhanced absorption coefficient α_ν, this optical depth corresponds to a larger radius. Therefore these frequencies sample a cooler spectrum and we see a dip in

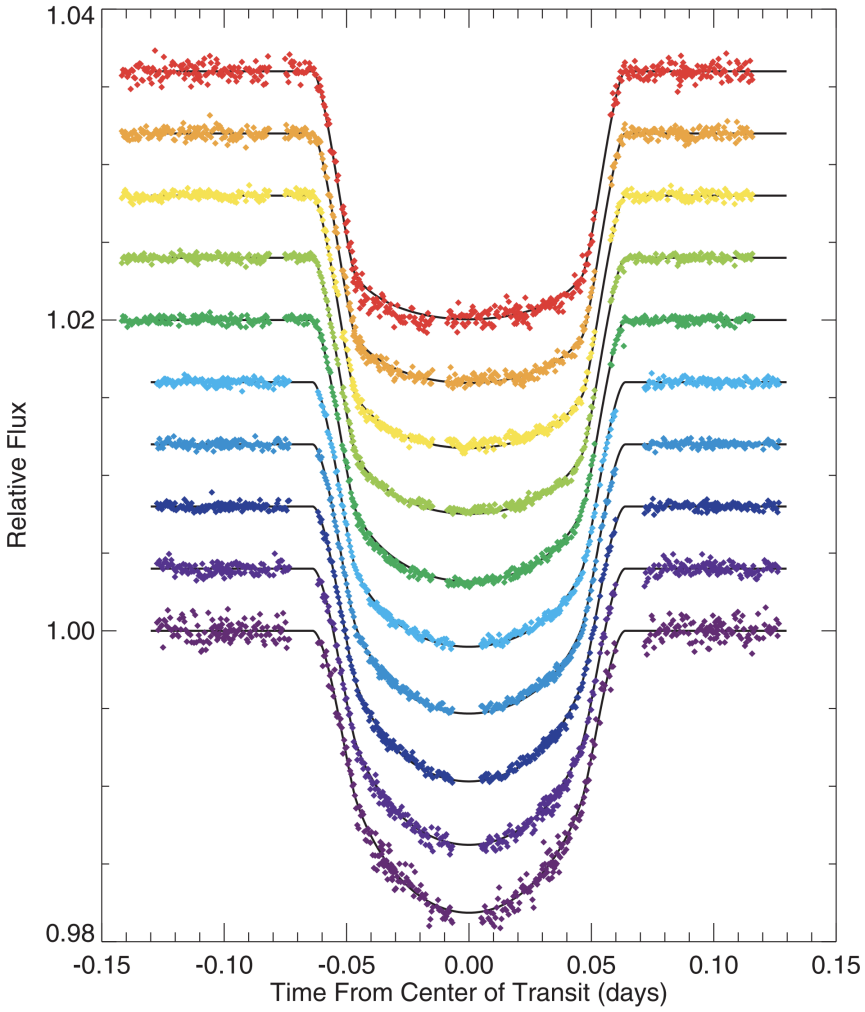

Figure 7.10: Transits of the exoplanet HD 209458b in front of its host star (Knutson et al 2007) at different wavelengths of light. The black lines represent the limb darkening model.

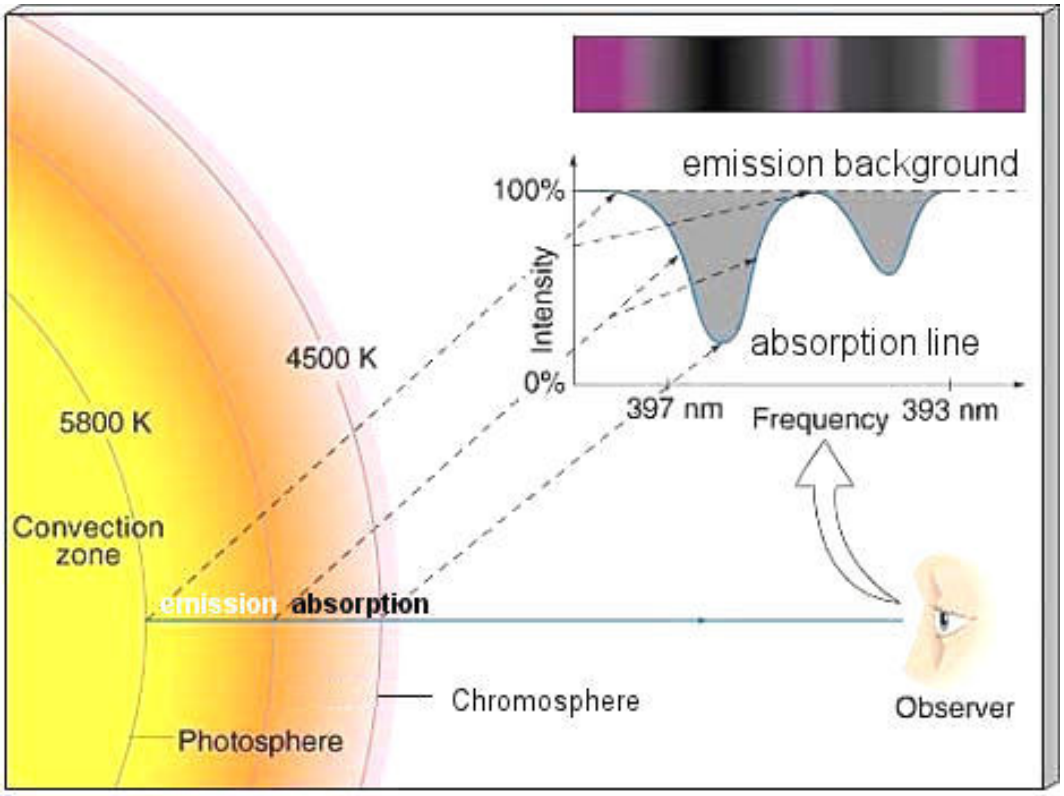

Figure 7.11: Schematic illustration of absorption line formation in the photosphere.

the overall spectrum. Clearly, the concept is the same whether we are talking about absorption lines or edges.

The lines and edges that we see in the spectrum of a given star depend on the form of the absorption coefficient, α_ν, which in turn depends on the ionization balance and excitation levels of bound electrons in the atmosphere. In stars, it is more common to talk in terms of the *opacity*. This is very simply related to the absorption coefficient via the mass density ρ: $\kappa_\nu = \alpha_\nu/\rho$ (units m^2/kg). We can therefore say that the nature of the absorption lines we see depends on what the dominant sources of opacity are in the atmosphere. There are three kinds of process that contribute to the opacity:

1. Bound-bound transitions. These are absorption lines: either photo-excitations in atoms or rotational-vibration transitions in molecules (which we will not be covering in this course).
2. Bound-free transitions. These are absorption edges resulting from photo-ionization events.
3. Free-free transitions. This covers all transitions whereby both particles start and finish unbound. For example, photons scattering off free electrons, electrons interacting with ions via the Coulomb force (bremsstrahlung), or electrons interacting with the magnetic field (synchrotron).

Fig 7.12 shows examples of optical spectra for stars across the range of stellar classifications, from O stars (hottest, top) to M stars (coolest, bottom). We see that the continuum changes across the classes, which is of course because the effective temperature is decreasing from $\sim 40,000$ K to $\sim 1,500$ K from O to M stars, meaning that O stars peak in the UV and M stars peak in the IR. The changes in absorption lines across the classes is dramatic. We see that Balmer lines and the Balmer edge are strongest for stars with intermediate effective temperatures, and molecular lines dominate for the coolest stars.

7.4.1 Absorption Lines

Fig 7.13 shows how the EW of different lines changes with spectral class. We see that hydrogen peaks for $T_{eff} \sim 10,000$K, metals are most important for $T_{eff} \sim 5,000$K, and molecules (TiO) become important for $T_{eff} \sim 3,000$K. Naively, it is remarkable that hydrogen does not always contribute the strongest lines, since it is *by far* the most abundant element in main sequence stars. So, why does H I only contribute significantly to the optical opacity for a small range of spectral classes? The answer is two fold:

1. The hydrogen lines that contribute to the optical opacity are the Balmer series lines. For a Balmer series absorption line to occur, there must be an electron already in the $n = 2$ shell. Therefore, for Balmer lines to be important, the star's atmosphere needs to be hot enough for a significant population to be excited to the $n = 2$ level.
2. To get hydrogen lines at all, there need to be neutral hydrogen atoms. Therefore, for H lines to be important, the star's atmosphere needs to be cool enough for there to be a

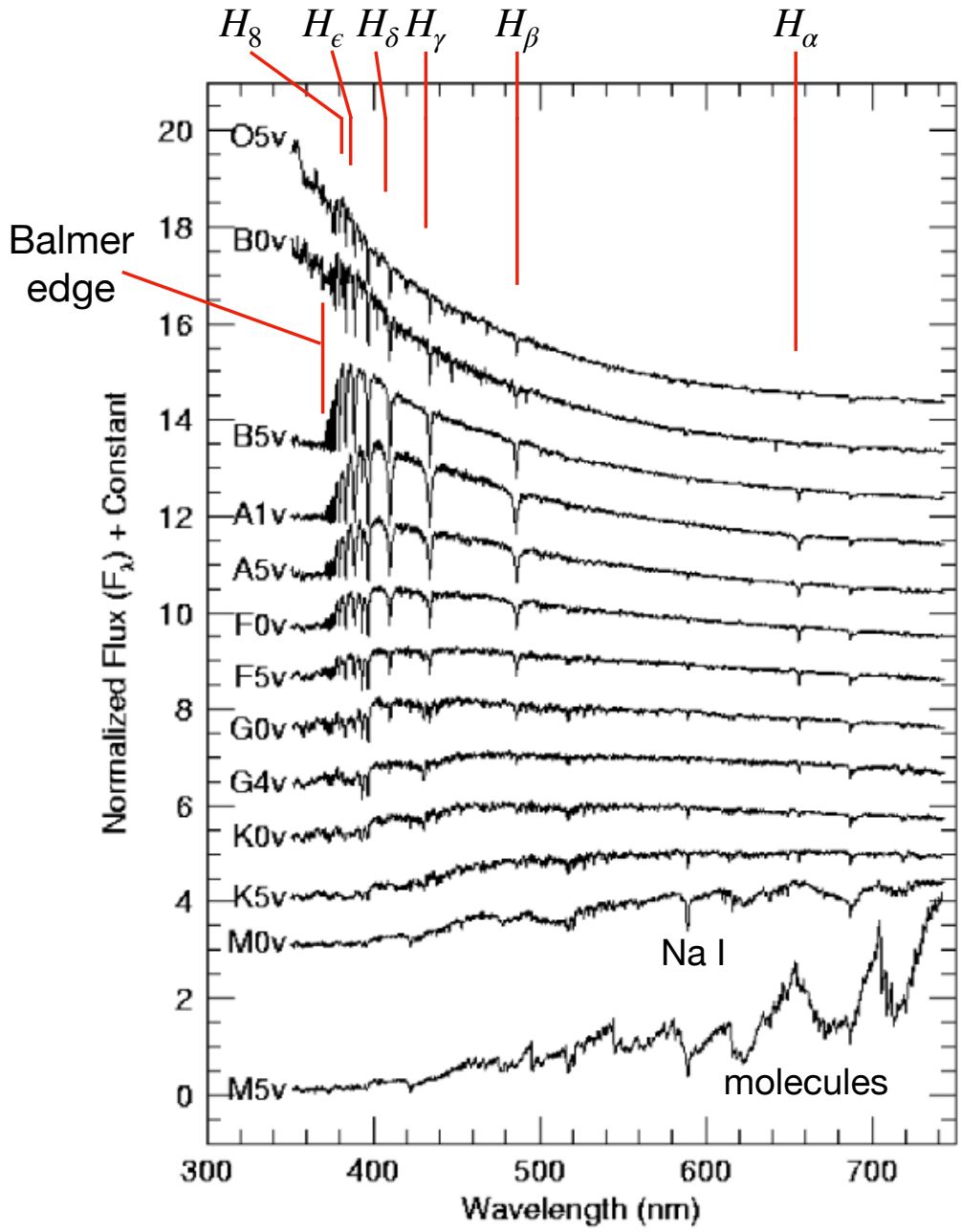

Figure 7.12: Example optical spectra for a range of stellar classes.

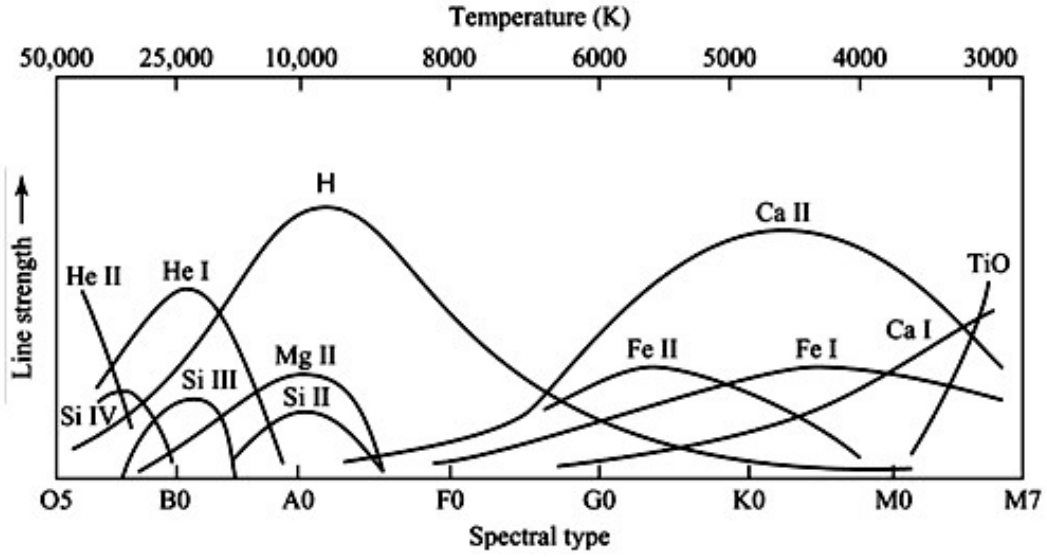

Figure 7.13: Line strengths for different spectral classes of stars.

significant population of neutral hydrogen atoms.

We can therefore understand the H line in Fig 7.13 as a trade off between two effects: the hottest stars have no hydrogen lines because all the hydrogen is ionized, and the coolest stars have no Balmer lines because there aren't enough H atoms with electrons in the $n = 2$ shell.

We can do this a little more quantitatively using what we learned in the previous lecture. For optically thin lines, the EW of a Balmer series absorption line (transition from $n = 2$ to $n = k$ in a neutral hydrogen atom) is

$$W_\lambda \propto \lambda_{2k}^2 \left(\frac{n_2}{n_{HI}}\right)_j (1-\zeta)\, f_{2k}(E), \tag{7.40}$$

where $\zeta = n_{HII}/n_H$ is the ionization fraction and f is the oscillator strength. The above assumes that $n_H = n_{HI} + n_{HII}$, and therefore $n_{HI}/n_H = (1-\zeta)$. Because the star is in LTE, we can use the Boltzmann distribution to describe the level populations. For hydrogen ($g_j = 2j^2$, $E_j = -13.6/j^2$), this gives:

$$\frac{n_j}{n_{HI}} = \frac{j^2 \exp[13.6\text{eV}/(j^2 kT)]}{\sum_i i^2 \exp[13.6\text{eV}/(i^2 kT)]}. \tag{7.41}$$

The resulting temperature dependence of n_2/n_{HI} is plotted in Fig 7.14 (top, red dashed line).

Now all that remains is to calculate the ionization fraction. In LTE, ionization balance is given by the *Saha equation*:

$$\frac{n_{i+1}}{n_i} = \frac{2}{n_e}\frac{g_{i+1}}{g_i}\left(\frac{2\pi m_e kT}{h^2}\right)^{3/2} \mathrm{e}^{-E_i/kT}, \tag{7.42}$$

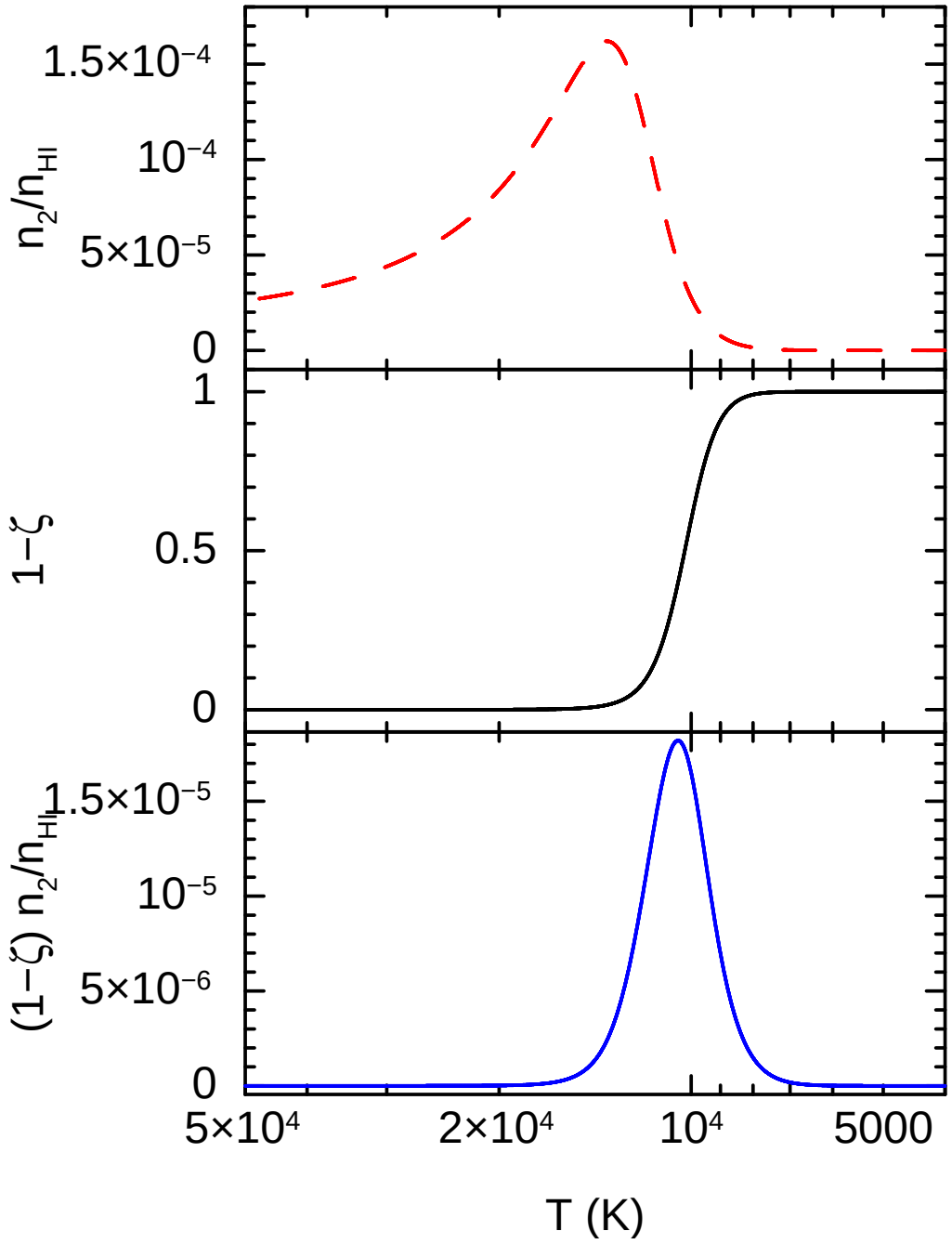

Figure 7.14: Estimates of excited fraction n_2/n_{HI} (top, dashed red line) and bound fraction $(1-\zeta)$ (middle, solid black line) for hydrogen, assuming $n_e = 5 \times 10^{20}\mathrm{m}^{-3}$. The product of these two quantities (bottom, solid blue line) is proportional to the EW of the Balmer series lines.

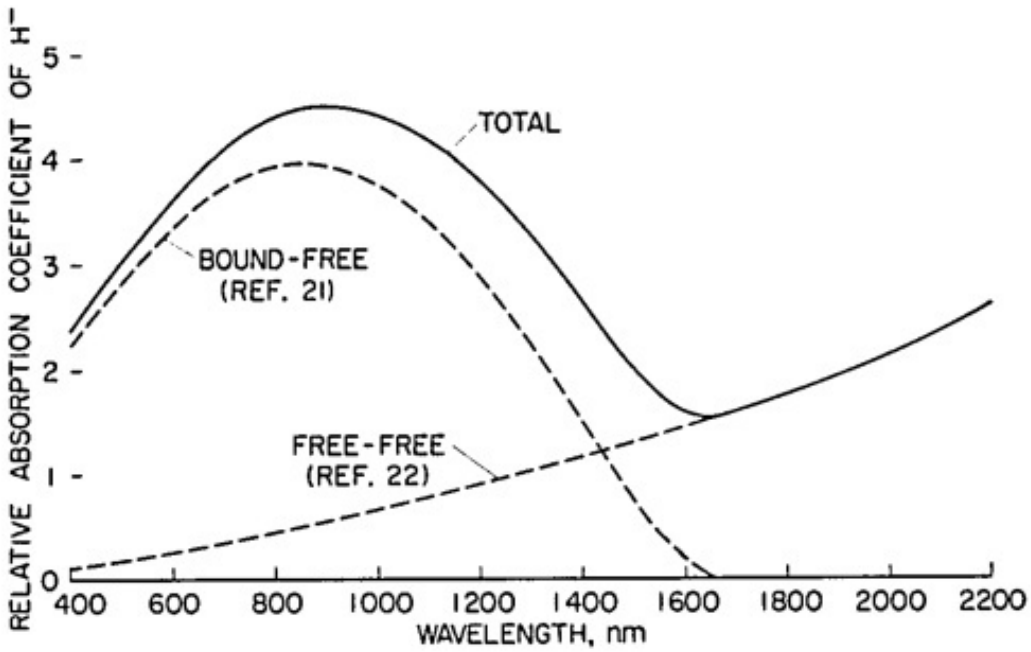

Figure 7.15: Opacity of H^-.

where n_{i+1} and n_i are ion number densities of the $(i+1)^{th}$ and i^{th} ionization state (*not* number densities of bound electrons), E_i is the ionization potential of the i^{th} ion (i.e. the energy required to liberate an electron for the *ground state* of the ion i), and g_{i+1} and g_i are the statistical weights of the *ground state* of the two varieties of ion. For hydrogen this becomes

$$\frac{\zeta}{1-\zeta} = \left(\frac{2\pi m_e kT}{h^2}\right)^{3/2} \frac{1}{n_e} \mathrm{e}^{-13.6\mathrm{eV}/kT}, \tag{7.43}$$

because the statistical weights are $g_{HII} = 1$, and $g_{HI} = 2$. The resulting temperature dependence of $(1-\zeta)$ is plotted in Fig 7.14 (middle, black solid line), assuming $n_e = 5 \times 10^{20}\mathrm{m}^{-3}$. We see that, as expected, the lowest temperature stars have plenty of neutral H atoms but very few of them are in the excited $n = 2$ state. On the other hand, the hottest stars have very few neutral H atoms. These two considerations balance out at $T \sim 10,000$ K (bottom, blue solid line), therefore explaining why A stars have the strongest Balmer lines. We can use similar reasoning to understand the temperature dependence of heavy element lines.

7.4.2 Absorption Edges and Continuum Opacity

Looking back at Fig 7.12, we see the Balmer edge – a sharp drop in flux blueward of 365 nm – only for intermediate spectral classes. This happens for exactly the same reason as for the Balmer lines: for the hottest stars there is not enough H I, and for the coolest stars there is enough H I, but too small a fraction of the H I atoms are in the $n = 2$ required for a Balmer

bound-free transition. Note however that the spectrum of the hottest stars with no Balmer jump continues to rise for $\lambda < 365$nm, whereas the spectrum of the coolest stars is still suppressed for $\lambda < 365$ nm, even though there is no Balmer jump.

This continuum suppression is primarily due to opacity of the negative hydrogen ion H^-. This is a hydrogen nucleus with two bound electrons, and has an ionization potential of 0.75 eV ($\lambda = 1,650$ nm). Fig 7.15 shows the absorption cross-section of H^-. We see there are two components. The bound-free contribution is just photo-ionization. This is a very different cross section to other bound-free transitions – we may naively expect to see a function going as λ^3 for $\lambda < 1,650$ nm and zero for $\lambda > 1,650$ nm. Instead, it is a broad bump for $\lambda < 1,650$ nm. The free-free contribution is the opposite of Bremsstrahlung radiation. For Bremsstrahlung radiation, an electron is decelerated by an ion due to the Coulomb force, and emits a photon to conserve energy. In the case of inverse Bremsstrahlung, the electron instead *absorbs* a photon during this deceleration, meaning that the electron keeps more kinetic energy than it otherwise would have.

Since the ionization potential of H^- is so low (0.75 eV), it is an important source of opacity in all stars that are cool enough to have a significant H^- population (solar and cooler). It is not important at all in the highest temperature stars, because all H^- atoms are 'ionized' to HI or HII (we can again use the Saha equation to calculate this). Finally, in the very hottest stars, electron-proton scattering becomes a dominant source of opacity, as there are so many free electrons.

8 Dust

8.1 Introduction

Dust consists of particles ranging in size from a few molecules to ~micrometers (Fig 8.1). It is very important in astronomy. Partly as a nuisance, since it absorbs and scatters light and re-emits it at longer wavelengths. Optical and UV light is preferentially absorbed / scattered, and re-emission is at longer wavelengths, therefore the process of dust scattering and absorption tends to be referred to as *extinction* or *reddining*. Clearly, the greater the column of dust we look through, the greater the reddening. This can be seen in the deep field images taken by HST (optical) and ALMA (sub-mm) that are shown in Fig 8.2. Dust re-emission is also polarised, which provides a challenge for experiments aiming to measure the polarisation of the cosmic microwave background (CMB) radiation. Most infamously, the BICEP2 experiment announced the detection of polarisation B-modes originating from gravitational waves during the epoch of inflation in 2014, but it was later realised that the contribution of Galactic dust had been slightly underestimated (Fig 8.3). The BICEP2 collaboration withdrew their claim when they re-calculated that foreground dust alone could potentially explain the detected signal within statistical errors. Dust is important as more than just a nuisance though. The process of planet formation relies on particles in a proto-planetary disc around a young star coagulating into larger and larger grains. These grains eventually become large enough to grow into 'planetesimals', which eventually become planets. This process is still not well understood and is the subject of active research.

In this lecture, we will cover the *extinction curve*, which governs the contribution of dust extinction as a function of wavelength, we will learn about some of the absorption and scattering processes that determine the shape of the extinction curve, and we will calculate dust heating and re-emission.

8.2 Extinction curve

8.2.1 The Form of the Extinction Curve

Dust extinction is quantified in terms of its affect on the apparent magnitude of an object. The apparent magnitude relative to some constant reference star (e.g. Vega) is

$$m_\nu \equiv -2.5 \log_{10} \left(\frac{F_\nu}{F_\nu^{ref}} \right). \tag{8.1}$$

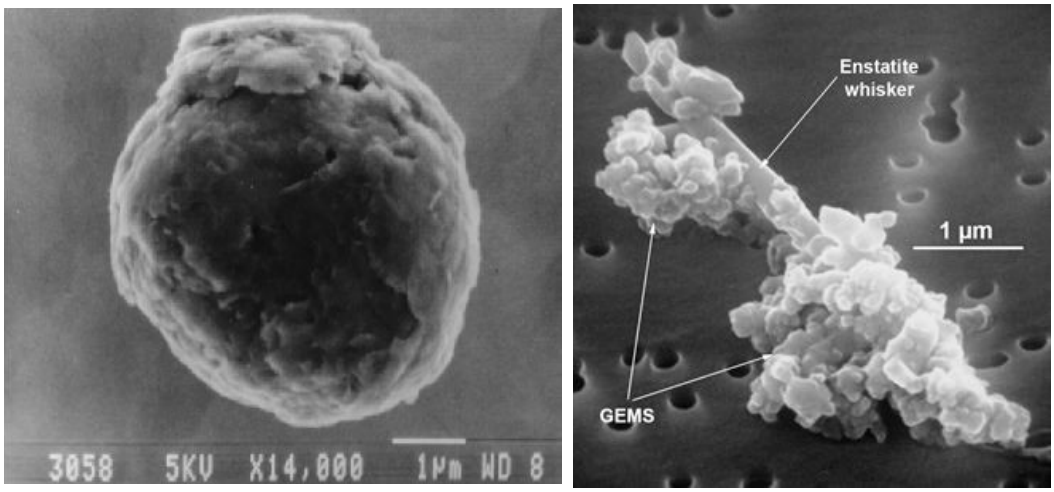

Figure 8.1: Dust grains grown in a lab.

If the specific flux of the object with no extinction is F_ν^0, then the apparent magnitude is

$$m_\nu \equiv -2.5\log_{10}\left(\frac{(F_\nu^0/F_\nu)F_\nu}{F_\nu^{ref}}\right) = -2.5\log_{10}\left(\frac{F_\nu}{F_\nu^{ref}}\right) - 2.5\log_{10}\left(\frac{F_\nu}{F_\nu^0}\right) = m_\nu^0 + A_\nu, \tag{8.2}$$

where $A_\nu \equiv -2.5\log_{10}(F_\nu/F_\nu^0)$ is the frequency-dependent extinction in terms of magnitudes. Note that larger A_ν makes the apparent magnitude more positive, which corresponds to lower observed flux (I know, I don't like magnitudes any more than you do!).

The form of A_ν can be determined empirically using a number of methods. First is the *pair method*, which involves comparing the spectrum of two stars of the same spectral type. If one of the stars has negligible foreground dust but the other is heavily reddened, then A_ν can be inferred by assuming $A_\infty = 0$. Say the apparent magnitude of the un-reddened and reddened stars are respectively $m_1(\nu)$ and $m_1(\nu)$. The two stars are assumed to have the same intrinsic spectral *shape*, but they are likely at different distances and so will have different integrated apparent magnitudes. Therefore, the un-reddened magnitudes of the two stars are $m_1^0(\nu)$ and $m_2^0(\nu) = m_1^0(\nu) + C$, where C is a constant (unknown if we do not know the distance to the two stars). Since star 1 is un-reddened, we simply have $m_1(\nu) = m_1^0(\nu)$, whereas the apparent magnitude of star 2 is $m_2(\nu) = m_2^0(\nu) + A(\nu)$. Combining these equations and assuming that extinction is not important at the longest wavelengths yields:

$$A(\nu) = [m_2(\nu) - m_2(\infty)] - [m_1(\nu) - m_1(\infty)]. \tag{8.3}$$

Another method involves using the known relative strengths of hydrogen recombination lines. Recall from Lecture 5 that the flux ratios of Balmer lines depend only very weakly on electron temperature, and so are fairly well determined theoretically. The same is true for longer wavelength series of H transitions, therefore an observed spectrum that contains H

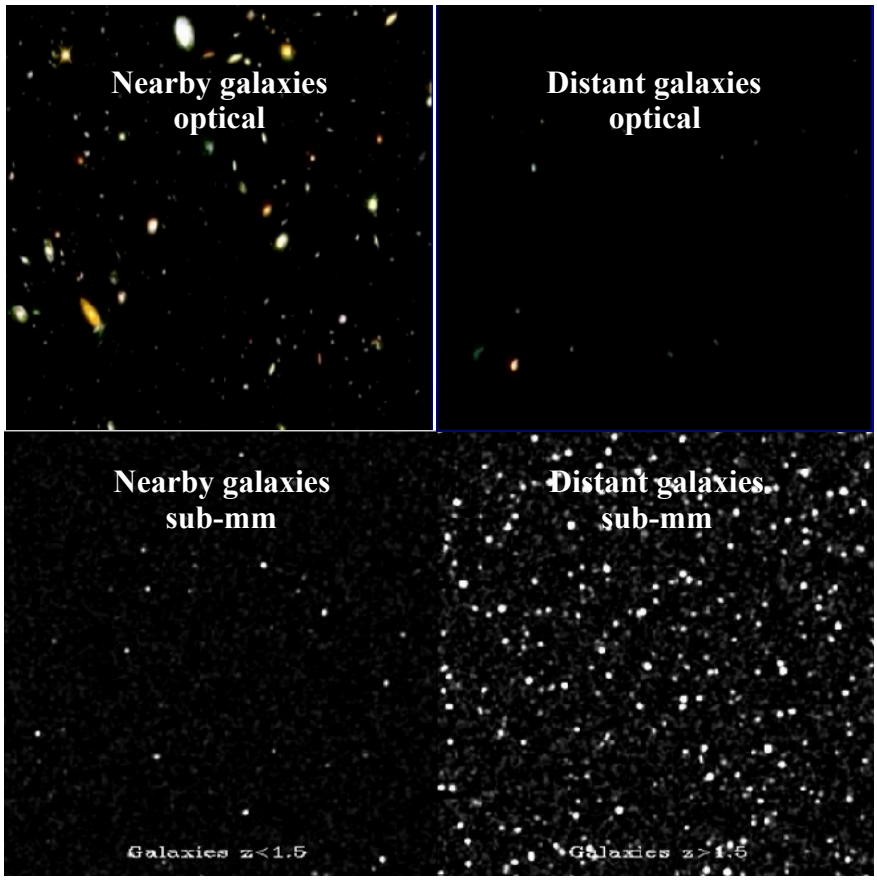

Figure 8.2: Near and far galaxies seen by Hubble (optical; source: K. Lanzetta, SUNY-SB) and ALMA (sub-mm; source: Wootten and Gallimore, NRAO). More distant galaxies are more reddened due to the greater column density of dust along the longer line of sight.

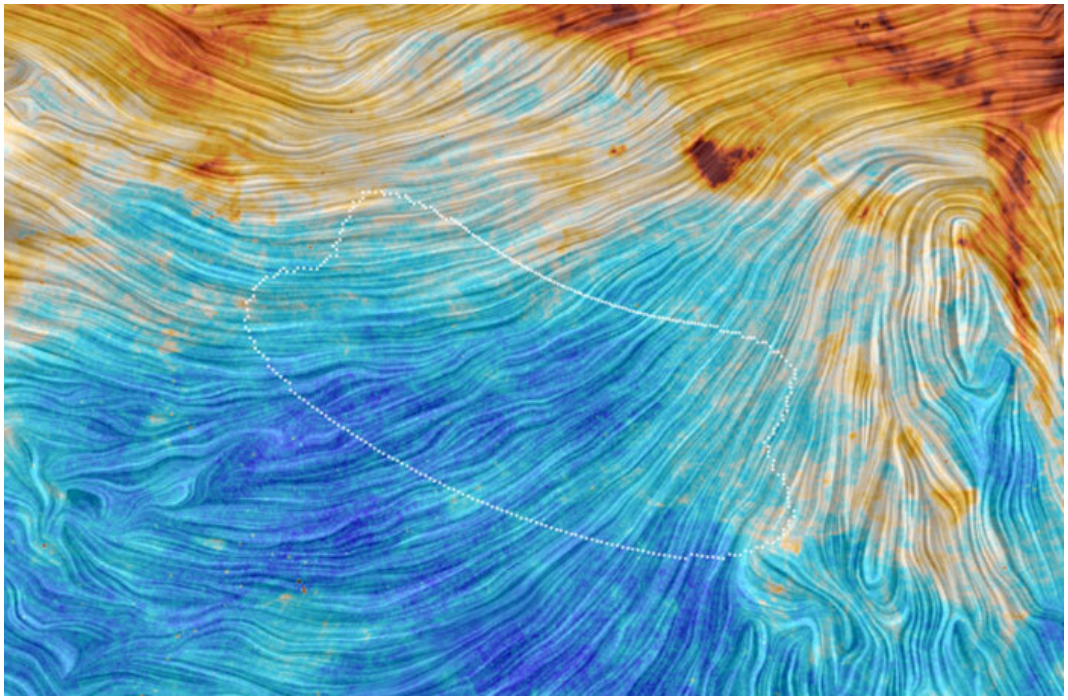

Figure 8.3: Polarization of 353 GHz radiation detected by Planck in the BICEP2 field. Colours are emission from dust, relief is orientation of the Galactic magnetic field, and the white patch depicts a region of the sky observed by both the Keck observatory and by BICEP2. Dust contributes polarised emission to the BICEP2 field that cannot be ignored. Source: ESA/Planck Collaboration, M-A Miville-Deschênes, CNRS – Institut d'Astrophysique Spatiale, Université Paris-XI, Orsay, France

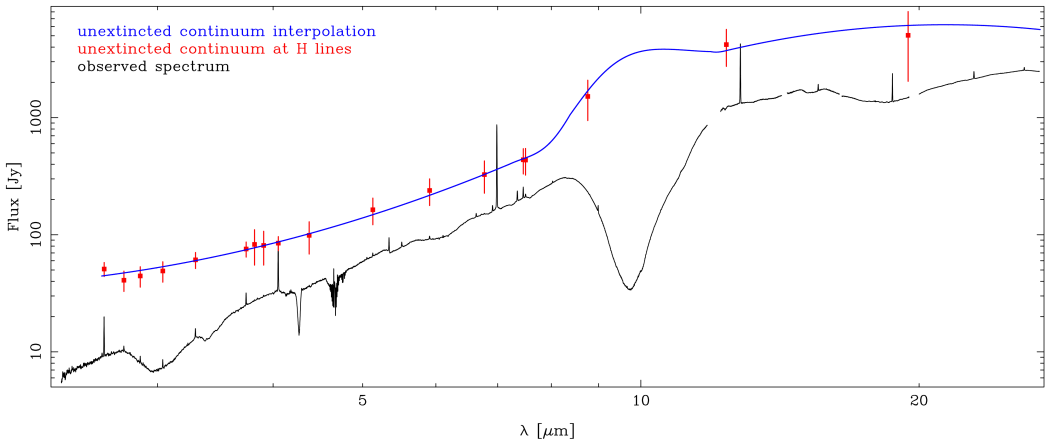

Figure 8.4: Observed spectrum of the Galaxy centre (black) corrected for extinction using H line ratios (red points). The blue line is a model for the un-extincted spectrum. From Fritz et al (2011).

recombination lines can be de-reddened by comparison to theoretical line ratios. Fig 8.4 shows an example of the IR spectrum of the Galaxy centre, Sgr A. The enhanced extinction at 10μm and 20μm is due to absorption by silicate dust.

These empirical methods have shown that the amount of dust extinction varies with line of sight (e.g. the Galaxy centre is very dusty), but the general *form* of A_ν is fairly universal in that it can be modelled with reasonably few parameters (see Draine 2003, Annual Review of Astronomy & Astrophysics, 41, pp.241-289). The dimensionless quantity $R_V \equiv A_V/(A_B - A_V)$ is a common measure of the slope of the extinction curve in the optical region. Here, the V and B bands are centered respectively on $\lambda \approx 551$ nm and $\lambda \approx 569$ nm. A gray extinction curve would have $R_V \rightarrow \infty$, and a very steep extinction curve of $A_\nu \propto \nu^4$ would give $R_V \approx 1.2$. The measured values of R_V for different sight lines range from $R_V \sim 2.1 - 5.8$.

Fig 8.5 shows the extinction curve for different values of R_V. Note that this is plotted as a function of wave number, so everything to the right of $1/\lambda \approx 2.5$ on this plot is UV. Clearly extinction occurs most dramatically for UV (as we expected). The curves all peak at $1/\lambda \approx 12.5$, such that extinction is not so extreme for X-rays. We see a large feature at ~ 220 nm, and we can even see the tiny silicate feature at $1/\lambda \approx 0.1$ that we already saw in the previous plot.

8.2.2 Processes Contributing to Extinction

The extinction curve A_ν is, to within a factor of ~ 1.09, equal to the optical depth of extinction, since

$$F_\nu = F_\nu^0 \exp(-\tau_\nu^{ext}), \tag{8.4}$$

and therefore

$$A_\nu \equiv -2.5 \log_{10}(F_\nu/F_\nu^0) = 2.5 \log_{10}(\mathrm{e})\tau_\nu^{ext} \approx \tau_\nu^{ext}. \tag{8.5}$$

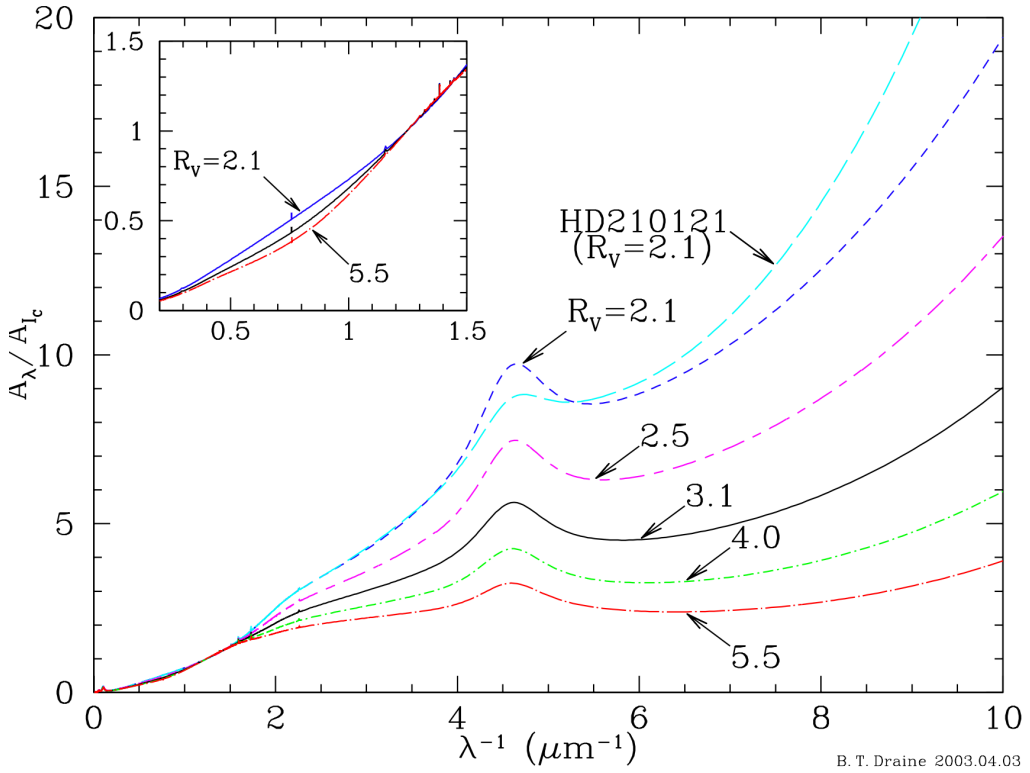

Figure 8.5: Extinction curve for different values of R_V as a ratio to A_I (I band centered on $\lambda \approx 806$ nm, $1/\lambda \approx 1.24 \mu\text{m}^{-1}$). The curves all peak and turn over at $\lambda \sim 80$nm, corresponding to $1/\lambda \sim 12.5 \mu\text{m}^{-1}$ which is just off the plot. Note that optical is $1/\lambda \sim 1.43 - 2.5 \mu\text{m}^{-1}$. From Draine et al (2003)

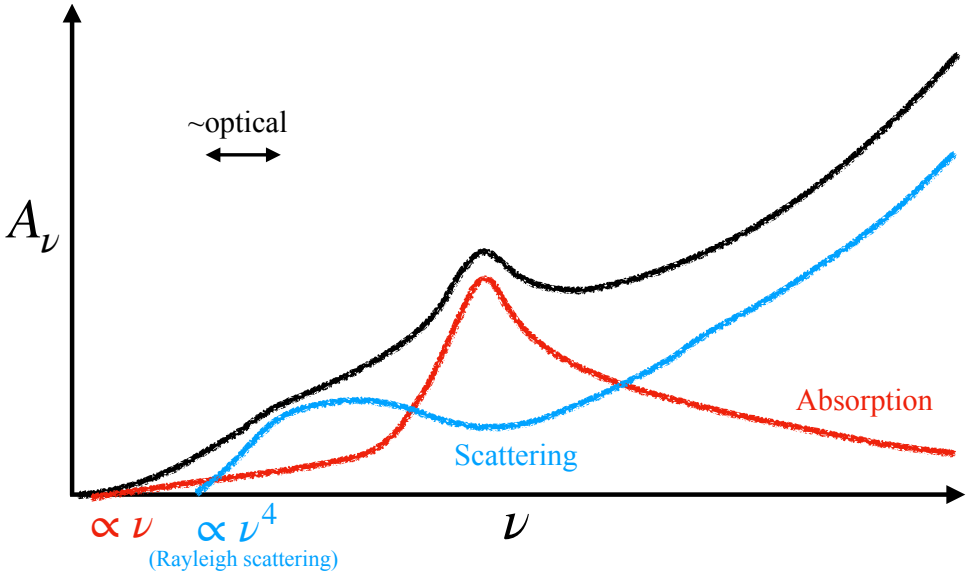

Figure 8.6: Schematic of extinction curve demonstrating the relative importance of scattering and absorption. At long wavelengths, the continuum of both processes can be represented by a power-law.

As usual, we can represent the optical depth in terms of a column density and a cross-section: $\tau_\nu^{ext} = N_{\rm dust}\sigma_\nu^{ext}$. We can then define a cross-section for absorption, σ_ν^{abs}, and a cross-section for scattering, σ_ν^{sca}, such that $\sigma_\nu^{ext} = \sigma_\nu^{abs} + \sigma_\nu^{sca}$. It is usual to represent the cross-sections in terms of their geometrical cross-section multiplied by a correction factor

$$\sigma_\nu^{abs} = \pi a^2 Q_\nu^{abs} \tag{8.6}$$
$$\sigma_\nu^{sca} = \pi a^2 Q_\nu^{sca} \tag{8.7}$$
$$\sigma_\nu^{ext} = \pi a^2 Q_\nu^{ext}, \tag{8.8}$$

such that $Q_\nu^{ext} = Q_\nu^{abs} + Q_\nu^{sca}$ is the *efficiency factor* for dust extinction. Here, we are assuming that the dust grains are ~spherical with radius a. The distribution of dust grain sizes is approximately:

$$\frac{dN}{da} \propto \begin{cases} a^{-3.5} e^{-a/a_0} & \text{for } a \geq a_{\rm min}, \\ 0 & \text{for } a < a_{\rm min}, \end{cases} \tag{8.9}$$

where $a_{\rm min} \sim 1$ nm and $a_0 \sim 0.25\ \mu$m.

Fig 8.6 shows a sketch of the extinction curve with contributions from absorption and scattering.

Scattering

Scattering in the $(a/\lambda) << 1$ regime is *Rayleigh scattering*, and the scattered flux is $\propto a^6/\lambda^4$. Therefore, in this regime, illustrated in Fig 8.7, bluer light is preferentially scattered over redder light. This is the regime of Earth's atmosphere on a cloudless day: the Sun appears to be yellow

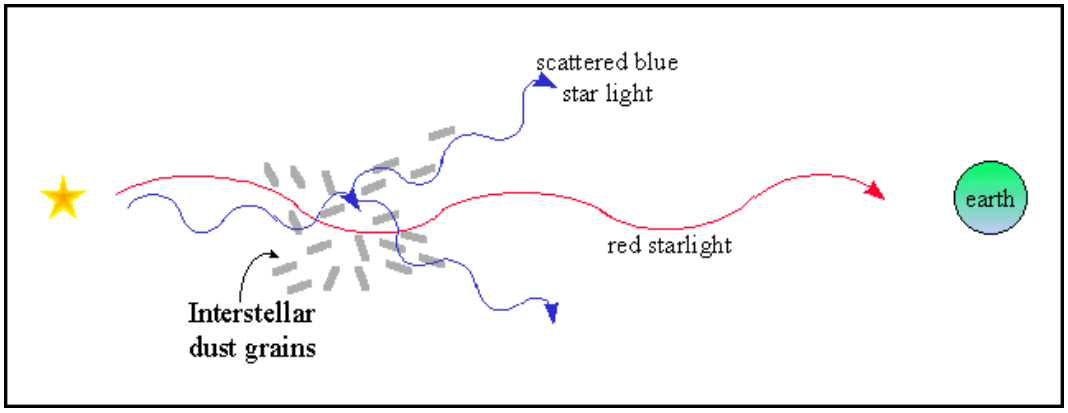

Figure 8.7: Schematic of Rayleigh scattering.

even though it is actually white, and the sky is blue, because we are seeing predominantly blue photons that came from the Sun and have been scattered. Another famous example of scattered light is the reflection nebulae surrounding the Pleiades. The blue filaments of light shown in Fig 8.8 are due to scattering of light from the stars into our line of sight.

Absorption

There are a number of narrow absorption features, and the continuum absorption goes as $A_\nu \propto \nu$ for the longest wavelengths. Absorption by molecules is beyond the scope of this course, and dust grains are made up of complex molecules, so we will only cover this qualitatively. I already said that the feature at $\sim 10\mu$m is due to absorption from silicate molecules (the Si-O bond stretching mode). The origin of the very large feature at $\lambda \sim 220$nm is actually still uncertain. Candidates include graphitic carbon (Draine & Lee 1984, ApJ, 285, 89) and Polycyclic Aromatic Hydrocarbon (PAH) molecules (Weingartner & Draine 2001, ApJ, 548, 296). These molecules have complex structures – see examples in Fig 8.10.

8.3 Dust heating

Whenever dust absorbs radiation, it is heated and the energy absorbed is then re-emitted at longer wavelengths. This happens in protoplanetary discs around young stars. Fig 8.11 shows an ALMA image of the young ($\sim$ 1 million years old) stellar system HL Tauri. The star is at the centre radiating in optical, and the protoplanetary disc around it is being heated by the star, and this energy is being re-emitted at wavelengths that ALMA is sensitive to ($\sim 0.3 - 3.6$ μm). The gaps in the disc are thought to be young planets clearing out dust lanes around their orbits. It is, however, difficult to understand theoretically how planets could have formed quite so quickly!

We can calculate the temperature of dust at a given distance from the star. If the luminosity of the irradiating star is

$$L = \int_0^\infty L_\nu d\nu, \tag{8.10}$$

Figure 8.8: The Pleiades. The blue fuzz around the stars is due to scattering of star light into our line of sight.

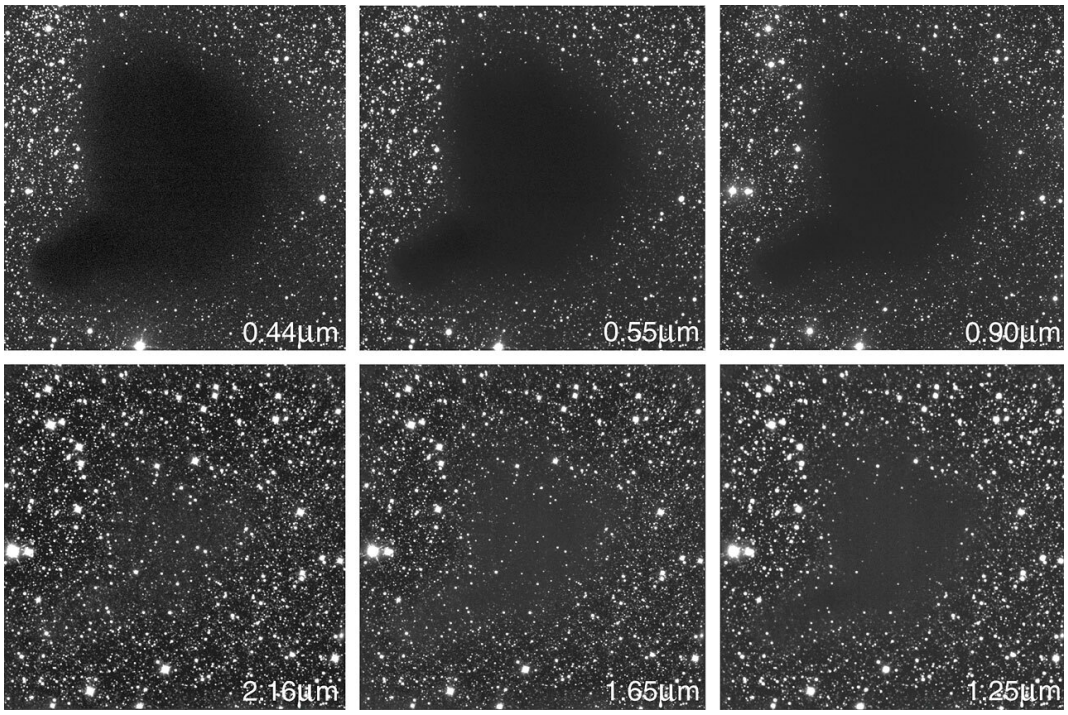

Figure 8.9: Images of the 'dark cloud' Barnard 68 at different wavelengths. Clearly, shorter wavelengths are preferentially absorbed. Source: ESO.

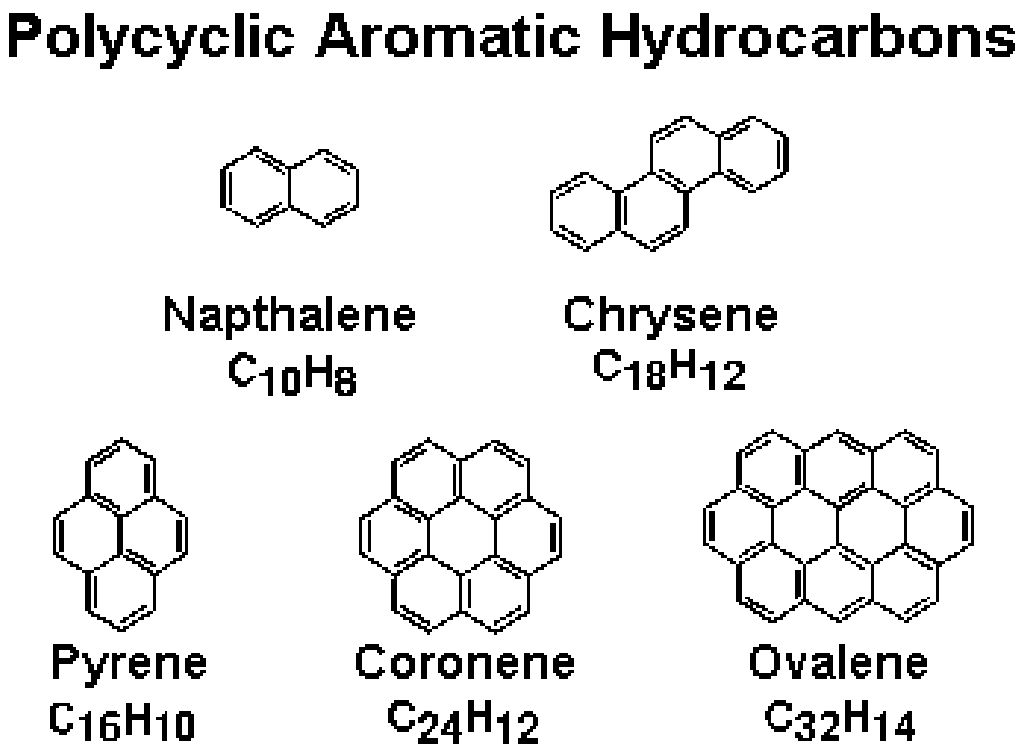

Figure 8.10: Examples of Polycyclic Aromatic Hydrocarbon (PAH) molecules.

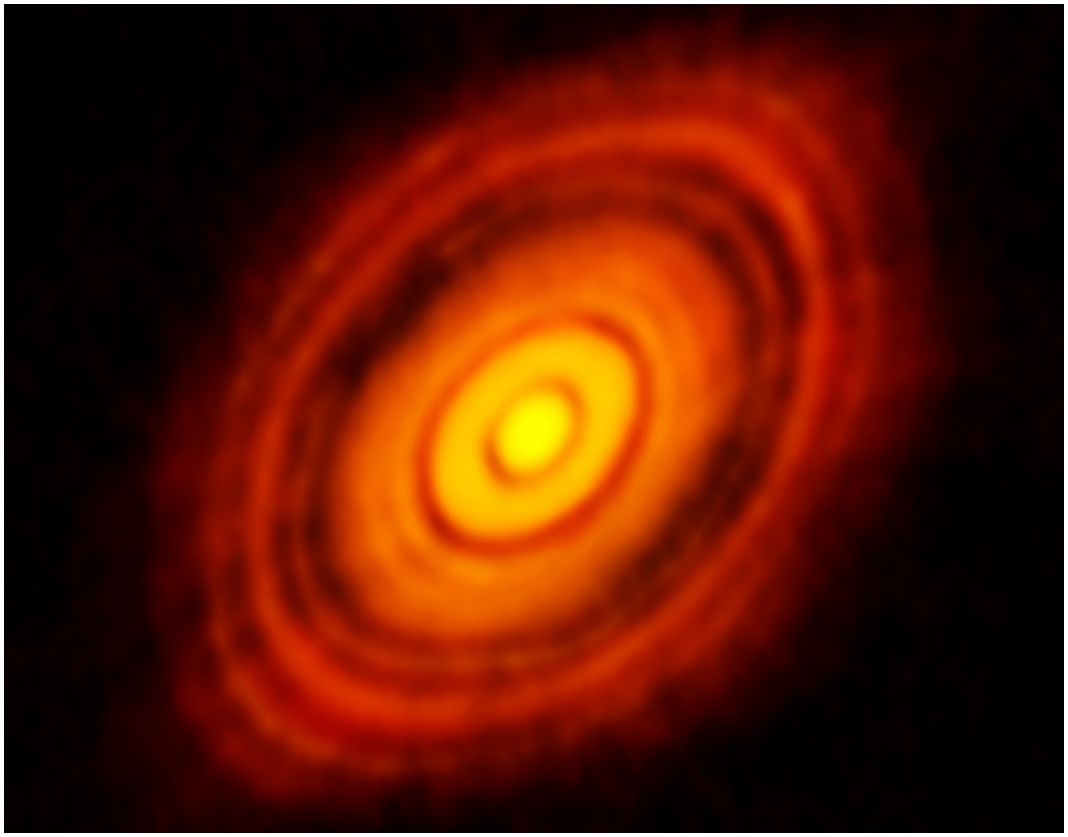

Figure 8.11: Protoplanetary disc around HL Tauri imaged by ALMA ($\lambda \sim 0.3 - 3.6$ mm). The distance to the star is $\sim$ 450 light years, and the disc is ~1,500 light minutes across. Image Credit: ALMA (ESO/NAOJ/NRAO), NSF.

then the power absorbed by spherical dust grains with radius a a distance d from the star is

$$L_{abs} = \int_0^\infty \frac{L_\nu}{4\pi d^2} \sigma_\nu^{abs} d\nu. \tag{8.11}$$

From before, we know that the cross-section is $\sigma_\nu^{abs} = \pi a^2 Q_\nu^{abs}$, therefore

$$L_{abs} = \frac{\pi a^2}{4\pi d^2} \int_0^\infty L_\nu Q_\nu^{abs} d\nu. \tag{8.12}$$

The dust grains radiate a with a specific intensity I_ν^{em}, such that the power re-emitted from the grains is

$$L_{em} = 4\pi a^2 \int_0^\infty \pi I_\nu^{em} d\nu, \tag{8.13}$$

where we recall that πI_ν is a specific flux to explain the factor of π in the integral. If the system is in equilibrium, the emitted power equals the absorbed power,

$$\frac{\pi a^2}{4\pi d^2} \int_0^\infty L_\nu Q_\nu^{abs} d\nu = 4\pi a^2 \int_0^\infty \pi I_\nu^{em} d\nu, \tag{8.14}$$

such that *all* of the ~optical/UV light absorbed by the dust grains is re-emitted. The spectrum re-emitted by the dust grains is not quite thermal, but it is useful to define a characteristic temperature for the grains. We can therefore assign an effective temperature (recall this from Lecture 1), such that $I_\nu = Q_\nu^{em} B_\nu$. We then have

$$\frac{\pi a^2}{4\pi d^2} \int_0^\infty L_\nu Q_\nu^{abs} d\nu = 4\pi a^2 \int_0^\infty \pi Q_\nu^{em} B_\nu(T) d\nu. \tag{8.15}$$

We could then calculate the effective temperature of the dust grains if we knew the exact spectrum of the star and the exact forms of Q_ν^{abs} and Q_ν^{em}. This is difficult in practice, but the equations can be simplified by introducing averaged quantities:

$$\frac{\pi a^2}{4\pi d^2} \langle Q_{UV} \rangle \int_0^\infty L_\nu d\nu = 4\pi a^2 \langle Q_{IR} \rangle \int_0^\infty \pi B_\nu(T) d\nu, \tag{8.16}$$

where

$$\langle Q_{UV} \rangle \equiv \frac{1}{L} \int_0^\infty L_\nu Q_\nu^{abs} d\nu, \tag{8.17}$$

and

$$\langle Q_{IR} \rangle \equiv \frac{\int_0^\infty Q_\nu^{em} B_\nu(T) d\nu}{\int_0^\infty B_\nu(T) d\nu}, \tag{8.18}$$

where the names come from absorption (emission) being primarily in the UV (IR). In one of the homework problems, you will be asked to calculate grain temperatures for given values of $\langle Q_{IR} \rangle / \langle Q_{UV} \rangle$. Note that the grain size a drops out of the above equations explicitly, but the absorption / scattering cross-section depends on a, and so the size of the dust grains governs the value of $\langle Q_{IR} \rangle / \langle Q_{UV} \rangle$.

Adam Ingram